CORROSION UNDER INSULATION OF CARBON STEEL AND THERMALLY SPRAYED ALUMINUM (TSA) COATING

by

Shahzad Karim

Submitted in partial fulfilment of the requirements
for the degree of Master of Applied Science

at

Dalhousie University
Halifax, Nova Scotia
August 2024

Dalhousie University is located in Mi'kma'ki, the
ancestral and unceded territory of the Mi'kmaq.
We are all Treaty people.

DEDICATION PAGE

This thesis is dedicated to the pursuit of knowledge and the relentless quest for understanding in the realm of Material Engineering. It is a tribute to the countless hours spent delving into technical intricacies, unravelling complexities, and pushing the boundaries of what is known.

To my mentors and academic advisors, whose guidance and expertise have been instrumental in shaping my understanding of Material Engineering and fostering a deep appreciation for research and innovation. Your mentorship has not only enriched my academic journey but has also instilled in me a passion for lifelong learning and contributing to the research community.

I dedicate this work to my colleagues and peers, whose collaboration, insightful discussions, and constructive feedback have been invaluable in refining ideas, challenging assumptions, and elevating the quality of research. Together, we have forged a community dedicated to advancing knowledge and addressing the pressing challenges facing our field.

With gratitude for the opportunity to learn, grow, and serve.

Shahzad Karim

Table of Contents

LIST OF TABLES

TABLE OF FIGURES

ABSTRACT

Corrosion, particularly Corrosion Under Insulation (CUI), poses significant challenges in industrial applications due to its covert nature and potential for severe, undetected damage. This research explores the mechanisms and implications of CUI through forensic investigations of rust scale samples from various industrial settings, highlighting the impact of environmental and operational factors. Comparative analyses of laboratory and field samples assess insulation aging and its effects on CUI, emphasizing the necessity of realistic simulation techniques for accurate predictions. Additionally, a case study on premature coating failure in boiler tubes underscores the critical role of appropriate material selection and maintenance practices in preventing CUI, providing practical insights for improving industrial corrosion management.

This study further examines the performance of Thermally Sprayed Aluminum (TSA) coatings under CUI and immersion conditions using both CUI simulation setups and autoclave immersion tests. Detailed microstructural characterizations reveal the distinct corrosion behaviors of TSA in varying environments, identifying significant degradation challenges under moisture-saturated thermal insulations due to factors such as flashing moisture and active iron dissolution. These findings offer critical insights into the limitations and potential improvements for TSA coatings, contributing to the broader goal of enhancing corrosion resistance and developing more effective prevention strategies in industrial applications.

LIST OF ABBREVIATIONS USED

AER	Alberta Energy Regulator
AI	Artificial intelligence
AISI	American Iron and Steel Institute
API	American Petroleum Institute
ASTM	American Society for Testing and Materials
BFW	Boiler feed water
CBN	Carbon boron nitride
CDU	Crude distillation unit
CE	Counter electrode
CF	Corrosion fatigue
CFU	Colony forming units
COE	Crude oil emulsions
CR	Corrosion rate
CR	Computed radiography
CS	Carbon steel
CUI	Corrosion under insulation
CW	Cyclic wet
DFT	Dry film thickness
DMs	Damage mechanisms
EDS	Energy dispersive spectroscopy
EIS	Electrochemical impedance spectroscopy
EN	Electrochemical Noise
EW	Equivalent weight
GDP	Gross domestic product
HAZ	Heat affected zone
HCF	High cycle fatigue
i_{corr}	corrosion current density
ICP	Inductively coupled plasma
IGSCC	Inter granular stress corrosion cracking

IOW	Integrity operating window
ISR	Insulation support ring
IW	Isothermal wet
LPR	Linear polarization resistance
LTCS	Low temperature carbon steel
MIC	Microbial influenced corrosion
MLCR	Mass loss corrosion rate
N/A	Not applicable
NACE	The National Association of Corrosion Engineers
NDE	Non-destructive examination
NDT	Non-destructive testing
NPS	Nominal pipe size
NRC IRAP	National Research Council Canada Industrial Research Assistance Program
OCP	Open circuit potential
PCM	Phase change materials
PECT	Pulsed eddy current testing
ppb / ppm	parts per billion / parts per million
PVDF	Polyvinylidene fluoride
RBI	Risk based inspection
R_{ct}	Charge transfer resistance
RE	Reference electrode
R_p	Polarization resistance
SAGD	Steam assisted gravity drainage
SCC	Stress corrosion cracking
SCE	Saturated Calomel Electrode
SEM	Scanning Electron Microscopy
SSRT	Slow strain rate tests
TOW	Time of wetness
TOW	Total oxygen weight
TSA	Thermally sprayed aluminum

UT	Ultrasonic testing
UV	Ultraviolet
WCO	World Corrosion Organization
WE	Working electrode
XRD	X-ray diffraction

GLOSSARY

Corrosion Current Density	Current per unit area indicating corrosion rate
Corrosion Fatigue	Cyclic stress and corrosion damage
Corrosion Inhibitor	Gross domestic product
Counter Electrode	Provides current in electrochemical corrosion cells
Cyclic Wet	Repeated wet and dry corrosion cycles
Electrochemical Noise	Fluctuations in current/potential during corrosion
Flashing Moisture	Non-destructive examination
Holiday	Corrosion under insulation
Insulation Leachate	The National Association of Corrosion Engineers
Isothermal Wet	Constant temperature wet corrosion condition
Linear Polarization Resistance	Measures corrosion rate by resistance to polarization
Open Circuit Potential	Voltage of an electrode in a solution
Passivation	National Research Council Canada Industrial Research Assistance Program
Phase Angle	Angle difference between reflected X-rays for material analysis
Polarization Resistance	Resistance to electrochemical reaction rates
Pores	Thermally sprayed aluminum
Reference Electrode	Provides stable reference potential in measurements
Sacrificial Anode	World Corrosion Organization
Scale	Artificial intelligence
Slow Strain Rate Testing	Tests susceptibility to stress corrosion cracking
Stress Corrosion Cracking	Crack growth due to stress and corrosion
Voids	Risk based inspection
Working Electrode	Electrode where corrosion reaction occurs

ACKNOWLEDGEMENTS

I extend my sincere gratitude to my supervisor, Dr. George Jarjoura, for his invaluable guidance and unwavering support throughout this dissertation. Their expertise and mentorship have been instrumental in shaping the quality and direction of this research.

Additionally, I would like to dedicate a special acknowledgment to Ahmad Raza (Integrity Products Inc.) for their generous support and guidance during the experimental phases of this study. Their commitment to advancing research and their contributions to practical applications have significantly enhanced the depth and relevance of this work. This research work received financial support from National Research Council Canada Industrial Research Assistance Program (NRC IRAP-Mitacs).

Lastly, I am deeply thankful to my wife Yusra Hafeez, my family, friends, and colleagues for their encouragement, understanding, and support. Their belief in my abilities and encouragement during challenging times have been invaluable and have motivated me to strive for excellence in this endeavor.

Shahzad Karim

August 2024

CHAPTER 1. INTRODUCTION

Corrosion can be defined as the surface degradation that occurs when metals are exposed to reactive environments, resulting in their gradual destruction. It is also characterized as an aspect of material decay caused by chemical or biological agents, representing an extractive metallurgy process in reverse, where metals revert to their original state due to environmental interaction. Another definition describes corrosion as the deterioration of materials due to reactions with their surroundings, while also highlighting it as a destructive attack on metals through chemical or electrochemical reactions with the environment [1].

Faraday (1791–1867) made significant contributions that marked a crucial turning point in understanding the relationship between chemical action and electric current, establishing a quantitative framework. His pioneering work, encapsulated in Faraday's first and second laws, laid the foundation for calculating corrosion rates in metals. The early nineteenth century witnessed the inception of ideas on corrosion control, with Whitney (1903) advancing this field by offering a scientific grounding through electrochemical observations. Evans, Uhlig, and Fontana are credited with making significant strides towards our contemporary comprehension of corrosion [1].

1.1 ELECTROCHEMISTRY OF CORROSION

Corrosion is an electrochemical process driven by a metal's tendency to revert to a more stable, oxidized state. This complex phenomenon involves intricate interactions between the metal, its environment, and the electrolyte. Understanding the electrochemistry of corrosion requires examining the anodic and cathodic reactions, the role of the electrolyte, and the environmental factors influencing these processes. In an electrochemical cell, corrosion involves two primary reactions occurring at the anode and cathode. At the anode, the metal undergoes oxidation, losing electrons. For iron, the anodic reaction can be represented as:

$$Fe_{(s)} \rightarrow Fe^{+}_{2\,(aq)} + 2e^{-}$$ Equation 1– 1

The released electrons travel through the metallic pathway to the cathode, where they participate in a reduction reaction to maintain electrical neutrality. In an aerated aqueous environment, the most common cathodic reaction is the reduction of dissolved oxygen:

$$O_{2\,(g)} + 4H^{+}_{(aq)} + 4e^{-} \rightarrow 2H_2O_{(l)}$$ Equation 1– 2

The overall corrosion process can be summarized by combining the anodic and cathodic half-reactions. For iron in an acidic environment, the complete reaction is:

$$2Fe_{(s)} + O_{2\,(g)} + 4H^{+}_{(aq)} \rightarrow 2Fe^{+}_{2\,(aq)} + 2H_2O_{(l)}$$ Equation 1– 3

In neutral or alkaline environments, the reduction of oxygen can proceed differently:

$$O_{2\,(g)} + 2H_2O_{(l)} + 4e^{-} \rightarrow 4OH^{-}_{(aq)}$$ Equation 1– 4

Here, the iron reacts with hydroxide ions to form iron hydroxide, which further oxidizes to form rust (hydrated ferric oxide). The electrolyte, a conductive medium containing ions, facilitates the movement of electrons and ions, completing the electrochemical circuit. Electrolytes can be acidic, neutral, or alkaline, significantly affecting the corrosion rate and type of corrosion products formed. For instance, chloride ions, prevalent in marine environments, are particularly aggressive, promoting localized corrosion such as pitting by disrupting the protective oxide layer on the metal surface.

Several environmental factors influence the electrochemical corrosion process. The acidity or alkalinity of the environment (pH level) can significantly impact the corrosion rate. Lower pH levels (acidic conditions) generally increase the corrosion rate of iron and steel by providing more hydrogen ions for the cathodic reaction. The availability of oxygen is crucial for the cathodic reaction, and areas with higher oxygen concentration tend to corrode faster due to the enhanced reduction of oxygen. Higher temperatures typically increase the rate of corrosion by accelerating electrochemical reactions. Chloride ions are

particularly harmful as they can penetrate and break down protective oxide layers, leading to pitting corrosion.

The nature of corrosion products can provide valuable insights into the kinetics and chemistry of the corrosion process. For example, in an aerated environment, iron corrosion often results in the formation of iron oxides and hydroxides, such as magnetite (Fe_3O_4) and goethite (α-FeOOH). The formation of these products depends on the local electrochemical conditions, including pH, oxygen concentration, and the presence of other ions. For instance, the presence of chlorides can lead to the formation of more soluble iron chloride complexes, which can exacerbate corrosion.

In corrosion processes involving iron, the flow of electrons between the anode and cathode constitutes the corrosion current, with the rate of corrosion directly proportional to its magnitude. The presence of an electrolyte, such as saltwater or a moist environment, facilitates this electron transfer, enabling the anodic and cathodic reactions to proceed. Therefore, understanding the electrochemical interactions and the environmental conditions that influence them is crucial for developing effective corrosion mitigation strategies. This knowledge helps in designing better protective measures, such as coatings, inhibitors, and cathodic protection systems, to prolong the lifespan of metallic structures and components.

1.2 COST OF CORROSION

The global annual cost of corrosion exceeds US $2.2 trillion, representing over 3% of the world's GDP. Despite this substantial economic impact, corrosion tends to receive limited attention from governments and industries, except in critical sectors like aircraft and pipelines. It is crucial for corrosion professionals to collaborate now, raising awareness among industries, governments, and the public about the significance of corrosion control. This collaboration presents an ideal opportunity to standardize practices worldwide, share corrosion mitigation technologies, and make a meaningful impact in safeguarding the environment, conserving resources, and ensuring human safety [2].

Recent surveys reveal that the direct global cost of corrosion ranges between approximately 2 to 3 trillion dollars annually, encompassing expenses related to repairing, maintaining, and replacing materials, equipment, and services affected by corrosion. However, this cost does not account for the environmental damage, resource wastage, production losses, or personal injuries resulting from corrosion. Corrosion experts estimate that applying existing corrosion control technologies could save around 20 to 25% of this annual cost, potentially leading to significant savings for the world's economies. Leaders from various corrosion-focused organizations joined forces to create a cooperative plan, culminating in the establishment of the World Corrosion Organization (WCO). Comprising key entities such as the Australasian Corrosion Association, the Chinese Society for Corrosion and Protection, the European Federation of Corrosion, and NACE International, the WCO aims to promote education and best practices in corrosion control, delivering economic and environmental benefits through resource conservation and environmental stewardship [3].

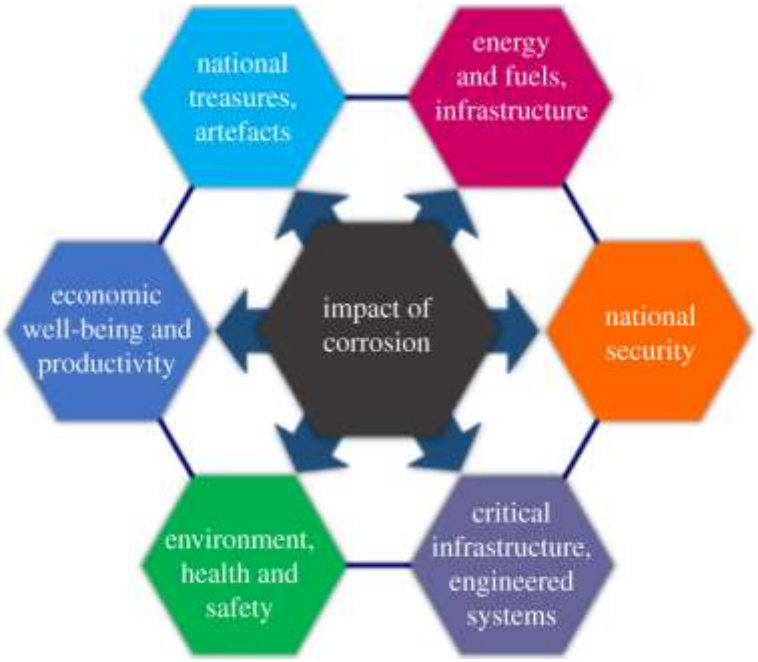

Figure 1-1. Impacts of corrosion [4].

1.3 RESEARCH OBJECTIVES

With previous findings in the literature considered and some case studies from field samples, the objectives are as follows:

1. Investigating the mechanisms, kinetics, and driving factors of Corrosion Under Insulation (CUI) through forensic analysis of rust scale samples.
2. Comparing laboratory-aged and field-aged insulation samples to understand corrosion modes and the implications of CUI.
3. Examining premature coating failure on boiler tubes and discussing the associated corrosion modes.
4. Analyzing the corrosion behavior of Thermally Sprayed Aluminum (TSA) at elevated temperatures under CUI and immersion conditions.

1.4 THESIS STRUCTURE

This thesis comprises seven chapters, beginning with an introduction to corrosion in Chapter 1. Chapter 2 provides a literature review on Corrosion Under Insulation (CUI), with a specific focus on Thermally Sprayed Aluminum (TSA) coating. Chapter 3 presents a study on CUI investigation through the analysis of corrosion products. Chapter 4 compares laboratory-aged and field-aged insulation samples, exploring the implications of CUI. Chapter 5 examines premature coating failure on boiler tubes, while Chapter 6 discusses the corrosion behavior of TSA at elevated temperatures under CUI and immersion conditions. Finally, Chapter 7 presents the overall conclusions and future works.

CHAPTER 2. LITERATURE REVIEW

2.1 CORROSION UNDER INSULATION (CUI)

The ongoing battle against corrosion under insulation (CUI) in the petrochemical industry took a significant turn with the publication of ASTM STP 880, "Corrosion of Metals Under Thermal Insulation" in 1985, which heralded the modern approach to CUI management. This pivotal publication analyzed CUI's causes and influencing factors, field experiences with different insulation types, and control measures such as coatings, specifications, system design, and inspection methods. A critical gap identified was the urgent need for a nondestructive on-stream examination (NDE) method to detect CUI without removing insulation. In 1989, the first NACE report on CUI was released as NACE Publication 6H189, titled "A State-of-the-Art Report on Protective Coatings for Carbon Steel and Stainless-Steel Surfaces Under Thermal Insulation and Cementitious Fireproofing." This report comprehensively reviewed the history and effectiveness of protective coatings under insulation and fireproofing. It also discussed the application of thermal spray aluminum to prevent CUI on insulated carbon steel surfaces. It highlighted the longstanding European use of aluminum foil to avoid external stress corrosion cracking (SCC) on austenitic stainless-steel surfaces [5].

Insulation materials such as glass wool, glass fibers, and polyurethane foam do not induce steel corrosion when kept dry. However, corrosion beneath the insulation becomes notable once exposed to moisture during storage or operation. Factors exacerbating this issue include moisture ingress, resulting in the leaching of low-pH soluble salts, chloride ion release, loss of steel passivity, and weather-induced corrosion acceleration. Additionally, insufficient moisture barriers due to inadequate insulation spacing contribute to the problem. To mitigate insulation-induced corrosion, strategies include avoiding flat surfaces, employing water-draining structural designs, ensuring appropriate insulation thickness, installing effective moisture barriers, and incorporating inhibitors like sodium silicate.

Thermal insulations are widely used in industrial, energy, and hydrocarbon processing facilities for heat conservation in pipes, pipelines, and equipment. Corrosion under insulation (CUI) is a common damage mechanism on thermally insulated systems that mainly manifests localized corrosion and pitting. Reportedly, 10% of the maintenance expenditures in a typical oil refinery result from CUI, whereas 40-60% of the piping failures (alone) are from CUI. The damage progression from CUI may go unnoticed during routine visual inspections unless it's inspected via stripping off the insulations or using specialized non-destructive examinations (NDE). Moreover, the CUI prediction is quite challenging as the CUI rate(s) are primarily non-linear and influenced by unique factors such as time of wetness (TOW), differential oxygen starvation, temperature swing, insulation aging, and coatings degradation, to name a few. Many of these factors remain un-quantified or even unnoticed in real-life inspection programs as the protocols for quantification of these factors are not even established [6].

The duration during which a metal surface remains wet before initiating corrosion is termed the time of wetness. A critical thickness of the water layer is necessary to generate an emf that surpasses a threshold, triggering corrosion. Factors influencing the time of wetness include temperature, porosity voids affecting water adsorption, degree of oxidation, grain boundaries, and surface roughness. Typically, a relative humidity exceeding 80% and a temperature above 32°C are considered critical conditions for wetness, with values ranging from 100 to 2700 hours per year in temperate zones and much higher values in tropical-humid regions. The hydrophobic and hydrophilic nature of the surface influences the quantity of water adsorbed [1].

Corrosion Under Insulation (CUI) remains a persistent threat in industries where equipment is insulated to maintain operational temperatures. The ingress of water, coupled with oxygen and salts, creates a corrosive environment within insulation systems, leading to metal degradation over time. For instance, a recent study by Smith et al. (2023) found that CUI accounted for 60% of all piping failures in offshore oil rigs due to inadequate insulation maintenance. The complexity of CUI arises from its heterogeneous nature; localized conditions under insulation vary widely, affecting corrosion rates and patterns.

Understanding these factors is crucial for implementing effective mitigation strategies. For example, using advanced non-destructive testing techniques, such as ultrasonic thickness measurements and infrared thermography, allows for early detection of moisture ingress points and insulation breaches, mitigating potential corrosion risks before they escalate [5].

Corrosion Under Insulation (CUI) occurs when moisture becomes trapped under insulation, leading to accelerated corrosion rates due to the prolonged exposure of metal surfaces to water and corrosive elements. This form of corrosion is insidious because it can go undetected until significant damage has occurred, often requiring complete insulation removal for inspection. Typical signs of CUI include rust staining on insulation, bulging or deformation of insulation material, and elevated iron levels in water samples taken from the insulation system. The risk of CUI is influenced by operating temperature, insulation type, and environmental conditions, making it a complex issue to manage [7].

The primary objective of the study by Hayrullin et al. was to evaluate the influence of moisture content and wet-drying cycles on the thermal conductivity and density of rock wool insulation materials commonly used in various industries such as petrochemical and power engineering. Experimental analysis was conducted on samples from three manufacturers, utilizing the guarded hot plate method to measure thermal conductivity. The results revealed that the thermal conductivity of the insulating materials increased significantly with higher moisture content, ranging from 1.33 to 4.42 times, depending on the sample's density and origin. Additionally, the wet-drying cycles enhanced thermal conductivity and density by up to 2 and 2.5 times, respectively. These findings underscore the importance of managing moisture levels in insulation materials to optimize their performance and durability in practical applications. The study provides valuable insights for improving energy efficiency in district heating systems and other relevant sectors [8].
Caines et al. tried to explore Corrosion Under Insulation (CUI) in harsh marine environments and discussed various aspects of corrosion affecting insulated materials, especially in offshore and coastal applications. Mechanisms of uniform corrosion, pitting corrosion, stress corrosion cracking (SCC), and microbial-influenced corrosion (MIC) were discussed in the study. The study emphasizes the importance of understanding these

corrosion mechanisms to develop accurate predictive models and effective mitigation strategies. The methodology includes laboratory simulations based on ASTM standards to replicate field conditions and assess the impact of factors such as temperature, chlorine content, and time of wetness on low-temperature carbon steel (LTCS). The findings aim to improve risk-based asset integrity evaluations and enhance the reliability of protective coatings in preventing CUI. The paper also highlights the need for accelerated testing methods to determine corrosion rates under varying environmental conditions, enabling better design and maintenance of insulation systems [9].

Xu et al. conducted a study that meticulously investigated the thermal insulation performance of composite energy storage pipelines incorporating phase change materials (PCM), which is crucial for enhancing oil and gas transportation efficiency. The research aims to determine the optimal structural parameters for these pipelines by comparing the effective insulation times under identical working conditions and utilizing the thermal resistance method. A sophisticated pipe-PCM-oil coupling thermodynamic model was developed, accounting for crude oil's nonlinear latent heat release and phase change properties. The study's outcomes reveal that composite pipelines with PCM provide superior thermal insulation and significantly extend the safe shutdown period, thereby ensuring stable and energy-efficient transportation of crude oil. Numerical solutions and heat transfer characteristics were analyzed under various conditions, with findings indicating that different PCM physical properties and structures substantially influence thermal performance. The research offers invaluable theoretical support for developing safe shutdown schemes and optimizing thermal insulation design in oil pipelines [10].

2.2 ATMOSPHERIC CORROSION

Morcillo et al. meticulously investigated the mechanisms and contributing factors of atmospheric corrosion of mild steel, highlighting the dual-layer structure of corrosion products formed over prolonged exposure. The primary objective is to elucidate the influence of environmental parameters, such as time of wetness (TOW), salinity, and sulfur dioxide (SO_2) concentrations, on mild steel's corrosion rates and characteristics. The research employs advanced analytical techniques, including X-ray microdiffraction

(μXRD), Mössbauer spectroscopy, and Raman spectroscopy, to characterize the morphology and composition of corrosion layers. The findings indicate that the exponent B in the corrosion rate equation ($C = At^{\wedge B}$) varies significantly with atmospheric conditions, showing higher values in marine atmospheres (0.6-0.9) compared to rural and urban atmospheres (0.3-0.7), thus underscoring the substantial impact of chloride presence. This research advances the understanding of atmospheric corrosion, providing valuable insights for predicting long-term corrosion behavior and enhancing protective measures for steel infrastructure in varying environmental conditions [11].

Antunes et al. focused on characterizing the corrosion products formed on carbon and weathering steels during the initial months of atmospheric exposure. They evaluated the influence of different atmospheric conditions on these corrosion products. The steels were exposed to industrial, urban, and humid environments, and their corrosion products were analyzed using Raman microscopy, X-ray diffraction, and Scanning Electron Microscopy (SEM). Key outcomes include the identification of predominant corrosion phases such as lepidocrocite (γ-FeOOH), goethite (α-FeOOH), and magnetite (Fe_3O_4). Notably, akageneite (β-FeOOH) was observed in weathering steel samples exposed to industrial atmospheres with high chloride concentrations. Raman microscopy revealed distinct spectral patterns correlating with different oxide colors, providing insights into the spatial distribution of corrosion phases. The study underscores the significant impact of atmospheric conditions on the corrosion behavior of steels and highlights the importance of advanced analytical techniques in characterizing corrosion products. For instance, lepidocrocite dominated in the early stages across all sites, while goethite and magnetite's presence increased with exposure time. This comprehensive analysis provides a deeper understanding of corrosion mechanisms and informs the development of improved corrosion-resistant materials [12].

2.3 PREVENTION OF CORROSION UNDER INSULATION

Effective Corrosion Under Insulation (CUI) prevention involves a holistic approach encompassing insulation design improvements, material selection, and protective coatings. For instance, in the chemical processing industry, implementing vapor barriers within

insulation systems has shown a significant reduction in moisture ingress, as demonstrated in the work of [13]. Applying hydrophobic coatings and wraps, like polyethylene or polyvinylidene fluoride (PVDF), helps repel water and maintain insulation integrity. These materials not only enhance the durability of the insulation but also minimize the contact between metal surfaces and corrosive agents, thereby extending equipment lifespan. Furthermore, proactive maintenance practices, including regular inspections and moisture monitoring, are essential for identifying early signs of CUI development and ensuring timely corrective actions to preserve asset reliability [5].

Preventing CUI involves a combination of protective coatings, insulation materials, and non-destructive testing methods. Protective coatings, such as 2-component phenolic epoxies and novolac epoxies, are commonly used due to their durability and resistance to high temperatures. These coatings form a barrier between the metal surface and any infiltrating water. Insulation materials are also critical; non-metallic jacketing materials, like thermoplastic and fibre-reinforced plastics, provide watertight seals more resistant to mechanical damage. Non-destructive testing (NDT) techniques detect CUI without removing insulation, such as infrared thermography and guided wave ultrasonic technology. These methods allow for early detection and targeted maintenance, reducing the risk of extensive damage and costly repairs [7].

The study presented by Rana et al. investigates the efficacy of various moisture management techniques to mitigate thermal losses and corrosion under insulation (CUI) in pipelines. Key findings indicate that adequate moisture barriers, such as perforated dimple wraps and ventilation windows, significantly reduce moisture levels within insulated systems. For instance, systems with these barriers exhibited lower moisture content than conventional setups, which lacked such protective measures. Perforated stand-offs were particularly effective in promoting air circulation and reducing drying time, thereby minimizing the risk of moisture-related damage. Additionally, compartmentalizing assets through modular approaches enhanced the focus and effectiveness of assessment and maintenance efforts by confining moisture near the intrusion point. Ultimately, these

findings underscore the importance of moisture management in maintaining the integrity and longevity of insulated pipelines [14].

The study's primary objective by Saito et al. was to develop an empirical model for predicting corrosion under insulation (CUI) in industrial piping systems by evaluating environmental and material factors influencing CUI rates. The research meticulously examined the effects of temperature, humidity, and insulation type on CUI progression using data from field observations and controlled experiments. A significant outcome was the identification of critical temperature zones where CUI was most prevalent, particularly between 50°C and 150°C. Statistical analyses demonstrated that chloride ions significantly accelerated corrosion rates, underscoring the necessity for stringent monitoring in coastal and industrial environments. The model's predictive accuracy, validated against historical CUI incidents with a correlation coefficient of 0.87, provides a robust tool for proactive maintenance and risk mitigation. The study highlighted that optimized epoxy coatings with specific chemical compositions significantly reduce CUI progression compared to traditional coatings, offering a cost-effective solution for long-term infrastructure maintenance. This comprehensive approach integrates empirical data with predictive modelling, enhancing the durability and safety of insulated piping systems in corrosive environments [15].

2.3.1 DESIGN PREVENTION

Many studies have emphasized the crucial role of design in mitigating CUI risks in industrial settings. One of the primary strategies is to challenge the necessity of insulation itself. Insulation is often added for various reasons, such as heat conservation, fire protection, and noise reduction. However, in many cases, the level of necessity is not critically assessed, leading to unnecessary insulation that increases CUI risk. Winnik et al. recommend using metal guards instead of insulation for personal protection. Another significant design consideration is plant layout, where adequate spacing between equipment and piping should be maintained to facilitate effective inspection and maintenance. This prevents the creation of inaccessible areas prone to CUI due to poor insulation system application [16].

Mechanical design elements also play a vital role in preventing CUI. Avoiding shapes that retain water, such as flat horizontal surfaces and insulation support rings, is crucial. Instead, designs should incorporate sloped weatherproofing at vulnerable points like column vacuum rings to prevent water accumulation. Winnik et al. also highlighted the importance of high-quality weatherproofing materials, such as aluminized steel or UV-curable glass-reinforced plastics, which provide robust protection against weather and mechanical damage. Weatherproofing joints should minimize the use of sealants and instead use overlapped joints with swaged edges to reduce water ingress points. Overall, implementing these design strategies during the early stages of a project and maintaining them throughout the plant's lifecycle can significantly reduce the occurrence of CUI, ensuring safer and more reliable operations [16].

2.3.2 COATING SYSTEMS

Industrial environments present a relentless assault on metallic structures, demanding robust solutions for corrosion mitigation. These meticulously engineered barriers isolate the metal surface from its aggressive surroundings. The specific coating chosen depends on the environment and the threat posed. For instance, epoxy coatings offer exceptional chemical resistance, making them ideal for environments saturated with harsh chemicals. Polyurethanes, with their superior abrasion resistance, are well-suited for pipelines and machinery constantly exposed to wear and tear. When aesthetics are a concern, powder coatings provide a durable and visually pleasing option. Beyond these basic categories lie a multitude of specialized coatings, boasting properties like flame retardancy or electrical conductivity to cater to specific industrial demands. The application of these coating systems often involves a multi-layered approach, with primers promoting adhesion and topcoats offering the final line of defense. A meticulous selection and application process ensures the chosen coating system effectively extends the lifespan of metallic assets, minimizing costly repairs, replacements, and disruptions.

Coatings are pivotal in mitigating CUI by preventing moisture from contacting metal surfaces. Common coatings include epoxy phenolics and novolacs, which provide excellent protection up to certain temperatures. For instance, epoxy phenolics can

withstand temperatures up to 205°C (401°F) but may degrade at higher temperatures. Recent advancements have led to the development of high-temperature coatings capable of withstanding up to 600°C (1112°F), such as titanium-modified inorganic copolymers and inert multipolymeric matrices. These coatings are often applied in multiple layers to ensure complete coverage and durability. Additionally, insulating coatings, such as spray-applied non-clad thermal isolative coatings, offer a monolithic barrier against water, chemicals, and UV rays while providing thermal insulation and personnel protection. These innovations in coating technology are essential for enhancing the longevity and reliability of insulated systems in harsh industrial environments [7].

One efficient approach for offshore environments is the application of thermally sprayed aluminum (TSA) coatings. These coatings offer a unique combination of properties. Aluminum serves as a sacrificial anode, preferentially corroding to protect the underlying steel substrate. Additionally, the inherent passivity of aluminum oxide formed on the coating surface enhances its barrier properties. TSA coatings boast excellent mechanical properties, withstanding the harsh conditions encountered offshore, including high winds, waves, and impact from debris. Furthermore, the application process allows for customization of the coating thickness, enabling engineers to tailor the level of protection to specific needs. The success of TSA coatings in offshore applications is exemplified by their widespread adoption in the oil and gas industry, where they effectively protect critical infrastructure like platforms and pipelines from the corrosive effects of seawater.

Cui et al. have done a study to elucidate the impact of water adhesion on the anti-corrosive behavior of superhydrophobic coatings applied to aluminum substrates. By varying the concentration of hydrophobic SiO_2 nanoparticles, the researchers could fabricate superhydrophobic surfaces with distinct levels of water adhesion. Electrochemical tests, including polarization curves and electrochemical impedance spectroscopy (EIS), were conducted to assess the corrosion resistance of these surfaces when exposed to a 3.5 wt% NaCl solution. The findings revealed a clear correlation between water adhesion and corrosion resistance: low-adhesion surfaces exhibited superior anti-corrosive properties, marked by a significant reduction in corrosion rate (CR) and an increase in polarization

resistance (Rp). Specifically, coatings with 100% OTS-SiO_2 demonstrated the lowest corrosion current and highest impedance modulus (R_{ct}), indicating exceptional protection against corrosion. These results underscore the critical role of water adhesion in designing superhydrophobic coatings for effective corrosion prevention, providing valuable insights for developing advanced anti-corrosive materials [17].

The investigation delineated by Cao et al. meticulously explores the degradation behavior of epoxy-based coatings under varying thermal exposures, specifically targeting temperatures up to 150°C. The study's primary objectives were to assess polyamine-cured epoxy coatings' chemical and mechanical stability on carbon and stainless-steel substrates insulated with mineral wool and elucidate the degradation's implications on the overall barrier properties. Key outcomes indicated that while prolonged thermal exposure did not significantly impact the pull-off adhesion strength, it did lead to notable increases in cohesive coating failures and chemical degradation, characterized by the irreversible formation of carbonyl functional groups and an increase in the glass transition temperature from 77.6°C to 116.5°C. Electrochemical impedance spectroscopy (EIS) revealed a decline in low-frequency total impedance under high-temperature conditions, although the coating capacitance remained unaffected. These findings are substantiated by quantitative data, such as the coating impedance fluctuating from 10^9 to 10^{11} $\Omega \cdot cm^2$. The study underscores the necessity for enhanced protective measures and advanced material formulations to mitigate the adverse effects of high-temperature environments on epoxy coatings in industrial applications [18].

Table 2-1. Typical protective coating systems for carbon steels under thermal insulation [7]

System	Temperature range	Generic first coat	Generic second coat
CS-1	-45 to 60°C (-50 to 140°F)	High build epoxy	N/A
CS-2 (shop application only)	-45 to 60°C (-50 to 140°F)	N/A	Fusion-bonded epoxy
CS-3	-45 to 150°C (-50 to 302°F)	Epoxy phenolic	Epoxy phenolic
CS-4	-45 to 205°C (-50 to 401°F)	Epoxy novolac or silicone hybrid	Epoxy novolac or silicone hybrid
CS-5	-45 to 595°C (-50 to 1100°F)	Thermal spray Al	Optional sealer
CS-6	-45 to 650°C (-50 to 1200°F)	Inert multipolymeric matrix coating or inorganic copolymer	Inert multipolymeric matrix coating or inorganic copolymer
CS-7	60°C (140°F) maximum	Thin film petrolatum or petroleum wax primer	Petrolatum or petroleum wax tape
CS-8 inorganic zinc shop-primed pipe	-45 to 400°C (-50 to 750°F)	N/A	Typically coatings from system CS-3/4/6
CS-9 under fireproofing	Ambient	Epoxy or epoxy phenolic	Epoxy or epoxy phenolic
CS-10 galvanized steel under fireproofing	Ambient	Epoxy or epoxy phenolic	Epoxy or epoxy phenolic

2.3.3 THERMALLY SPRAYED ALUMINUM COATING (TSA)

Protective coatings are a well-established method for corrosion protection in both above-ground and below-ground structures. Additional strategies include cathodic protection, modifying the environment, selecting appropriate materials, and designing structures effectively. Unlike rust formation on steel, oxide formation provides a protective layer against corrosion by increasing electrolyte resistivity and slowing electron flux, thereby reducing corrosion rates. Coatings like epoxies, vinyl, and chlorinated rubbers with high resistivity hinder electric current flow to the metal surface, and thicker coatings offer greater electrical resistance, making them effective in preventing corrosion through increased metal electrical resistance.

Thermally sprayed aluminum (TSA) is a widely utilized metallic coating to combat Corrosion Under Insulation (CUI). TSA boasts a maximum operating temperature of 595°C (1103°F) and is applied without surface temperature restrictions using arc or flame

methods. Proper surface preparation, such as SSPC-SP10 near-white blast cleaning, is essential for optimizing TSA's corrosion-resistant qualities. The correct application and preparation play a pivotal role in TSA's longevity, with instances of up to 20 years without requiring maintenance. While TSA doesn't act as a sacrificial anode in rural settings, it exhibits this protective capability in marine environments rich in chlorides. The presence of Al_2O_3 on the TSA surface forms a protective barrier, decreasing the corrosion rate. However, due to its porosity ranging from 5% to 15%, sealer paints are commonly used as a final coat to enhance protection. This is necessary as the porous nature of TSA provides an ideal substrate for the adhesion and efficacy of paint coatings [7], [19].

TSA involves the high-velocity deposition of aluminum or aluminum alloy particles onto metal substrates, forming a dense, impermeable barrier against moisture and aggressive chemicals. This technique has been extensively utilized in the marine industry, where offshore platforms face constant exposure to saltwater environments. Research by Johnson et al. (2021) highlights TSA's effectiveness in protecting critical components from CUI-related failures by maintaining coating integrity under varying temperature and humidity conditions. Surface preparation is crucial in TSA application; abrasive blasting to achieve surface cleanliness and roughness ensures optimal adhesion and longevity of the TSA coating. Moreover, advancements in TSA formulations, such as alloy modifications and nanostructured coatings, continue to enhance its performance in challenging industrial settings, reinforcing its role as a cornerstone in comprehensive CUI prevention strategies [5].

The study by Ortega et al. aimed to evaluate the effectiveness of three protective coating names: Thermally Sprayed Carbide with an organic sealant (C1), Thermally Sprayed Aluminum with an organic sealant (C2), and an epoxy-based organic coating reinforced with ceramic particles (C3) in combating corrosion and tribo-corrosion in offshore environments. Using techniques like Electrochemical Impedance Spectroscopy (EIS) and Potentiodynamic Polarization, the study found that all coatings significantly enhanced the steel substrate's resistance to corrosion and wear. Notably, the Thermally Sprayed Aluminum coating (C2) demonstrated the best performance, exhibiting the lowest friction coefficient and the highest resistance to sliding-induced corrosion. The conclusion

underscores the importance of these advanced coatings in extending the lifespan and reducing the maintenance costs of offshore structures, highlighting the superior suitability of the C2 coating for harsh marine conditions [20].

Thermal Spray Aluminum (TSA) coatings have demonstrated exceptional effectiveness in protecting riser pipes in high-temperature seawater environments, offering significant implications for the oil and gas industry. The performance evaluation of TSA-coated carbon steel, exposed to synthetic seawater at boiling temperatures for up to 5,000 hours, revealed the formation of stable brucite [$Mg(OH)_2$] layers in defective areas, which substantially mitigated corrosion. This resulted in a remarkably low corrosion rate of approximately 0.008-0.015 mm/year and a stable potential of around -800 mV (SCE). The ability of TSA to facilitate the formation of calcareous deposits further enhances its protective capabilities, providing an additional barrier against seawater. Advanced techniques such as X-ray diffraction (XRD) and scanning electron microscopy (SEM) confirmed that these deposits were primarily composed of brucite, a novel finding at elevated temperatures. These results underscore TSA's potential to extend the service life of riser pipes and reduce maintenance costs, even when coatings are compromised, highlighting its valuable role in mitigating corrosion in harsh marine environments [21].

The investigation into the electrochemical behavior of thermally sprayed aluminum (TSA) coatings subjected to damage and their implications for corrosion under insulation (CUI) unveils several critical insights. Firstly, this study underscores the pervasive issue of CUI in industrial settings, where insulated systems experience accelerated corrosion due to moisture ingress, leading to substantial maintenance costs and safety hazards. Various CUI prevention techniques were evaluated, revealing that effective strategies often involve the use of protective coatings, enhanced insulation materials, and rigorous maintenance protocols. Among these, TSA coatings emerged as a superior choice due to their robust barrier properties and sacrificial anodic behavior, which significantly mitigate corrosion even when the coating is mechanically compromised. Through detailed electrochemical testing, it was demonstrated that TSA maintains its protective efficacy by forming a stable passive oxide layer, which acts as a secondary defense against corrosion. Additionally, this

study highlighted the practical application of TSA in diverse industrial scenarios, reinforcing its role as a cost-effective and durable solution for long-term CUI management. Overall, the findings advocate for the broader adoption of TSA coatings in industrial maintenance programs, emphasizing their capacity to enhance asset longevity and operational safety [22].

The comprehensive analysis of thermal spray aluminum (TSA) coatings underscores their pivotal role in combating corrosion under insulation (CUI), particularly in challenging environments characterized by high humidity and temperature fluctuations. TSA coatings, renowned for their robust barrier properties, effectively mitigate electrochemical corrosion by forming a protective oxide layer on the metal substrate. This layer significantly reduces the ingress of corrosive agents such as water, oxygen, and chloride ions. The efficacy of TSA in preventing localized corrosion is further enhanced by its ability to maintain structural integrity even when mechanically damaged, as evidenced by electrochemical impedance spectroscopy (EIS) studies. These studies demonstrate that TSA coatings exhibit superior impedance values, indicative of low corrosion rates, despite the presence of defects. The longevity and performance of TSA are also attributed to its sacrificial anodic behavior, wherein the aluminum coating preferentially corrodes, thereby protecting the underlying steel substrate. This self-healing capability, coupled with a low maintenance requirement, positions TSA as a cost-effective solution for extending the service life of insulated piping systems and equipment in the oil and gas industry. Notably, field studies corroborate the laboratory findings, showcasing minimal corrosion rates and extended inspection intervals for TSA-coated assets, thereby affirming its practical applicability and reliability in real-world scenarios [23].

Lee et al. have investigated the electrochemical behavior of thermal spray aluminum (TSA) coatings, and significant insights were gained into the mechanisms of corrosion protection, the influence of environmental conditions, and the effectiveness of TSA in various scenarios. Their research highlights the critical role of TSA in polarizing steel to protective potentials, with rapid achievement of potentials below -800 mV for steel samples coated with TSA. Notably, this study delineates the divergent behaviors of samples in aerated and

deaerated synthetic seawater, where the deaerated sample maintained a potential close to -1050 mV. In comparison, the aerated sample gradually shifted from -800 mV to below -900 mV, eventually stabilizing at higher anodic values. This disparity is attributed to the dissolution of air-formed oxide films on TSA and the subsequent formation of water-based corrosion products that influence the electrochemical properties. Furthermore, the findings underscore the significance of the relative cathode-to-anode area ratio, as the exposed steel area directs TSA's polarization and dissolution rate. The research also discusses the formation of protective passive films and the impact of corrosion product deposition on the TSA surface, which act as barriers to aggressive ions, thereby enhancing the longevity and efficacy of the coating. Advanced analytical techniques, such as Field Emission Scanning Electron Microscopy (FE-SEM) and Electrochemical Impedance Spectroscopy (EIS), were employed to characterize the morphology, kinetics, and mechanisms underlying the corrosion processes, providing a comprehensive understanding of TSA's protective capabilities. These technical details and examples illustrate the intricate interplay between coating properties, environmental factors, and electrochemical dynamics, offering valuable insights for optimizing TSA applications in corrosive environments [24].

The investigation focused on determining the corrosion rate of thermally sprayed aluminum (TSA) coatings, both sealed and unsealed, in simulated marine environments was done by Paul et al. The primary objective was to evaluate these coatings' long-term performance and stability under alternate immersion conditions in synthetic seawater. The research demonstrated that Al_5Mg coatings, sealed and unsealed, exhibited an impressively low stable corrosion rate of less than 0.002 mm/year over 400 days. In contrast, unsealed aluminum and AlZnIn coatings showed higher corrosion rates and potential for coating failure, mainly when the sealant degraded. Electrochemical measurements, such as linear polarization resistance (LPR), revealed that sealed coatings maintained more negative potentials, enhancing their corrosion resistance. This study underscores the critical importance of sealants in prolonging the efficacy of TSA coatings and highlights the need for further research to optimize coating formulations for marine applications [25].

2.4 STRESS CORROSION CRACKING

Stress corrosion cracking (SCC) poses a significant threat to the integrity of metallic components in a wide range of industrial applications. This insidious form of failure arises from the synergistic interaction of three key factors: sustained tensile stress, a specific corrosive environment, and, in some cases, susceptible metallurgical characteristics of the metal itself. Unlike other forms of corrosion that manifest as gradual degradation, SCC can lead to the rapid initiation and propagation of microscopic cracks, often culminating in catastrophic and unexpected component failure. These elongated cracks, characteristic of SCC, can develop and spread over time, even in components that have functioned satisfactorily for extended periods.

The critical factor governing the initiation and propagation of SCC lies in the delicate balance between passivity and reactivity at the metal surface. In environments conducive to SCC, a specific equilibrium must be established. If the system is excessively reactive, the protective oxide layer on the metal surface breaks down, leading to localized corrosion (pitting) or general corrosion. Conversely, if the environment is overly passive, no significant corrosion occurs. However, the crucial danger zone lies within this delicate balance. When a susceptible metal is exposed to a specific corrosive environment while under sustained tensile stress, the synergistic interaction can disrupt the passive oxide layer, triggering the initiation and propagation of SCC cracks; understanding this interplay between stress, environment, and material properties is paramount for selecting appropriate materials and implementing preventative measures to mitigate the risk of SCC in industrial settings.

SCC is insidious because it can occur in materials resistant to general corrosion due to protective film formation. Cracks can propagate at varying velocities, from extremely slow (10^{-12} m/s) to relatively rapid (10^{-3} m/s), depending on the specific alloy and environmental conditions. The crack propagation can be intergranular, occurring along the grain boundaries, or transgranular, cutting through the grains. This duality is influenced by minor changes in the environment, such as pH or ionic concentration, and the material's microstructure. For instance, austenitic stainless steels sensitized by heat treatment become susceptible to intergranular SCC in environments that would not normally induce such

cracking. SCC is influenced by three primary factors: the material properties, the environmental conditions, and the stress applied. For example, AISI 316L stainless steel in a hot magnesium chloride solution can exhibit intergranular and transgranular SCC, depending on the specific stress and environmental conditions [26].

Ralston et al. seek to elucidate the mechanisms and contributing factors to stress corrosion cracking (SCC) observed in an above-ground, mineral wool-insulated oil emulsion pipeline. The research aims to determine whether SCC mechanisms known from buried pipelines apply to above-ground pipelines. A root cause analysis (RCA) identified stress, environment, and material properties as critical factors. Laboratory testing involved cyclic potentiodynamic polarization (CPP) and slow strain rate tests (SSRT) using leachate solutions derived from mineral wool insulation. Key findings indicate that insulation degradation, notably binder burnout leading to acidic conditions, significantly contributes to SCC. The metallurgical investigation showed intergranular fracture morphology in cracks unaffected by the pipe's heat treatment or supplier, suggesting environmental factors as primary SCC drivers. This study provides critical insights into mitigating SCC in similar pipeline systems, emphasizing the role of insulation quality and environmental control [27].

2.5 CORROSION FATIGUE

The relentless interplay of cyclic stress and corrosive environments presents a significant challenge for engineers in material selection and design. This challenge manifests in the phenomenon known as corrosion fatigue, a process that dramatically reduces the lifespan of metallic components. Unlike fatigue, where repeated loading induces cracks and eventual failure, corrosion fatigue combines this cyclic stress with the detrimental effects of a corrosive environment. This synergistic interaction leads to premature material failure at stress levels far lower than those that would cause fatigue failure in a non-corrosive setting.

Even without the additional threat of corrosion, metals and alloys are susceptible to fatigue. When subjected to repeated cyclic loading over extended periods, microscopic cracks can

initiate and propagate within the material. The number of cycles required for failure decreases as the applied stress increases. However, a critical threshold, known as the "Endurance Limit," exists below which the material can theoretically withstand cyclic stresses indefinitely. However, the presence of a corrosive environment disrupts this established limit. The synergistic interaction between stress and corrosion disrupts the protective passive layer on the metal surface, accelerating crack initiation and propagation. This reduces the endurance limit significantly, leading to premature failure at stress levels well below the material's fatigue limit in a non-corrosive environment. Understanding the mechanisms of corrosion fatigue and its dependence on factors like stress magnitude, corrosive environment, and material properties is crucial for engineers to predict material behavior and design components that can withstand the combined effects of cyclic loading and corrosive attack.

Corrosion fatigue (CF) is closely related to SCC but generally affects a broader range of materials and environmental conditions. Almost all active or passive metals experience reduced fatigue life in corrosive environments. For example, ferritic stainless steels used in turbine blades can develop transgranular cracks initiated from pits, which differ from the branching cracks typical of SCC. The CF process has four stages: cyclic plastic deformation, microcrack initiation, small crack growth to linkup and coalescence, and macrocrack propagation. High-cycle fatigue (HCF) studies using smooth or notched cylindrical specimens plot the applied cyclic stress amplitude against the number of cycles to failure, revealing a decrease in stress amplitude with an increase in cycles until a fatigue strength or endurance limit is reached. In corrosive environments, this fatigue strength decreases continuously, indicating the significant impact of corrosion on fatigue life. Crack growth rates in CF are influenced by factors such as stress intensity range, stress ratio, and loading frequency, with the presence of corrosive agents often accelerating crack propagation through synergistic effects with cyclic loading [26].

Choi et al. investigated the impact of cyclic stress on the corrosion fatigue properties of thermally insulated pipelines, particularly within synthetic groundwater environments. The research employed advanced electrochemical testing, including Linear Polarization

Resistance (LPR) and Electrochemical Impedance Spectroscopy (EIS), alongside Scanning Electron Microscope (SEM) analysis, to elucidate the underlying mechanisms. The experimental findings revealed that the corrosion fatigue life of pipelines is significantly diminished in the presence of cyclic stress and corrosive environments, as evidenced by the reduction in fatigue life on the S–N curves. Moreover, it was observed that the insulation's effectiveness in mitigating corrosion was contingent on forming a protective rust layer, which decelerated both corrosion progression and fatigue crack propagation. These conclusions were substantiated by detailed EIS measurements and SEM observations, highlighting the crucial role of stress magnitude over water content in determining corrosion rates. The study underscores the importance of considering both mechanical and environmental factors in the design and maintenance of thermally insulated pipelines to prevent premature failure [28].

2.6 NONDESTRUCTIVE INSPECTION TECHNIQUES TO PREVENT CUI FAILURES

Corrosion under insulation (CUI) presents a significant challenge to the integrity of piping and pressure vessels in various industries. The primary difficulty arises from the need for thorough inspection, often requiring complete removal of the insulation layer. This poses a substantial logistical and financial burden. Dismantling insulation is time-consuming and expensive and carries the risk of damaging the underlying pipework and potentially exposing personnel to hazardous materials. Additionally, the disruption to ongoing operations can significantly impact production and profitability. Recognizing these limitations, researchers have actively developed reliable nondestructive evaluation (NDE) techniques designed explicitly for CUI inspection.

These advancements have yielded a diverse toolbox of portable NDE methods that can be effectively deployed on-site, eliminating the need for insulation removal. These techniques offer a compelling alternative to traditional methods, providing piping networks with cost-effective and comprehensive inspection capabilities. Some of the most prominent NDE methods employed for CUI inspection include neutron backscatter, infrared thermography, guided wave ultrasonic testing (UT), profile radiography, computed radiography (CR), and

pulsed eddy current testing (PECT). Notably, profile radiography and guided wave UT have received formal recognition within the industry standard API 581 as viable alternatives to insulation removal for CUI inspection purposes. The successful implementation of these NDE techniques offers a significant advantage by enabling proactive identification and mitigation of corrosion threats without disrupting ongoing operations. This not only translates to substantial cost savings but also enhances overall plant safety and operational reliability [7].

2.7 CUI MONITORING UNDER COATINGS AND INSULATION

Corrosion monitoring under coatings and insulation is paramount for ensuring the durability and reliability of industrial infrastructure. Advanced monitoring techniques, such as Electrochemical Impedance Spectroscopy (EIS) and Electrochemical Noise (EN), have emerged as crucial tools in detecting and mitigating corrosion. EIS facilitates non-destructive analysis of coating performance by assessing parameters like coating capacitance, pore resistance, and charge transfer resistance. These metrics are essential for understanding water uptake in coatings, which directly impacts their protective efficacy. EN offers additional insights by identifying early signs of coating delamination and underlying corrosion, often undetectable by visual inspections. The complexities of corrosion under insulation (CUI) necessitate these sophisticated real-time monitoring solutions, as traditional visual methods are insufficient for comprehensive detection. Adopting these advanced techniques not only preemptively addresses potential corrosion issues but also significantly reduces maintenance costs and enhances the structural integrity of industrial assets. This approach underscores the imperative of integrating innovative monitoring methodologies to safeguard infrastructure against the pervasive challenge of corrosion [29].

2.7.1 RISK BASED INSPECTION (RBI) METHODOLOGY

Risk-Based Inspection (RBI) for Corrosion Under Insulation (CUI) is a sophisticated and strategic approach that prioritizes inspection efforts based on the risk of failure due to corrosion in insulated piping and equipment. This methodology integrates probabilistic risk

assessment with engineering judgment, focusing on both the likelihood of CUI occurrence and the potential consequences of such failures. In developing an RBI plan, critical factors such as operating temperatures, insulation types, exposure to moisture, and historical corrosion data are meticulously analyzed. This process begins with a high-level screening to identify high-risk areas, followed by detailed risk assessments using semi-quantitative or quantitative models. Advanced techniques, such as non-destructive testing (NDT) and real-time monitoring systems, are employed to gather accurate data on the condition of insulation and underlying metal surfaces. The outcomes of an RBI program include a prioritized inspection schedule, optimized maintenance strategies, and the allocation of resources to areas with the highest risk, thereby enhancing plant safety, reliability, and operational efficiency. Additionally, this approach is dynamic, allowing for continuous updates and refinements as new data becomes available, ensuring the most effective management of CUI over the lifecycle of the facility.

The primary objective of the study by Winnik is to establish a robust Risk-Based Inspection (RBI) methodology tailored specifically for addressing Corrosion Under Insulation (CUI) in industrial settings. This methodology involves a comprehensive, multi-step process designed to prioritize inspection efforts based on the risk of CUI failure. The initial step entails high-level prioritization, focusing on identifying plant areas most susceptible to CUI that could significantly impact health, safety, environment, and business continuity. Subsequent steps involve data validation, challenging the necessity of insulation, and employing both qualitative and semi-quantitative RBI assessments to determine the probability and consequences of potential failures. The ultimate outcome is a detailed, risk-based CUI inspection plan that not only guides inspection priorities but also integrates maintenance strategies tailored to the specific risk levels of different plant units. Through this meticulous approach, the study aims to enhance the reliability and safety of industrial operations by systematically mitigating the risks associated with CUI [30].

2.7.2 CUI MONITORING WITH ARTIFICIAL INTELLIGENCE (AI)

The integration of AI technologies in corrosion monitoring represents a transformative advancement in the oil and gas industry, significantly enhancing the accuracy, efficiency,

and effectiveness of corrosion detection, prediction, and mitigation. Traditional corrosion monitoring methods, such as corrosion coupons, electrical resistance probes, and ultrasonic inspections, have been pivotal but are limited by their inability to provide real-time and precise data. AI, particularly through machine learning and deep learning algorithms, addresses these limitations by analyzing complex data patterns and relationships, thus predicting corrosion rates with higher accuracy. For instance, AI-driven predictive models can proactively identify potential corrosion issues, allowing for timely intervention and reducing the risk of catastrophic failures. Furthermore, AI enhances data analysis and integration capabilities, enabling the processing of vast amounts of data from various sources, such as sensors, laboratory tests, and historical records. This capability is crucial for real-time decision-making and the development of comprehensive corrosion management strategies. An example includes the use of AI to analyze data from ultrasonic sensors in pipelines, which can detect and predict corrosion-related anomalies with greater precision than traditional methods.

Additionally, AI's role in corrosion monitoring extends to the identification of corrosion patterns that may not be easily discernible through human inspection. Techniques such as pattern recognition can detect localized or complex forms of corrosion, including pitting and crevice corrosion, which can rapidly deteriorate material integrity. AI-powered systems also facilitate the creation of predictive models that simulate corrosion behavior under various conditions, such as changes in temperature, pressure, and chemical composition. This modeling capability aids in understanding corrosion mechanisms and predicting outcomes, thereby informing more effective corrosion mitigation strategies. Moreover, AI enhances non-destructive testing methods like visual inspections, ultrasonic techniques, and electromagnetic testing by providing advanced data analysis and pattern recognition, thus improving the detection and assessment of corrosion damage. In summary, the integration of AI technologies in corrosion monitoring not only improves the accuracy and timeliness of data but also enables proactive and real-time management of corrosion, ultimately enhancing the safety, integrity, and longevity of oil and gas industry infrastructure [31].

CHAPTER 3. FORENSIC INVESTIGATION OF CORROSION UNDER INSULATION FROM RUST SCALE SAMPLE

3.1 ABSTRACT

Corrosion under insulation (CUI) stands as a prominent challenge in oil refining and hydrocarbon production establishments, accounting for 40-60% of piping-related repairs and constituting approximately 10% of total maintenance expenditures. While conventional and advanced inspection methods aim to detect and assess CUI occurrences, understanding the underlying reasons and kinetics of CUI formation remains a complex task. Rust scale samples, akin to other corrosion types, offer valuable insights into CUI mechanisms. A clear comprehension of these drivers and kinetics can significantly enhance root cause analysis and decision-making processes for effective CUI management. This article delves into three distinct case studies focusing on forensic investigations of CUI through the chemical analysis of rust scale samples. These samples, extracted from various assets within downstream and upstream facilities, underwent x-ray diffraction (XRD) analysis, revealing a spectrum of corrosion products such as hematite (Fe_2O_3), goethite (α-FeOOH), akageneite (β-FeOOH), magnetite (Fe_3O_4), among others. The study further delves into the kinetics associated with these corrosion products and proposes practical strategies for leveraging forensic insights from rust scales. [32]

3.2 INTRODUCTION

Corrosion under insulation (CUI) stands as a formidable challenge in the hydrocarbon production and processing industries, driving a substantial portion of piping failures, estimated between 40-60% [5]. This insidious form of corrosion predominantly manifests as localized corrosion, posing intricate hurdles in its prediction and mitigation strategies [33]. Historical data underscores the detrimental impact of CUI, showcasing instances where process pipes experienced significant thinning, leading to a cascade of leakage events [34]. The traditional arsenal of inspection methods, primarily non-destructive

examinations (NDEs), has evolved with advancements like digital radiography and moisture detection imaging, streamlining the screening process for CUI damage. These technological leaps have made damage assessment quicker and more cost-effective. Yet, the precise quantification of short-term and long-term corrosion rates remains challenging, often requiring the laborious process of stripping off insulations for thorough inspection and corrosion rate determination.

Despite these advancements, the localized and highly non-linear nature of pitting damage under thermal insulations complicates predictive assessments. Factors such as insulation type, chemistry, aging, and system design significantly influence pitting severity and environmental variables like temperature, time of wetness (TOW), moisture chemistry, and oxygen concentration cells [35]. While NDEs offer valuable insights into CUI risk extent and near-future susceptibility through time of wetness assessments, they often fall short of providing comprehensive information on underlying drivers and chemistry, creating uncertainties in CUI assessments, especially with extended inspection intervals [6]. In response, industries reliant on hydrocarbon, energy, and chemical processes employ corrosion inhibition and oxygen-scavenging chemicals, complemented by scale/rust analysis to evaluate internal corrosion management effectiveness, thereby enhancing their understanding of corrosion drivers for more effective mitigation strategies. For example, the boiler feed water (BFW) should be de-aerated to facilitate the formation of a uniform magnetite scale on the inner surfaces of the tubes. Even trace amounts of oxygen, in parts per billion (ppb), can support the formation of goethite, resulting in heterogeneous scale formation as illustrated by the following reaction [6].

$$\frac{3}{4}O_2 + 3Fe_3O_4 + \frac{9}{2}H_2O \rightarrow 9FeOOH \qquad \text{Equation 3– 1}$$

The heterogeneous nature of corrosion scale plays a pivotal role in localized damage and anodic dissolution, often leading to failures in boiler tubes. Understanding the composition and kinetics of corrosion products become crucial in deciphering the underlying chemistry of the environment. Extensive studies have been conducted to analyze corrosion scales on steel, especially in atmospheric and marine exposures, correlating environmental conditions with kinetic behaviors [36], [37], [38], [39]. Furthermore, chemical analyses of

corrosion scales have provided valuable insights into downhole applications, shedding light on corrosion mechanisms in diverse environments [40].

Metal-environment parameters significantly influence corrosion under insulation (CUI), impacting reaction kinetics and forming specific corrosion products. Analyzing these corrosion products offers insights into reaction kinetics, aiding in understanding the drivers and managing non-linear pitting rates associated with CUI. Despite advancements, there remains a gap in understanding the nature of corrosion compounds formed under insulation due to CUI. Research by Pojtanabuntoeng et al. delves into the chemistry of compounds formed on coupons in closed insulation systems with fibrous mineral wool insulation, shedding light on the intricacies of CUI-related corrosion [41].

Recent developments include deploying newer insulation grades with corrosion inhibitors to combat CUI. However, there's a shortage of long-term field verifications regarding the inhibitive properties of such insulations. Analyzing scale chemistry offers insights into the long-term effectiveness of corrosion-inhibitive insulations. This paper presents three distinct case studies analyzing scale samples from CUI on equipment in downstream facilities of hydrocarbon processing plants, pipelines in upstream facilities, and ambient temperature CUI simulation test cells. Through x-ray diffraction (XRD) analysis and comparison with international databases, the composition of compounds is unveiled, alongside discussions on associated kinetics and engineering outcomes for each case, providing a comprehensive understanding of CUI-related corrosion dynamics.

3.3 CASE STUDIES

3.3.1 CASE STUDY 1 – CUI SCABS FROM A VINTAGE OIL REFINING FACILITY

This study analyzes scale samples obtained from the crude distillation unit (CDU) column of an aging oil refining facility situated at a North American harbor, which has been operational for over five decades. The CDU column features vintage-grade fibrous stone wool insulation with varied temperature zones tailored for refining diverse petroleum fractions. Visual inspections of the column's exterior revealed significant scabbing at the top dome and around the insulation support ring (ISR), characterized by dense and prominently raised formations. Extensive interconnected pitting was observed upon closer examination and removal of loosely adhered scabs. Figure 3-1 illustrates the column's layout and the areas of damage, while Figure 3-2 provides detailed field images capturing the rust scabs and the underlying pit formations.

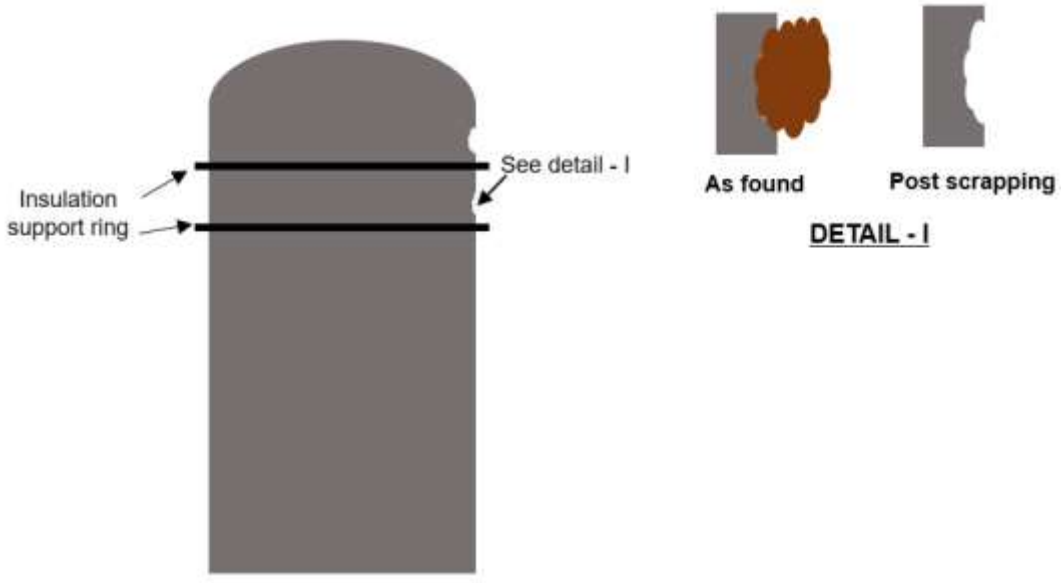

Figure 3-1. Schematic of CUI damage on crude oil distillation column

Non-destructive examination (NDE) through ultrasonic thickness measurements identified substantial pit depths, resulting in up to a 50% loss in wall thickness at these locations. Complementing this, visual assessments of the insulation and jacketing were conducted, followed by chemical analyses utilizing X-ray diffraction (XRD) on scale samples collected from the upper dome area and surrounding the insulated support ring (ISR).

Figure 3-3 summarizes the XRD spectra for the scale powders, while Table 3-1 outlines the diffraction angles corresponding to each identified compound.

Figure 3-2. Field visuals of the rust scab and underlying inter-connected pits

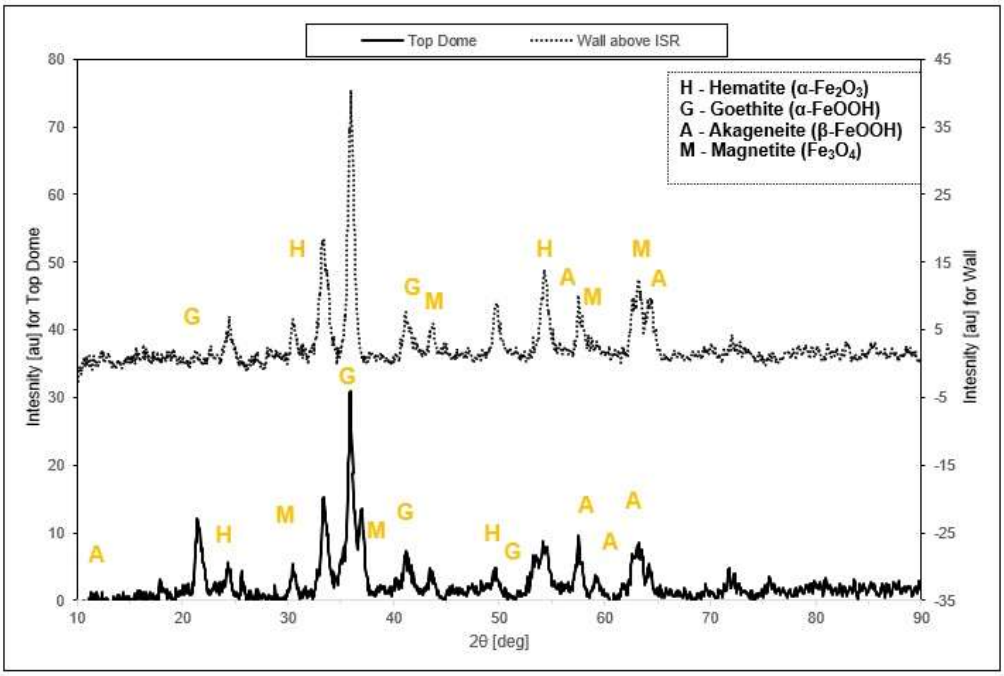

Figure 3-3. XRD spectra of CUI scabs from the crude distillation column

Table 3-1. Diffraction angles for various corrosion products (for CUI on crude distillation column)

SAMPLE LOCATION	DIFFRACTION ANGLE (2θ)			
	Goethite (α-FeOOH)	**Akageneite (β-FeOOH)**	**Magnetite (Fe_3O_4)**	**Hematite (Fe_2O_3)**
Top dome	35.8º, 40.95º, 52.9º	11.85º, 46.7º, 55.9º, 59.25º, 61.05º, 64.3º	30.2º, 35.2º, 37.1º	24º, 49.4º
Wall around ISR	21º, 41º	56º, 64.3º	35.5º, 43.1º, 53.35º, 57.4º, 62.7º	33.15º, 54.15º

3.3.2 CASE STUDY 2 – CUI SCABS FROM IN-SERVICE CRUDE OIL EMULSION & STEAM PIPELINES

In steam-assisted gravity drainage (SAGD) operations, crude oil emulsions (COE) are a mixture of crude oil and moisture from injected steam in underground formations. The pipelines used to transport these COEs typically operate within the range of 90°C to 170°C, while the steam lines, as discussed in this study, operate at around 350°C. Figure 3-4 (a-b) illustrates the appearance of scales on the COE and steam pipelines, respectively. Figure 3-5 displays the X-ray diffraction (XRD) spectra of corrosion compounds, and Table 3-2 summarizes the corresponding angles for each identified corrosion compound.

Figure 3-4. Rust scale on the pipe skin for (a) crude oil emulsion pipeline (b) Steam pipeline

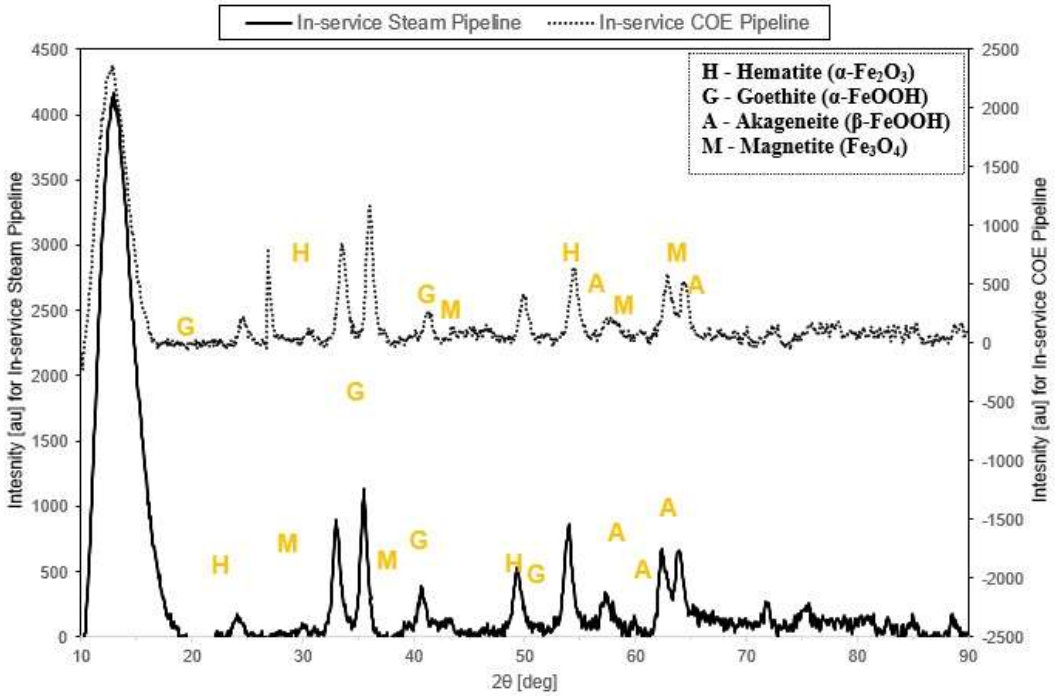

Figure 3-5. XRD spectra for COE & steam pipelines

Table 3-2. Diffraction angles for various corrosion products (for CUI on COE & steam pipelines)

SAMPLE LOCATION	DIFFRACTION ANGLE (2θ)			
	Goethite (α-FeOOH)	Akageneite (β-FeOOH)	Magnetite (Fe_3O_4)	Hematite (Fe_2O_3)
COE pipeline	21.23º, 33.17º, 34.72º, 36.06º, 36.66º, 53.29º,54.19º, 58.98 º	11.65º, 16.79º, 26.87º, 34.27º, 39.56º, 43.35º, 44.25º, 46.80º, 49.50º, 52.54º, 56.44º, 61.43º, 62.58º, 64.98º, 84.75º	30.22º, 35.46º, 37.16º, 43.34º, 53.64º, 57.28º, 62.83º, 74.46º, 79.30º, 87.01º	24.13º, 33.12º, 35.66º, 40.91º,49.40º, 54.04º, 57.73º, 62.48º, 63.99º, 71.92º, 75.36º
Steam pipeline	21.28º, 33.07, 35.81, 36.81º, 40.06º, 41.16º	11.7º, 16.7º, 26.83º, 34.07º, 35.21º, 39.61º, 46.35º, 52.04º, 55.74º,	30.5º, 35.46º, 53.8º, 57.13º, 62.43º	24.28º, 33.07º, 35.6º, 40.7º, 49.4º, 54.14º, 62.68º, 63.9º

3.3.3 CASE STUDY 3 – CUI SCABS FROM OUT OF SERVICE PIPES WITH AND WITHOUT EGRESS DESIGN(S)

Case study 3 examines scale analysis from corrosion under insulation (CUI) simulation tests conducted at ambient temperatures. These tests spanned a full year and involved two sets of cells, each housing steel coupons with different insulation configurations. The first

test cell utilized non-metallic stand-off membranes and low-point drains, replicating a design that facilitates moisture removal (see Figure 3-6 (a)) [42]. In contrast, the second assembly (Figure 3-6 (b)) featured fibrous stone wool insulation directly applied over the coupons without specific moisture egress provisions. Figure 3-7 presents the X-ray diffraction (XRD) spectra of compounds found in scale samples from each design, with their corresponding diffraction angles summarized in Table 3-3 [35].

Figure 3-6. Comparison of the test cells

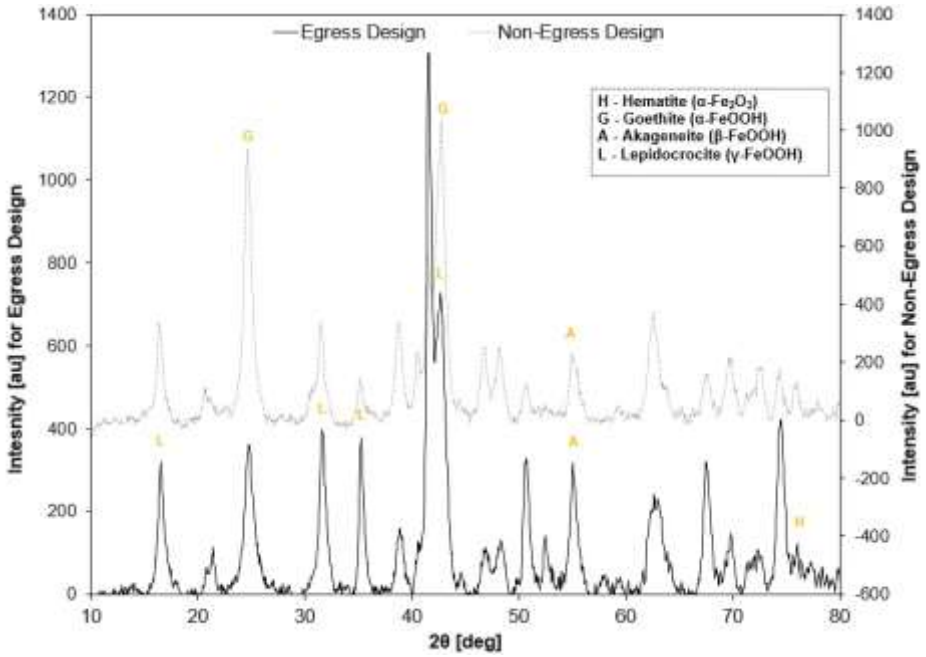

Figure 3-7. XRD spectra for moisture egress & non-egress designs

Table 3-3. Diffraction angles for various corrosion products w.r.t Insulation System's design

INSULATION SYSTEM'S DESIGN	DIFFRACTION ANGLE (2θ)				
	Goethite (α-FeOOH)	**Akageneite (β-FeOOH)**	**Lepidocrocite (γ-FeOOH)**	**Magnetite (Fe_3O_4)**	**Hematite (Fe_2O_3)**
Egress design	Not detected	54.86º, 62.2º	16.43º, 31.52º, 42.4º	Not detected	68º
Non-egress design	27.47º, 24.64º	54.92º	Not detected	Not detected	Not detected

3.3.4 DISCUSSION

Managing external corrosion from corrosion under insulation (CUI) could benefit from existing protocols used for chemical assessment in internal corrosion scenarios such as in-process pipes, pipelines, and downhole applications. Generally, corrosion compounds like hematite and magnetite are favored under specific conditions, reflecting the environmental conditions that led to their formation. In Case Study 1, scale composition analysis from the top dome and ISR of the CDU column reveals similar compounds, though with higher concentrations of akageneite and goethite in the top dome than around the ISR. Elevated goethite levels are attributed to higher temperatures at the top of the column, which are influenced by compounds like SO_2 and carbonates, while akageneite is linked to chloride-rich environments [39]. The CDU column's skin temperature is approximately 200°C, decreasing along its height, with areas studied at around 70°C. Historical data from the 1980s indicates low pH acid rain from effluents (NOx, SO_2), correlating with the presence of goethite, especially at the top, and akageneite due to chloride exposure from the nearby harbor. The top dome's higher water infiltration likely contributed to the observed compounds. Higher temperatures around the ISR promote the transformation of goethite and akageneite into hematite, as seen in lower portions. Despite favorable conditions, potential leachates from insulation materials necessitate further study to ascertain their role and aging in corrosion compound formation.

Case study 2 examines scale samples gathered from crude oil emulsions (COE) and steam pipelines in western Canada. Table 3-3 shows identical scales in both cases, with goethite presence attributed to high total oxygen weight (TOW) and carbonate ions likely from insulation or water sources. Despite these pipelines being distant from the harbor, incidents of moisture-saturated insulations have occurred, potentially linking to reported stress

corrosion cracking (SCC) incidents [43]. The presence of akageneite suggests chloride exposure, possibly from insulation leachates or waterborne ions on the pipe surface. Operating at temperatures exceeding 100°C, the presence of hematite indicates the transformation of goethite and akageneite. Magnetite is favored due to high temperatures but poses challenges due to oxygen concentration cell formation at insulation-pipe interfaces, creating heterogeneous magnetite patches that can lead to localized anodic dissolution, emphasizing the need for cautious interpretation considering system design and kinetics [6].

The composition and kinetics of rust scales in corrosion under insulation (CUI) scenarios are influenced not only by operating conditions and moisture chemistry but also by the design of the insulation system. Case study 3 delves into how the design of the insulation system can impact the nature of corrosion compounds, contrasting egress design, which allows moisture removal, with non-egress design [34]. Visual comparisons in Figure 3-6 illustrate the differences in corroded steels between these designs. Table 3-3 highlights that the egress design exhibits lepidocrocite, possibly due to its lower total oxygen weight (TOW) compared to the non-egress design, where magnetite is absent likely because of the near-neutral pH of water exposure and absence of heat [35].

While acknowledging exceptions related to kinetics beyond this study's scope, Table 3-4 provides a summary of general drivers for corrosion compound formation applicable to CUI forensic analysis. Meaningful interpretation of CUI scab analysis necessitates considering various factors from design, operations, non-destructive examinations (NDEs), and environmental perspectives. It requires expertise in CUI kinetics and physical factors to grasp their implications on CUI rates in pipelines and facilities. Scale analysis as a forensic tool in CUI management is an evolving field that requires further exploration to reduce uncertainties associated with CUI damage assessment.

Table 3-4. Common corrosion compounds and formation drivers [38], [42]

Typical Drivers	**Goethite (α-FeOOH)**	**Akageneite (β-FeOOH)**	**Lepidocrocite (γ-FeOOH)**	**Magnetite (Fe_3O_4) ***	**Hematite (Fe_2O_3)**
TOW	High	-	Low	-	Fully de-hydrated
Promoting Ions	Carbonates, SO_2	Chlorides	-	-	-
Oxygen levels	High	High	High	Low	High
pH	Neutral/ mildly acidic	Neutral/ mildly acidic	Neutral/ mildly acidic	Alkaline	Neutral & acidic
Temperature	Low		Low	Higher	High
Non-egress insulated system	Yes	Yes	No	Yes (at high temp.)	Yes
Egress-type insulated system	No	Yes	Yes	Low probability	Yes

* No direct correlation between the extent of dissolved oxygen and the magnetite

3.3.5 CONCLUSION

This paper explores scale sample analysis through three distinct case studies, focusing on x-ray diffraction (XRD) results that summarize corrosion compounds and subsequent interpretations. The following conclusions emerge:

1 The presence of effluents like SO_2 and marine vapors likely exacerbates corrosion under insulation (CUI) rates, necessitating further investigation through insulation leachate analysis.

2 Direct contact between insulation and metal fosters oxygen concentration cells, heightening pitting risks by generating heterogeneous scales in high-temperature CUI scenarios.

3 The design of insulation systems, operational conditions, and environmental influences collectively impact CUI rates and the nature of corrosion compounds.

4 Forensic analysis via scab studies represents a nascent area in CUI management, requiring further development to enhance understanding and predictive capabilities regarding CUI damage.

CHAPTER 4. INSULATIONS AGEING & CUI IMPLICATIONS – A COMPARISON OF LAB & FIELD SAMPLES

4.1 ABSTRACT

Corrosion under insulation (CUI) is a predominant damage mechanism in the hydrocarbon industry, with its prediction often shrouded in uncertainty due to numerous unknown variables. The condition of insulation is pivotal in assessing CUI risk within modern risk-based inspection (RBI) programs. However, predicting insulation conditions is challenging, as insulations typically alter their physical properties when exposed to heat and environmental factors, and established baselines to accurately gauge insulation aging are lacking. This study seeks to elucidate the aging behaviors of two commonly used insulations-mineral wool and calcium silicate (CalSil), by subjecting them to both laboratory and field conditions. Leachates were prepared per ASTM C871 and analyzed using inductively coupled plasma (ICP) spectroscopy, followed by corrosion tests via autoclave immersion, ASTM C1617 dripping, and ASTM G189-07 CUI simulation. Corroded steel samples and insulations were further characterized through weight loss methods to determine corrosion rates, and confocal laser topography and scanning electron microscopy (SEM) to elucidate corrosion modes. By integrating these advanced analytical techniques, the study aims to provide a comprehensive understanding of insulation aging and its impact on CUI, thereby enhancing predictive capabilities and risk management strategies in the hydrocarbon industry. [44]

4.2 INTRODUCTION

Corrosion under insulation (CUI) is recognized as a major damage mechanism in the hydrocarbon production and processing industries, accounting for 40-60% of piping failures. [33] CUI primarily manifests as localized corrosion, presenting significant challenges for prediction and mitigation. This form of corrosion has caused severe thinning in process pipes, leading to numerous leakage incidents. [34] In recent years, risk-based

inspection (RBI) has become a crucial methodology for understanding and predicting the criticality of assets such as pipes, equipment, and pipelines in the hydrocarbon sector. RBI operates on the fundamental principle of risk assessment by estimating both the probability and consequence of failure. In a typical semi-quantitative RBI assessment, the prediction of corrosion rates (Cr) for CUI is performed using the following equation. This approach helps in systematically evaluating and managing the risks associated with CUI, thereby enhancing the safety and reliability of hydrocarbon infrastructure [27].

$$C_r = C_{rB} \times F_{INS} \times F_{CM} \times F_{IC} \times \max\left[F_{EQ}, F_{IF}\right] \qquad \text{Equation 4– 1}$$

Whereas

C_r = Adjusted corrosion rate (or CUI CR)

F_{CM} = Complexity factor (1.0 for non-complex geometry)

F_{IC} = Insulation condition adjustment factor (1.0 for average condition)

F_{INS} = Insulation type adjustment factor (1.25 for mineral wool)

F_{EQ} = Equipment/ design factor (1.0 for the moisture egress, 2.0 for the non-egress design)

C_{rB} = Base CR (based on ambient condition & operating temperature)

F_{IF} = Soil and/ or water Interface factor (1.0 for no interface, 2 for interface)

The suggested numbers are primarily based on operator and personnel feedback derived from both field experiences and laboratory tests. However, assigning these numbers presents several challenges due to the varying quality and aging characteristics of insulation materials, which can differ significantly. Assessing insulation condition and accurately classifying it with ratings such as 0.75 (above average) or 1.0 (average) is complex, as there are generally no standardized practices to evaluate the chemical and corrosive nature of in-service insulation. Aging of fibrous insulation materials, due to the heat from the pipes or equipment they insulate, often results in physical degradation (e.g., binder burnout) and chemical changes [27], [45].

The Alberta Energy Regulator (AER) recently issued a bulletin regarding novel external inter-granular stress corrosion cracking (IGSCC) in aboveground thermally insulated pipelines, where moisture-saturated insulation was suspected as the cause, though investigations are ongoing. In a related study, Ralston et al. examined the aging of fibrous

mineral wool insulations using inductively coupled plasma (ICP) spectroscopy to identify chemical changes resulting from aging. [27] The study also explored the corrosion implications of insulation aging by testing in an autoclave environment to simulate stress corrosion cracking behaviors [27].

Unlike traditional immersion tests, CUI simulation uniquely incorporates the effects of insulation along with moisture and corrosive ions, providing a comprehensive understanding of corrosion dynamics. Various test methods exist, each differing in their effectiveness at determining the CUI rating for insulation materials based on their type (e.g., F_{INS}). The latest edition of API 581 endorses F_{INS} ratings for different insulation materials based on ASTM C1617, which primarily evaluates the corrosivity of leachates extracted from insulation. In contrast, ASTM G189-07 involves wrapping insulation around coupons to simulate CUI behavior accurately. This study delves into the thermal aging effects on fibrous stone (mineral) wool and calcium silicate (CalSil) insulations, comparing their performance from chemical and corrosion standpoints in both field and laboratory settings. It also assesses the efficacy of different test methods ASTM G189-07, ASTM C1617, and autoclave testing in replicating CUI behaviors, offering valuable insights for improving CUI prediction and mitigation strategies.

4.3 EXPERIMENTAL WORKS

Comprehensive testing scheme was developed to simulate the aging of insulation and understand the resultant chemical changes, a. This included chemical analysis using inductively coupled plasma (ICP) spectroscopy and corrosion tests conducted via three different methods. Representative samples of stone wool and calcium silicate (CalSil) insulations were aged for two weeks in a furnace at 200ºC. These samples, referred to as lab-aged insulation throughout the study, were then removed. Additional samples from the same insulation batch were applied to a steel pipe, wrapped with jacketing, and placed outdoors. This insulated assembly was continuously heated for six weeks using an immersion heater to induce aging effects. The insulation was then stripped off and designated as field-aged insulation for the study.

A small portion (20 g each) of both field-aged, lab-aged, and new insulation samples were mixed with deionized water in a stirring jar, boiled, and further mixed with deionized water to prepare leachate extract (volume: 0.5 liters) as per the ASTM C871 method. These leachate extracts were characterized using ICP spectroscopy to analyze their chemical composition. The extracts were also used for immersion and dripping tests according to ASTM C1617. Figure 4-1 (a-c) illustrates the arrangements for the autoclave immersion test, ASTM C1617 dripping test, and ASTM G189-07 CUI simulation test. Leachate solutions from the candidate insulation samples were utilized for three-day immersion tests in the autoclave and drip tests per ASTM C1617. Additionally, new and aged insulation materials were used in the test cell shown in Figure 4-1 (c) to conduct a three-day CUI simulation test under isothermal wet (IW) conditions as per ASTM G189-07. Upon completion of the tests, the coupons were cleaned, and weight loss measurements were taken to determine the corrosion rate, termed mass loss corrosion rate (MLCR), using the equation provided below [46], [47].

$$CR = \frac{KM}{ATD} \qquad \text{Equation 4– 2}$$

Whereas,

M = Mass loss (gm)

A = Surface area of steel coupons (cm^2)

K = constant (8.76×10^4)

T = Exposure time (hours)

D = Density (7.87 g/cm^3 for steel)

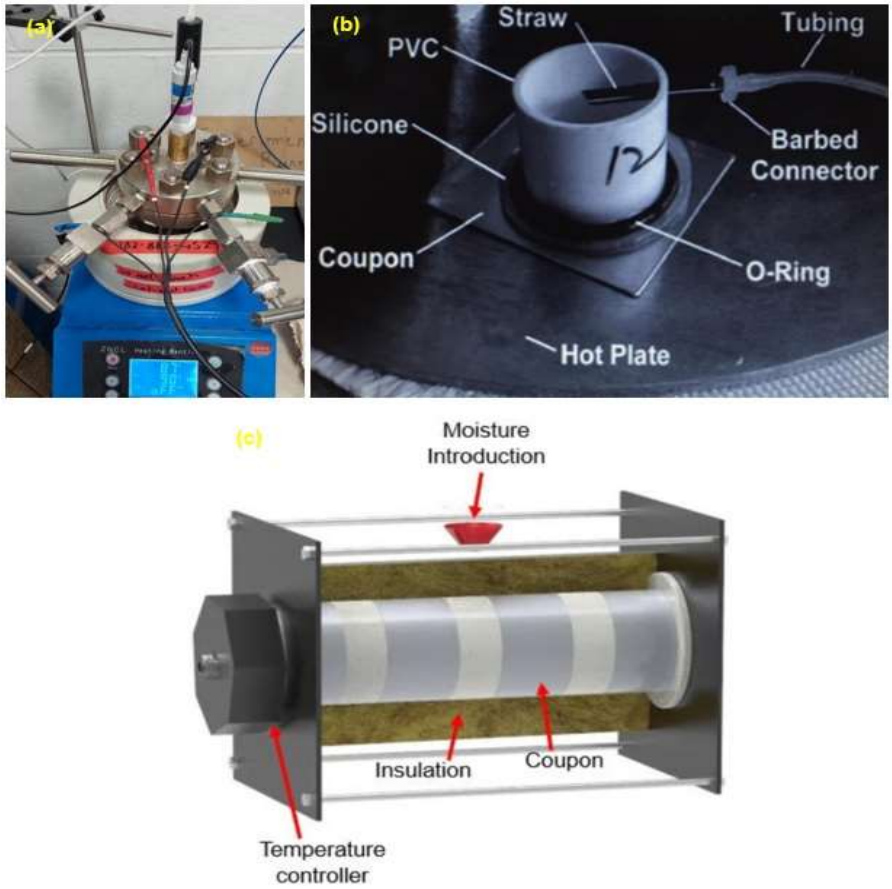

Figure 4-1. Arrangement for (a) autoclave immersion test (b) ASTM C1617 drip test (c) ASTM G189-07 CUI simulation test

4.4 RESULTS & DISCUSSION

The ICP results for the leachate extracts from the candidate insulation samples, summarized in Table 4-1, reveal that aging significantly impacts calcium silicate (CalSil) insulation, with both lab-aged and field-aged samples showing increased concentrations of alkaline ions, indicating a higher release of ions from the insulation matrix into the deionized water. Conversely, mineral wool samples exhibit more minor and less straightforward variations in ion concentration, necessitating further investigation. Figure 4-2 shows that mineral wool and CalSil consistently display higher corrosion rates for aged samples than pristine ones, as measured by ASTM G189-07, a trend corroborated by ASTM C1617 tests with some exceptions. However, autoclave immersion tests did not yield significant weight loss. Post-test images in Figure 4-3 illustrate the corroded coupons exposed to lab-aged insulation/leachates across different testing methods. This underscores

the varied corrosion impacts observed in autoclave, ASTM C1617 dripping, and ASTM G189-07 simulation tests.

Table 4-1. ICP Results

INSULATION DESCRIPTION	ELEMENTS (ppm)					
	Ca	Fe	K	Mg	Na	Si
Fibrous stone wool (Pristine)	7.8	0.28	46.4	2.4	11.1	7.5
Fibrous stone wool (Lab aged)	3.98	0.24	44.4	2.05	10	5.5
Fibrous stone wool (Field aged)	6.4	0.56	48.4	2.5	10.6	9.0
Calsil (Pristine)	76.1	0.04	8.5	0.3	11.6	10.6
Casil (Lab aged)	157	0.03	14	0.28	15.9	25
Calsil (Field aged)	144	0.62	13.1	0.5	18.1	52.9

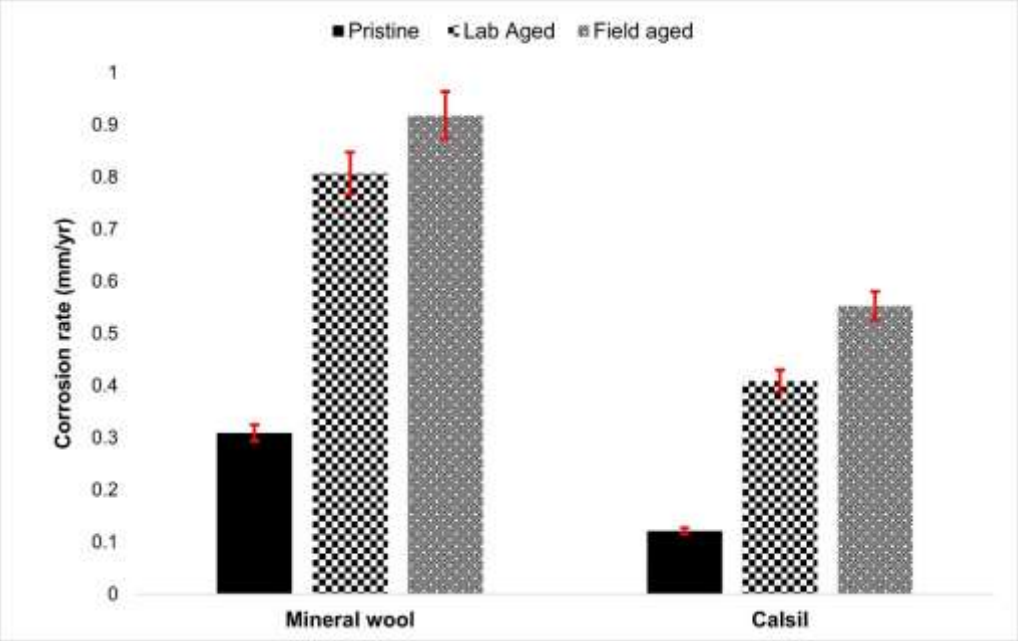

Figure 4-2. Corrosion rate (MLCR) trends for pristine and aged insulations as measured from ASTM G189-07 CUI simulation test

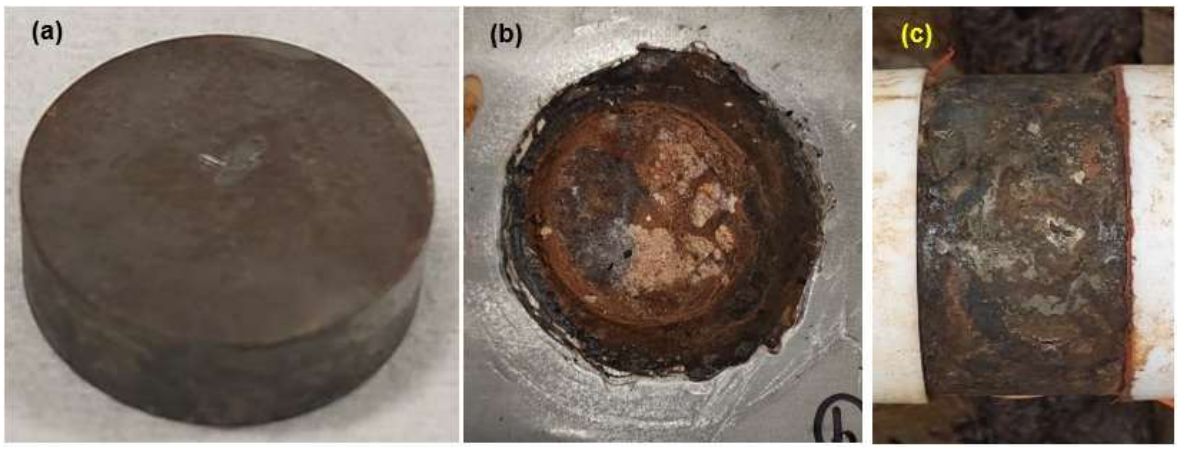

Figure 4-3. Post-test condition of coupon after exposed to lab aged Insulation/ leachates in (a) autoclave immersion test (b) ASTM C1617 dripping test (c) ASTM G189-07 CUI simulation test

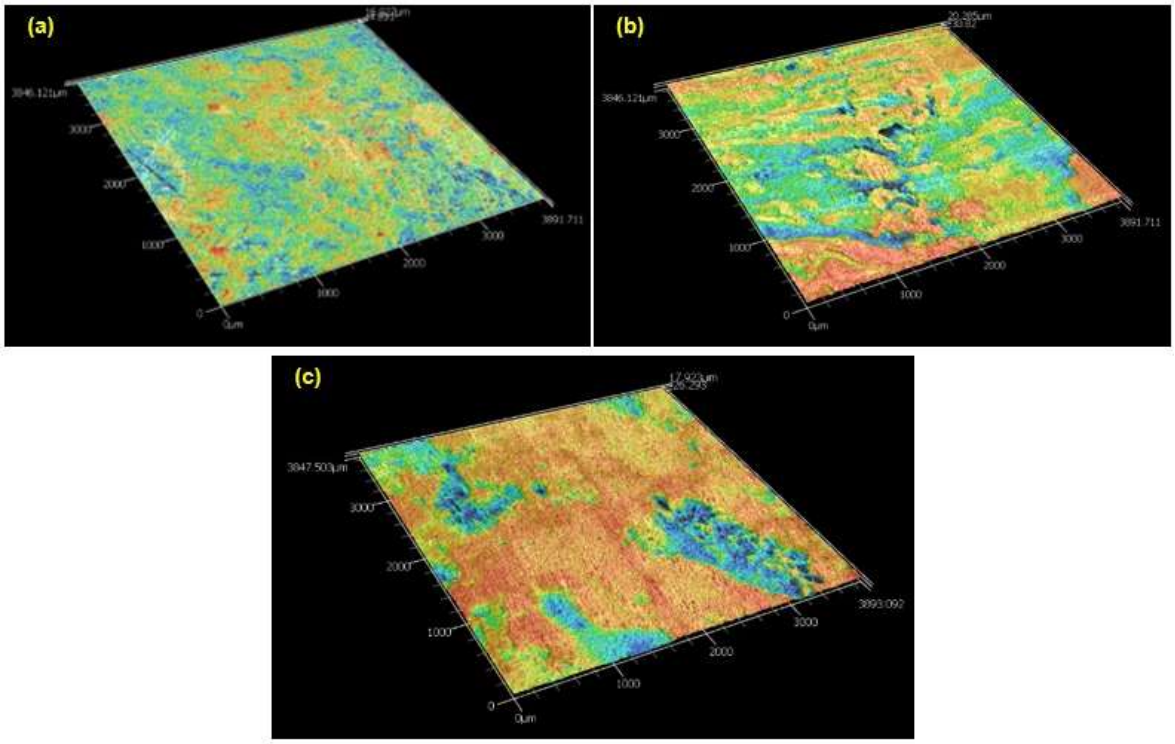

Figure 4-4. 3D topographs (mag. 100x) for the post-test coupons exposed to lab aged Insulation/ leachates in (a) autoclave immersion test (b) ASTM C1617 dripping test (c) ASTM G189-07 CUI simulation

In addition to exhibiting higher corrosion rates compared to pristine insulation, aging also induced notable physical changes in the insulation materials. Figure 4-5 illustrates the post-test conditions of the insulations following ASTM G189-07 testing. The lab-aged mineral wool insulation displayed a significant color change compared to the pristine sample,

indicating physical alterations. Conversely, aged CalSil insulation showed increased brittleness, as evidenced by the shattered samples. This brittle behavior was also observed in the field-aged CalSil samples. The fractures are indicative of CalSil's inherent brittleness. During the ASTM G189-07 tests, the CalSil samples emitted chattering sounds, suggesting cracking due to boiling moisture at the metal-insulation interface.

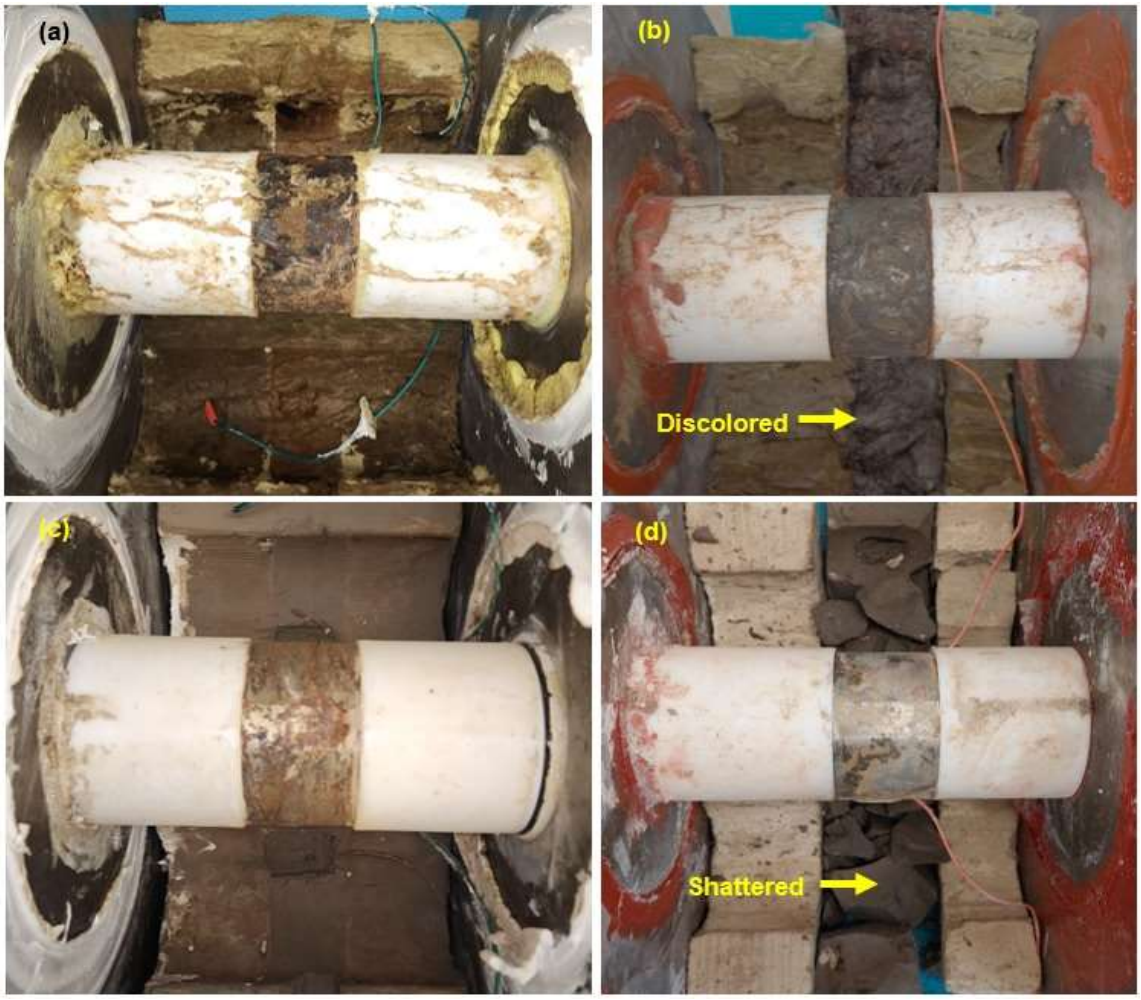

Figure 4-5. Post-test condition (a) pristine mineral wool (b) lab aged mineral wool (c) pristine Calsil (d) Aged Calsil

The testing methodology plays a critical role in the quality and accuracy of corrosion under insulation (CUI) simulations. To assess the impact of testing methodology, the corrosion modes were examined on corroded coupons from each test method: autoclave immersion test, ASTM C1617 dripping test, and ASTM G189-07 CUI simulation test. Figure 4-6

presents the scanning electron microscope (SEM) micrographs of coupons from each test scheme after exposure to field-aged mineral wool insulation/leachate, as applicable. Similarly, Figure 4-7 displays the SEM micrographs for field-aged calcium silicate (CalSil). These images provide insights into the corrosion mechanisms observed under different testing conditions, highlighting the importance of selecting an appropriate testing method for accurate CUI simulations.

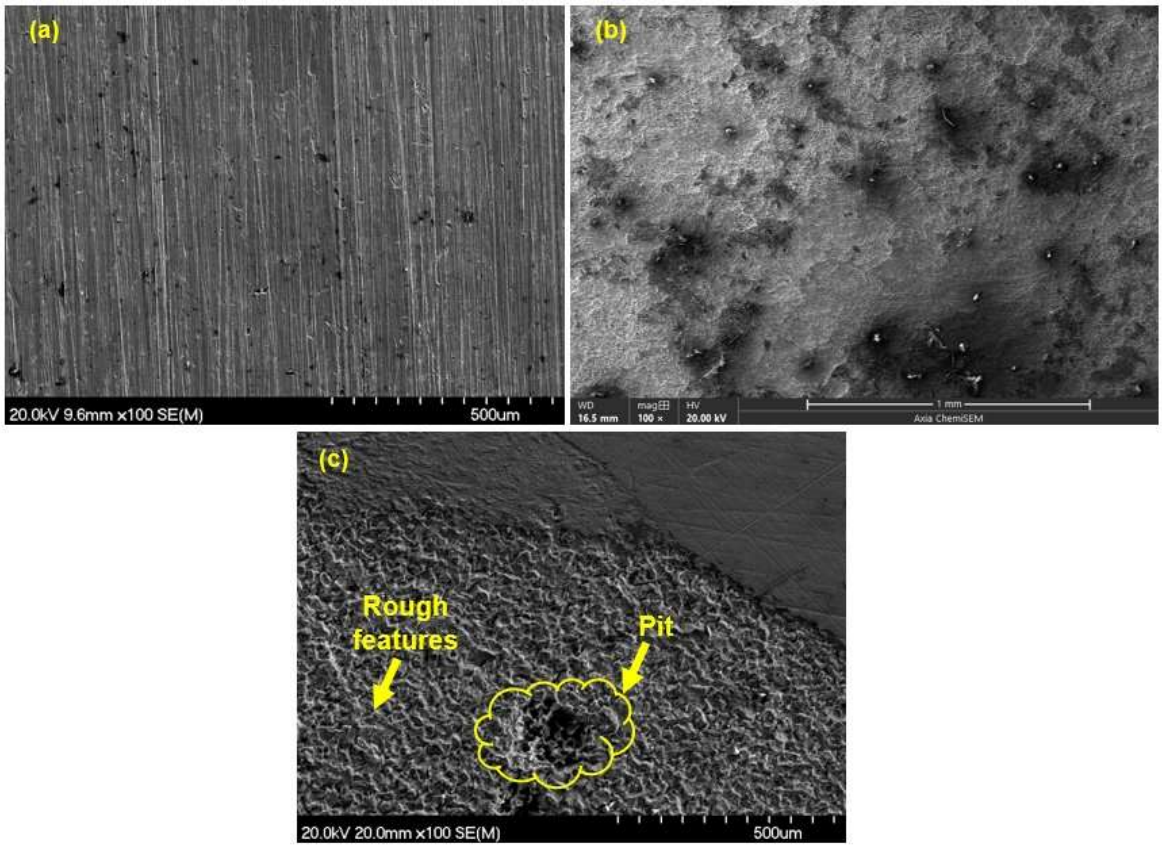

Figure 4-6. SEM micrographs (mag. 100x) for samples from (a) autoclave immersion test (b) ASTM C1617 dripping test (c) ASTM G189-07 CUI simulation test after exposed to field aged mineral wool insulation/ leachates

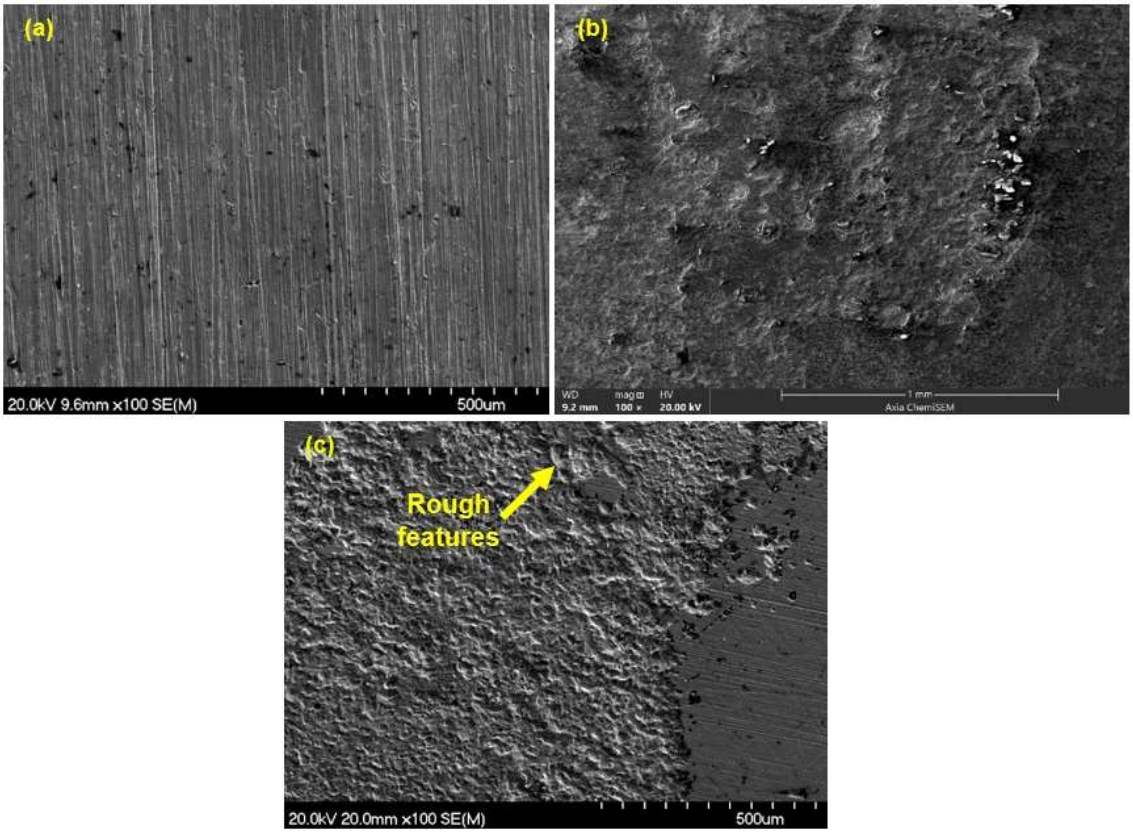

Figure 4-7. SEM micrographs (mag. 100x) for samples from (a) autoclave immersion test (b) ASTM C1617 dripping test (c) ASTM G189-07 CUI simulation test after exposed to field aged Calsil insulation/ leachates

The analysis of Figure 4-6 (a) and Figure 4-7 (a) indicates that the autoclave immersion test did not reveal significant surface damage, providing limited insights into aging effects. Conversely, Figure 4-6 (b) and Figure 4-7 (b) display noticeable, predominantly uniform surface damage without pitting. In contrast, Figure 4-6 (c) and Figure 4-7 (c) from ASTM G189-07 demonstrate localized damage and pitting, highlighting this method's ability to reveal the most concerning damage mode in CUI pitting, unseen in the ASTM C1617 dripping method or autoclave immersion test. Any CUI simulation test lacking direct insulation-to-steel contact may introduce ambiguities, as it overlooks a crucial aspect of the corrosion mechanism. Direct contact between insulation and metal generates oxygen concentration cells, leading to the formation of heterogeneous scales like magnetite and goethite. Magnetite, being more cathodic, triggers anodic dissolution underneath, resulting in pitting and localized corrosion. Therefore, selecting a method that accurately mimics such drivers, such as oxygen concentration cells, can reduce ambiguities in corrosion rate

assessments and improve the accuracy of assigning various insulation factors (e.g., F_{INS} and F_{IC}) in a typical RBI program.

4.5 CONCLUSION

This study delves into the impact of aging, both in field and laboratory settings, on two commonly utilized insulation materials: mineral wool and calcium silicate (Calsil). The effects of aging were meticulously characterized through the analysis of leachate extracts via Inductively Coupled Plasma Spectroscopy (ICP), coupled with comprehensive corrosion tests. The corrosion tests for leachate extracts were conducted employing autoclave immersion tests and ASTM C1617 dripping tests, while CUI simulation tests were carried out using the insulation materials in accordance with ASTM G189-07 methodology. From this thorough investigation, several significant conclusions emerge:

1 Both field and laboratory aging led to increased corrosion rates when compared to pristine mineral wool and Calsil insulations.
2 Autoclave immersion tests failed to replicate noticeable differences in corrosion rates between new and aged insulations.
3 The ASTM G189-07 test method effectively demonstrated localized pitting, a prevalent damage mode in real-life CUI applications.

CHAPTER 5. CASE STUDY OF THE PREMATURE COATING FAILURE ON THE BOILER TUBES

5.1 ABSTRACT

Boiler tubes in the penthouse sections are engineered to extract heat from flue gases, with materials and coatings specifically selected to mitigate high-temperature oxidation and other metallurgical damage mechanisms. These tubes are not designed to endure aqueous corrosion from external environmental factors, necessitating boilers to be strategically designed to minimize the ingress of moisture and corrosive ions from sources such as wind and cooling tower drift. This paper presents a case study on the failure of primer coatings on boiler tubes due to an upset condition that resulted in flooding inside the penthouse, leading to severe corrosion on the tube surfaces. The study examines multiple corrosion modes observed, detailing their mechanisms and impacts, and recommends corrective measures to prevent recurrence. Additionally, it highlights the role of insulation materials in contributing to heterogeneous corrosion morphologies, emphasizing the importance of selecting appropriate insulation and implementing effective moisture control strategies to enhance the reliability and durability of boiler systems. [48]

5.2 INTRODUCTION

Boilers are extensively utilized across various industries, including petroleum, manufacturing, chemicals, pulp and paper, and power generation, primarily to convert boiler feed water into steam. Due to their intricate construction, which involves diverse geometries and metallurgies for components like boiler tubes, casing, burners, and accessories, boilers are susceptible to multiple damage mechanisms. Beyond operating conditions, environmental factors can also pose additional risks. For example, chlorides from wind or cooling tower drift can infiltrate the combustion chamber, leading to stress corrosion cracking on the tubes. To mitigate the risk of airborne contaminants such as sulfur and chloride ions, facility layout designs incorporate strategic adjustments to boiler locations and the positioning of manways and air inlet points. Additionally, operational

practices recommend maintaining minimum temperatures during startup and shutdown phases to prevent the deposition of corrosive compounds through condensation, thereby minimizing the risk of dew-point corrosion [33]. With its unique attributes, the boiler's penthouse section is particularly vulnerable to moisture ingress from rain and cooling tower drift. Studies have documented various leakage events in penthouse sections, leading to multiple damage mechanisms [49]. Figure 5-1 illustrates the general arrangement of a typical boiler, highlighting the penthouse and thermally insulated pipes, which are pertinent to the discussion on coatings failure later in this study.

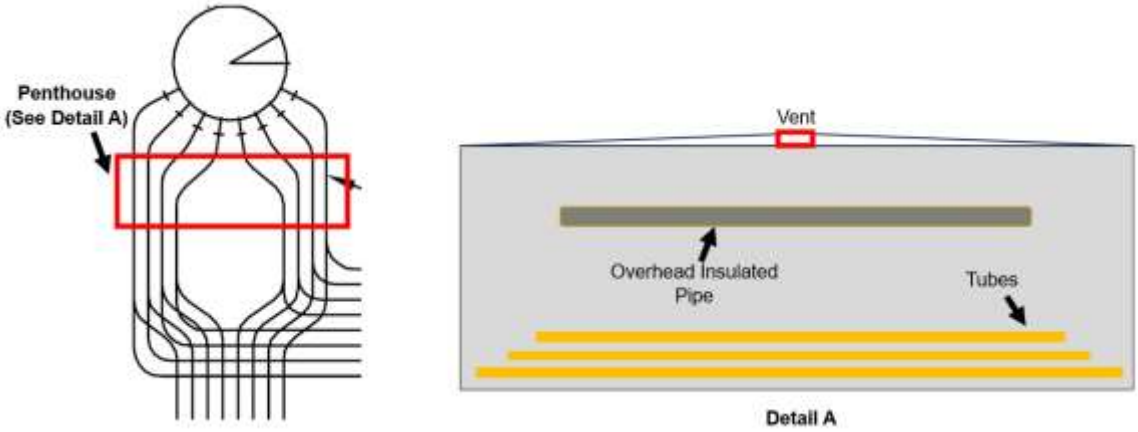

Figure 5-1. Schematics of penthouse and the associated tubes and overhead pipe

Boiler tubes are often coated to shield against atmospheric corrosion encountered during transportation, installation, and operation. These coatings primarily target damage mechanisms resulting from high-temperature exposure and dew-point corrosion. While they effectively address high-temperature corrosion risks like oxidation and fuel ash corrosion, they generally do not account for hydrated corrosion from moisture. Inorganic zinc silicate epoxies are a popular choice for corrosion protection in structural and high-temperature applications, offering resilience up to 400º C or 750º F. Their composition, with metallic zinc embedded in a silicate matrix, provides robust weathering protection even in the presence of corrosive pollutants like SO_2, CO_2, and NOx. Known for their toughness, these coatings are ideal for safeguarding surfaces during handling, storage, and construction. [50] Their low viscosity enables them to fill voids and cover complex geometries without leaving pinholes or holidays. Furthermore, the galvanic effects of zinc

offer sacrificial protection against surface damage such as scratching, dents, or tears. However, these coatings are unsuitable for buried or immersion conditions [50]. This article delves into a case study investigating the failure of inorganic zinc epoxy coating on penthouse boiler tubes due to unforeseen leaks in the boiler system. It examines the damage patterns and proposes remedial measures. Additionally, beyond boiler tubes, the study explores the potential of inorganic zinc epoxy coatings in preventing corrosion under insulation (CUI).

5.3 CASE STUDY

In a Middle Eastern power generation facility situated along the coastline, a water tube boiler was successfully commissioned and operating at full capacity. However, after five months of operation, anomalies arose when the steam temperature in the penthouse section consistently remained lower than expected. Upon external examination of the boiler and penthouse, crushed sections of jacketing were discovered. Subsequently, the jacketing was removed to inspect the insulation and penthouse area, revealing a flooded penthouse likely due to external water ingress, possibly from rain. The condition of the penthouse, with submerged tubes, is depicted in Figure 5-2 (a-b).

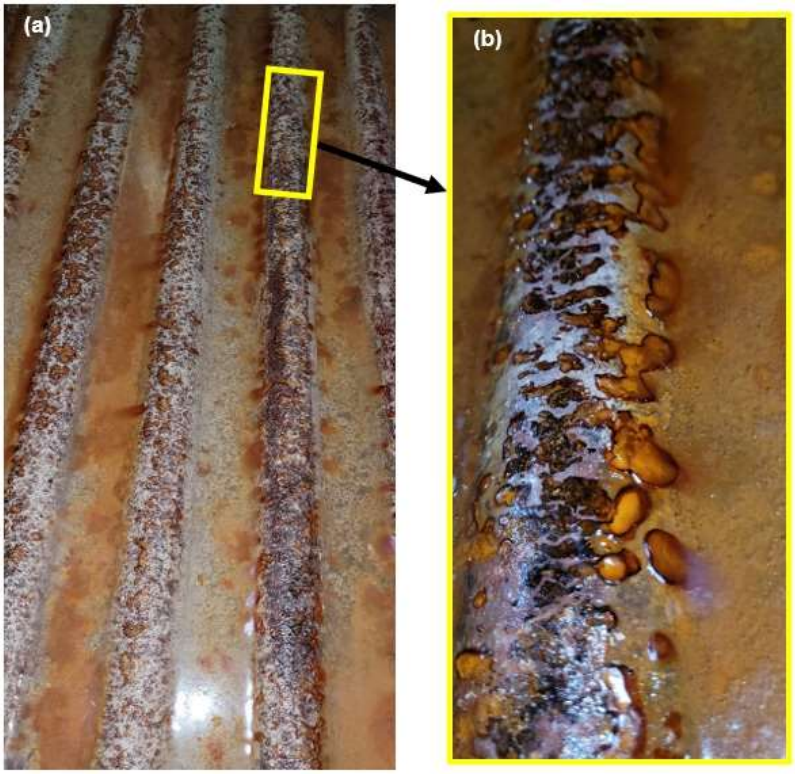

Figure 5-2. Submerged tubes in the flooded penthouse of the boiler

The boiler underwent immediate decommissioning, followed by the dewatering and thorough cleaning of the penthouse area, with a focus on the tubes. Samples were collected from the stagnant water and sent for laboratory analysis. Visual inspections revealed multiple failures in the tube coating, exhibiting holidays, localized corrosion, detachment, and under-deposit corrosion. Damage to the coating and underlying substrate is depicted in Figures 5-3 to 5-5. Furthermore, stains were observed on the fibrous stone wool insulation covering the overhead piping. Upon removing the insulation and conducting further inspections, significant localized damage was discovered on the surface of the overhead pipes, as shown in Figure 5-6.

Figure 5-3. Coating detachment and the localized corrosion on the tubes

Figure 5-4. Coating blistering and under-deposit corrosion on the tubes

Figure 5-5. (a) Pitting corrosion on the tubes skin (b) Dye penetrant test on the tubes

Figure 5-6. (a) Stains on thermal insulation and (b) coating damage & localized corrosion on the pipe skin for the overhead piping

The removal of rust scale and debris from the tubes and overhead pipes was accomplished using powered wire brushing, followed by inspections to evaluate the remaining thickness and its suitability for continued service. It was determined that the tube thickness remained above the retirement threshold. Subsequently, the insulation on the overhead pipes and penthouse enclosure was reinstated, followed by commissioning and startup procedures. A comprehensive investigation was also undertaken to ascertain the factors contributing to moisture ingress and subsequent damage to the coating. Finally, recommendations were made for periodic in-service inspections and future repairs to the coatings.

5.4 DISCUSSION

The boiler under investigation was included in the asset integrity management program, undergoing thorough assessment during design and throughout operation to screen for potential damage mechanisms (DM's) such as fuel ash corrosion, high-temperature oxidation, carburization, and corrosion under insulation (CUI), among others, in accordance with relevant industry standards [33]. During the DM screening process, no significant risks were identified concerning the penthouse area and specifically the primer-coated tubes. A review of construction records (i.e., dossiers) also confirmed the absence of any notable non-conformance during construction and pre-commissioning activities. The dry film thickness (DFT) of the inorganic zinc epoxy coating ranged from 40 to 80 μm, falling within the specified range. Additionally, the insulation used in the penthouse compartment and overhead piping within the compartment was fibrous stone wool, meeting the applicable specifications.

Despite meeting these requirements, the failure of the coating raised concerns, considering that inorganic zinc epoxy is known for its ability to protect the underlying steel through galvanic protection, acting as a more active element (anode) in the event of coating damage such as holidays. In response, a comprehensive investigation was carried out, involving laboratory testing of collected water samples to analyze their chemistry, pH levels, microbial content, possible sources, and more. Simultaneously, thorough inspections of the coatings on the tubes, overhead piping, and insulation were conducted. Laboratory reports confirmed that the water accumulated in the penthouse compartment was rainwater, ruling

out the possibility of steam or polished feed water leaks. Regarding moisture and rainwater intrusion, it became evident that the jacketing had suffered damage, with fish-mouth openings exposing the underlying insulation to moisture ingress along the edges. Figure 5-7 illustrates a typical example of fish-mouth in the jacketing.

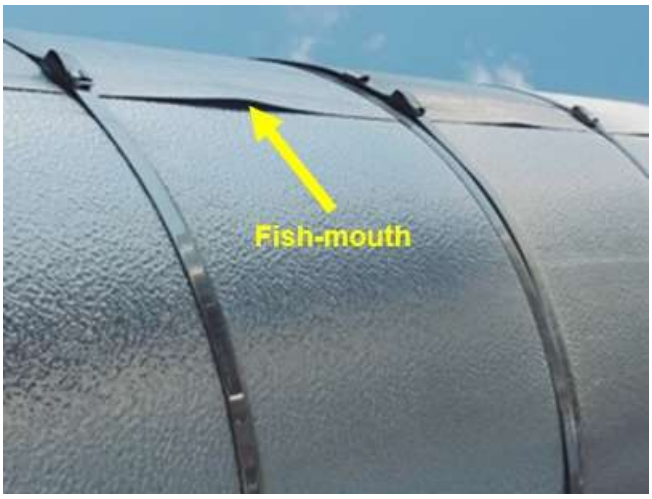

Figure 5-7. Typical fish-mouthing in the jacketing over thermal insulation

The jacketing damage was primarily due to human activity around the penthouse. The deformed jacketing remained unaddressed because there were no follow-up inspections or reinstatements during post-construction punch list items. Proper attention to such details could have significantly reduced the potential for rainwater intrusion. Visual inspection and odor indicated the water had been stagnant for some time, confirmed by laboratory analysis showing high microbial counts and colony-forming units (CFU). Industry practices for hydrostatic testing of large-volume equipment recommend disposing of the water within 15 days or using oxygen scavengers to prevent microbial growth [51]. Therefore, the stagnation of rainwater could have triggered microbiologically influenced corrosion (MIC) [33].

Inorganic zinc oxide epoxies are recognized for their galvanic protection during handling, transportation, and dry operating conditions. The penthouse tubes operated at around 400°C, ensuring arid conditions on and around the tubes and the inorganic zinc epoxy coatings. However, the intrusion of rainwater created submerged conditions around the

coated tubes. In the hot and moist environment, with temperatures exceeding 60°C, a galvanic reversal occurred, where the zinc-containing primers acted as a cathode relative to the underlying substrate [52], [53]. Any holidays or defects in the coating then acted as anodes, leading to accelerated corrosion at these locations, as explained below:

$$\text{Galvanic corrosion} \propto \frac{\text{Surface area}_{\text{Cathode}}}{\text{Surface area}_{\text{Anode}}} \qquad \text{Equation 5– 1}$$

Referring to Figure 5-4 (a), coating blisters are clearly visible, while Figure 5-4 (b) illustrates localized damage to both the coating and substrate (tubes) at the weld joints and heat-affected zone (HAZ). Figure 5-5 (a) shows localized damage accompanied by multi-colored scale deposits. Figure 5-5 (b) reveals underlying damage, such as pits, discovered after the removal of scale deposits and subsequent dye penetrant examination. Conventional epoxy coatings, unless specifically designed for immersion service, often contain micro-sized pores resulting from factors like paint atomization, deposition patterns, environmental conditions, and workmanship. These pores can allow moisture and waterborne nano-sized ions (e.g., chlorides, carbonates) to penetrate, leading to under-deposit (crevice) corrosion and subsequent blistering. Localized corrosion around welds and the HAZ can be attributed to defects or holidays in the paint at these locations. Zinc-rich primers or coatings are renowned for their self-healing properties, which can be compromised when exposed to chlorides, sulfides, or alkalis. The presence of chlorides, in addition to causing galvanic reversal, likely impaired the healing properties and the protective effect of the inorganic zinc primer [53].

Despite the insulation applied to the penthouse enclosure and overhead piping, the risk of corrosion under insulation (CUI) was considered low due to the operating temperature being well above the typical CUI temperature range [33]. However, visual inspections of the overhead piping revealed significant corrosion and damage to the coating beneath the insulation. This occurred because rainwater dripped onto the overhead pipe, soaking the insulation and creating a moist environment on the pipe's surface through wicking. The overhead piping was coated with inorganic zinc epoxy, which exhibited failure due to galvanic reversal effects similar to those observed on the submerged tubes (refer to Figure

5-6) [51]. Additionally, the chemical nature of the insulation can exacerbate the risk of corrosion through the release of aggressive leachate ions (e.g., chlorides, sulfates, carbonates). These leachate ions, along with waterborne ions from rainwater, can penetrate the coating's pores due to their nano size, accelerating the degradation process [6]. Figure 5-8 illustrates the schematic of the coating damage sequence resulting from submersion conditions.

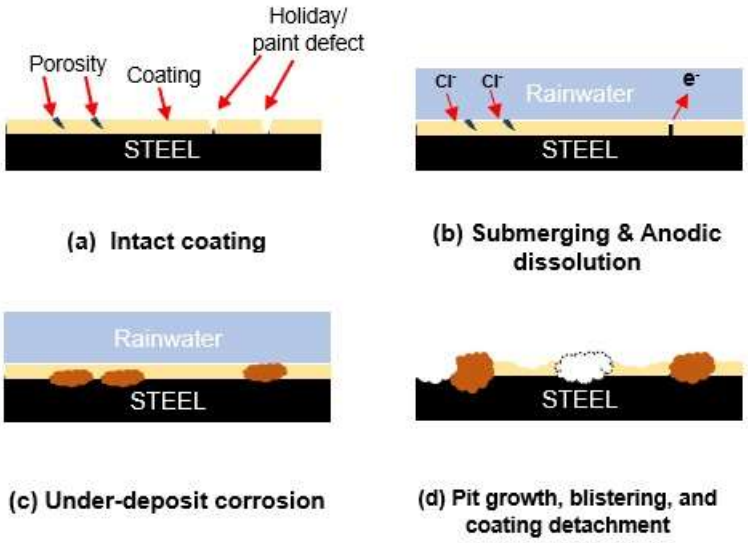

Figure 5-8. Schematic of coating degradation from coating defects on the tubes and overhead pipe from submerging with rainwater

As seen in Figures 5-2 through 5-6, the rust on the tubes and overhead pipe exhibits a variety of colors and morphologies. The rust scale is present in yellowish, reddish-brown, and even black hues. High-temperature oxidation of steel, known as dehydrated corrosion, typically produces magnetite (Fe_3O_4), which appears black and can protect the underlying steel unless damaged or formed intermittently. However, when magnetite undergoes hydrolysis in the presence of oxygen, it transforms into reddish-brown goethite (α-FeOOH) through the following reaction [45].

$$\frac{3}{4}O_2 + 3Fe_3O_4 + \frac{9}{2}H_2O \rightarrow 9FeOOH \qquad \text{Equation 5– 2}$$

The rust scale on the overhead pipe's surface exhibits heterogeneous morphology and varying rust colors due to the presence of insulation, which creates oxygen-concentration

cells at the insulation-pipe interface. In oxygen-rich areas, the moist conditions lead to the formation of reddish-brown oxyhydroxides such as goethite (α-FeOOH) and akaganeite (β-FeOOH). Conversely, oxygen-deprived spots result in the formation of dark black magnetite (Fe_3O_4) patches, as shown in Figure 5-6 (b). The presence of chlorides may further contribute to the formation of akaganeite (β-FeOOH). Additionally, the appearance of orange-colored scale or stains can be attributed to the presence of iron chlorides [34].

In addition to waterborne leachates from insulation and rainwater, boiler tubes may also be subjected to airborne leachates carried by air or cooling tower drift. To mitigate such risks, facility layouts generally position the boiler, particularly the air intake sections, away from cooling tower drift to avoid dew point corrosion [33]. Additionally, operating conditions and integrity operating window (IOW) programs recommend specific operating and mothballing temperatures to prevent dew point corrosion and other related damage mechanisms. Despite these proactive measures taken during the early design phase, the risk of submerging and flooding remains remote. In this instance, the flooding resulted primarily from mechanical damage to the insulation and jacketing. This issue could have been mitigated through design modifications, such as structural platforms to provide access to the penthouse surroundings. Additionally, using an insulation system with high compressive strength, incorporating stand-off membranes, could have prevented the deformation of the jacketing and insulation [27].

In addition to boilers, inorganic zinc primers are extensively used on thermally insulated equipment and pipes. Thermal insulations often absorb moisture through condensation or direct intrusion, leading to moisture-saturated conditions. These conditions can trigger galvanic reversal at temperatures exceeding 60°C (140°F), resulting in accelerated corrosion and undermining the protective purpose of these coatings. Implementing insulation designs that either prevent moisture ingress or facilitate the drying of insulation can significantly reduce the failure rates associated with inorganic zinc epoxies and other coatings on thermally insulated systems [6].

5.5 CONCLUSIONS

This study delves into a critical failure incident concerning the primer coatings applied to boiler tubes and the overhead insulated pipe within a boiler's penthouse section, treated with inorganic zinc epoxy primer. Through a meticulous analysis of field observations and relevant literature, the study uncovers key insights and offers practical recommendations. Here are the key takeaways from this investigation:

1 Coating failure inquiries should encompass a comprehensive review of surrounding conditions and external factors, recognizing that coatings can succumb to unforeseen external influences.
2 While inorganic zinc epoxies are prevalent in high-temperature applications, vigilant measures must be taken to shield them from moisture exposure, which can trigger galvanic reversal and subsequent coating breakdown.
3 Thermal insulation's vulnerability to moisture infiltration poses a risk to underlying inorganic zinc coatings, especially under high-temperature conditions where galvanic reversal can occur. Instituting strategies to ensure insulation dryness is essential in mitigating the risk of inorganic zinc epoxy coating failures.
4 Design provisions should be incorporated in susceptible areas to minimize moisture ingress, human-induced damage, and mechanical stresses. This includes utilizing structural platforms and implementing high-strength jacketing and insulation materials to fortify critical components against potential failure scenarios.

CHAPTER 6. AN INVESTIGATION OF CORROSION BEHAVIORS OF THERMALLY SPRAYED ALUMINUM (TSA) AT ELEVATED TEMPERATURES UNDER THERMAL INSULATIONS AND AUTOCLAVE IMMERSION CONDITIONS

6.1 ABSTRACT

Thermally Sprayed Aluminum (TSA) offers protection against internal and external corrosion across various industrial applications. Despite extensive research on TSA coatings, there remains a need for deeper insights into their degradation mechanisms, particularly under immersion conditions and moisture-saturated thermal insulations.

This study explores the corrosion behavior of TSA in a Corrosion Under Insulation (CUI) simulation setup (per ASTM G189-07) and autoclave immersion. Corrosion tests were conducted over three and four days under isothermal wet (IW) and cyclic wet (CW) conditions. Linear polarization resistance (LPR) scans were performed during both the CUI simulation and autoclave immersion tests to gain a comprehensive understanding of TSA's corrosion behaviours. Post-corrosion testing, detailed microstructural examinations were carried out using confocal laser microscopy, 3D topography, scanning electron microscopy (SEM), and energy-dispersive spectroscopy (EDS) to analyze the microstructural and tribological changes due to corrosion.

Results showed that TSA coating under insulation experienced significant degradation through flashing moisture and active iron dissolution at the insulation-metal interface. Unlike immersion conditions, the wear of TSA caused by flashing moisture under thermal insulation created crevices, leading to active corrosion of the steel substrate. The results underscore the crucial importance of considering the complete environmental context when selecting and implementing corrosion protection strategies for industrial applications. [54]

6.2 INTRODUCTION

Thermal insulation is extensively employed in industrial, energy, and hydrocarbon processing facilities to conserve heat in pipes, pipelines, and equipment. However, corrosion under insulation (CUI) is a prevalent damage mechanism in these thermally insulated systems, often manifesting as localized corrosion and pitting [33]. Reports indicate that CUI accounts for 10% of maintenance expenditures in a typical oil refinery, and 40-60% of piping failures are attributed to CUI [5]. This type of damage can progress unnoticed during routine visual inspections unless the insulation is stripped off or specialized non-destructive examinations (NDE) are employed. Predicting CUI is challenging due to its non-linear progression, influenced by factors such as time of wetness (TOW), differential oxygen starvation, temperature fluctuations, insulation aging, and coating degradation. Many of these factors remain unquantified or unnoticed in real-life inspection programs as protocols for their quantification are not well-established [45]. Industry practices often consider coatings as the last line of defense against corrosive moisture under thermal insulation [55]. Various coatings are applied to mitigate CUI, but their effectiveness varies depending on the application, type of coating, operating conditions, and external factors. Thermally sprayed aluminum (TSA) is one system known for managing internal and external corrosion across different applications. TSA offers advantages over conventional epoxy coatings, such as a solvent-free matrix, better adhesion, hardness, and toughness. Unlike traditional epoxy coatings, TSA is less prone to degradation issues like blistering, peeling, or layer detachment under thermal insulation. Despite being adopted for over four decades to protect structures, the degradation mechanisms of TSA in CUI applications are not fully understood [23], [56].

Numerous studies have explored the corrosion behaviours of thermally sprayed aluminum (TSA). A study by Hornus et al. examined deposit formation on TSA surfaces during seawater immersion, with and without cathodic protection [56]. This research focused on deposit growth in seawater rather than corrosion under insulation (CUI). Knudsen et al. investigated the high-temperature behavior of TSA in subsea mud and the effectiveness of barrier coatings on TSA under seawater immersion [57]. This study used different electrolyte and test cell configurations, making them less representative of TSA

degradation under thermal insulation. Arrabel et al. studied TSA behavior in a salt fog cabinet at 35°C, reflecting atmospheric corrosion rather than CUI [58]. Lee et al. examined TSA's seawater immersion behavior at ambient temperatures, which differs from the conditions typically seen in CUI, focusing on immersion rather than crevice conditions [24]. Ortega et al. reported on TSA's tribological behavior in an artificial seawater environment, while Paul studied the corrosion behavior of intact and scribed TSA coatings under seawater immersion [20], [22]. Despite these efforts, there remains insufficient research on the degradation behavior and corrosion modes of TSA under moisture-saturated thermal insulations, a common issue in the industry and a primary cause of CUI.

High temperatures and crevices at the insulation-TSA interface result in a unique form of TSA degradation compared to immersion conditions. Kane et al. previously studied the CUI behavior of TSA coatings under two types of insulation: fibrous stone wool and calcium silicate (Calsil), utilizing a CUI simulation test cell according to ASTM G189-07 [59] This study tested at 82°C and 110°C under both wet and dry conditions. ASTM G189-07 quantifies CUI rates using the in-situ linear polarization resistance (LPR) method, which necessitates a wet system with proper counter electrode (CE) placement away from the working electrode (WE) [46]. Consequently, the standard requires a gap between the insulation and the coupon to allow for CE placement. However, in most real-life applications, insulations are tightly held against the pipe’s surface. This gap in the CUI simulation tests, intended for CE placement, may have overlooked the effects of oxygen concentration cells, which drive localized pitting under typical fibrous stone wool insulation, as highlighted in Rana et al.'s study [6].

This study examines the high-temperature corrosion behavior of TSA coatings by investigating the impact of crevices formed from direct contact between moisture-saturated insulation and the TSA-coated pipe, as well as comparing it to simple boiling water immersion without insulation, an aspect previously unaddressed. To accomplish this, two distinct test environments are utilized: autoclave immersion and CUI simulation per ASTM G189-07 [46]. Detailed microstructural characterizations follow these tests to provide comprehensive insights.

6.3 EXPERIMENTAL INVESTIGATIONS

Ring-shaped steel coupons, 2 inches wide, were machined from a 3-inch nominal size (NPS) carbon steel pipe (A106 Gr. B). In this study, these are referred to as ring-shaped coupons. Additionally, cylindrical pucks with a diameter of 16 mm and a thickness of 5 mm were machined from a mild steel billet (AISI Gr. 1018). The outer surfaces of the ring-shaped coupons and the top faces of the cylindrical pucks were cleaned using high-pressure blasting with alumina particles (grit size: 16), achieving a surface finish of 3.2 per SP-5 blasting grade. The prepared surfaces were thermally sprayed in multiple passes with Grade 1350 aluminum powder (particle size: 38-90 μm) using a flame spray gun with a thermal power of 28 kW, mixing oxygen at 4 bar and 2,000 L/hr with acetylene (C_2H_2) at 0.7 bar and 1,800 L/hr. The application parameters are summarized in Table 6-1. Ultrasonic thickness measurements confirmed a TSA thickness of 12-20 mils (300-500 μm). Figure 6-1 (a-b) shows the morphology and EDS map of iron Kα1 (a contaminant) for the Grade 1350 aluminum powder, with the chemical composition summarized in Table 8.

Table 6-1 TSA application parameters

Parameter	Particle speed (avg.)	Material feed rate	Spray stand-off distance	Transverse gun displacement
Value	300 m/s	1 gm/ s	20 cm	150 cm/ minute

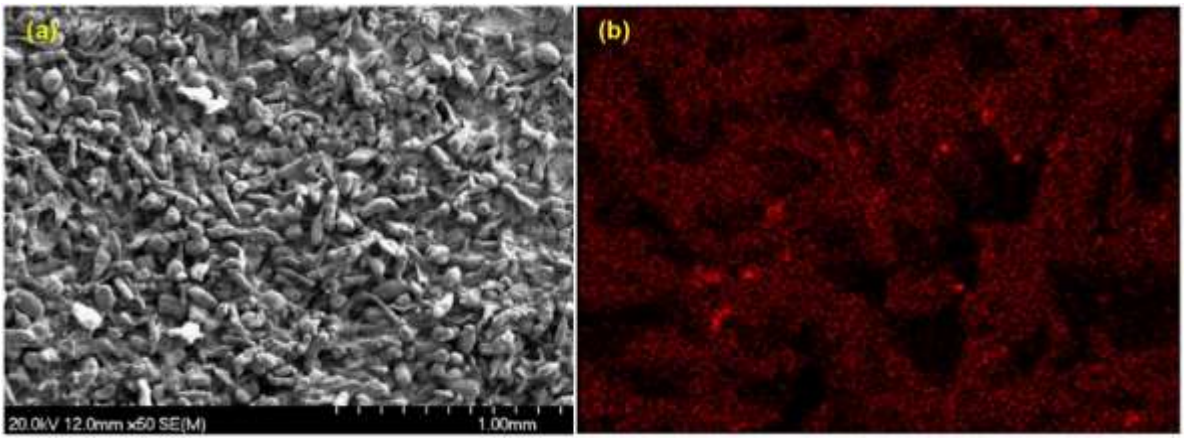

Figure 6-1 (a) SEM micrograph and (b) EDS map of iron Kα 1 for aluminum 1350 powder

Table 6-2 Chemical composition of typical grade 1350 aluminum powder

Element	Si	Iron	Others	Al
Conc. (wt.%)	0.03	0.1 - 0.4	0.300	Bal.

Figure 6-2 (a) and Figure 6-2 (b) depict the setups for the CUI simulation test cell (according to ASTM G189-07) and the autoclave immersion test cell, respectively. In the CUI simulation test cell, the insulation is partially removed to reveal the arrangement of the coupons and spacing rings. The ring-shaped coupons were affixed with epoxy and carbon fibre mesh and allowed to cure. After curing, the coupons were mounted in the test cell and then wrapped with fibrous stone wool insulation and aluminum jacketing (thickness: gauge 18). The coupon served as the working electrode (WE), the carbon fibre mesh as the counter electrode (CE), and a saturated calomel electrode (SCE) was used as the reference electrode (RE).

A typical setup for the CUI simulation test (per ASTM G189-07) includes an annular gap between the insulation and the coupon (i.e., WE) to allow for the placement of a CE, facilitating the measurement of corrosion current between the CE and WE. However, this gap does not accurately reflect real-world conditions, where thermal insulations are usually in direct contact with pipes. This direct contact typically leads to oxygen concentration cells, resulting in localized pitting via anodic dissolution, as observed in a study by Rana et al. [6]. The annular gap, designed to accommodate the CE, creates an environment lacking significant crevices and oxygen concentration cells, resulting in lower corrosion rates than actual crevice conditions. In the current study, the CUI simulation test employs a ring-shaped coupon with a carbon fibre mesh as the CE, adhered to the coupon (or WE) using epoxy (see Figure 6-2). The protruding carbon fibre mesh over the epoxy is tightly connected to the insulation. A small notch was created in the insulation to accommodate the protruding carbon fibre mesh and epoxy while ensuring tight contact between the insulation and the coupon/WE surface. This modified design facilitates electrochemical readings while mimicking the direct contact between the insulation and the coupons.

Type IV de-ionized water with 100 ppm NaCl was used as the electrolyte. A pre-measured volume of this electrolyte was added each day to maintain wet conditions. Open circuit potential (OCP) measurements were taken for 30 minutes daily, followed by potential scanning within a range of +/- 50 mV around the OCP at a scan rate of 0.125 mV/sec. As detailed in Table 9, CUI simulation tests were conducted under isothermal wet (IW) and cyclic wet (CW) conditions for 72 hours and 96 hours, respectively [46]. Throughout the testing period, the surface temperatures of the coupons were monitored to set the parameters for the subsequent autoclave immersion tests. For the autoclave immersion tests, an electrical wire was attached to the uncoated side of the cylindrical pucks. The pucks were then encased in waterproof epoxy, ensuring that only the TSA-coated surface was exposed to the electrolyte during the autoclave immersion testing.

The autoclave electrolyte was prepared using leachate extracts from stone wool insulations, following ASTM C871 to simulate the chemical effects of insulations. This approach was taken because fibrous stone wool insulations can leach various ions, such as Cl^- and carbonates, which influence CUI rates. A 20 g sample of stone wool insulation was mixed with 300 ml of de-ionized water to create the leachate. The mixture was thoroughly stirred and then filtered. The resulting leachate extract solution was heated to 85°C and diluted with de-ionized water to a final volume of 500 ml. The solution's pH was measured with a pH meter, and its elemental composition was analyzed using inductively coupled plasma mass spectroscopy (ICP-MS) [60]. The final leachate solution was then transferred to an autoclave where the cylindrical pucks (WE) were submerged, simulating continuous immersion. A platinum mesh served as the CE, and a saturated calomel electrode (SCE) was used as the RE. The temperature in the autoclave was maintained to match the surface temperature of the ring-shaped coupons during CUI simulation tests, ensuring consistent testing conditions. Table 9 outlines the testing conditions for both the CUI simulation and autoclave immersion tests. Polarization resistance (R_p) was determined from the slope of the E/I (voltage/current) graphs, and the corrosion current density (i_{corr}) was calculated using the Stern-Geary equation [35].

$$i_{corr} = \frac{b_a \times b_c}{R_p \times 2.303 \times (b_a + b_c)} \qquad \text{Equation 6– 1}$$

Since the polarization was limited to a very small scanning region, the slopes of the anodic and cathodic branches, b_a and b_c, were both assumed to be 120 mV/decade. This is generally considered a safe assumption because it ensures $b_a/2.303$ and $b_c/2.303$ are greater than $E\text{-}E_{oc}$. The corrosion current density (i_{corr}) calculated from equation (1) was then converted to the corrosion rate (CR) using equation [61].

$$CR = 0.00327 \times i_{corr} \times \frac{EW}{\rho} \qquad \text{Equation 6– 2}$$

The density of the TSA matrix, denoted by ρ, was determined using the fractional densities of its constituent elements (Al and iron). The equivalent weight (EW) was calculated using the equation below [62].

$$EW = \frac{1}{\left\{\frac{f_1 \times e_1}{Z_1}\right\} + \left\{\frac{f_2 \times e_2}{Z_2}\right\}} \qquad \text{Equation 6– 3}$$

Whereas

f = Weight fraction of constituent element (wt. % from EDS results)

e = Ion exchanging capacity (i.e., valency) of constituent element (e.g. 3 for Al, 2 for iron)

Z = Atomic weight of constituent element (grams)

The mentioned tests were performed twice on every TSA sample, which were prepared in two distinct batches by the same contractor within a commercial environment.

6.4 MICROSTRUCTURAL CHARACTERIZATIONS

Following the completion of corrosion tests, the coupons underwent extraction from the cells and subsequent cleaning and visual inspections. Utilizing a confocal laser microscope (Keyence VK-X1000), the coupons were scanned at multiple points (each spot measuring 4 mm x 4 mm) and stitched together to produce detailed 2D micrographs and 3D topographs corresponding to the scan areas. Surface roughness data was extracted from the

generated 3D topographs [63]. Additionally, the surfaces of the coupons underwent characterization through scanning electron microscopy (SEM) and energy dispersive spectroscopy (EDS) to analyze the damage mechanisms and chemical composition of the TSA, respectively. Cross-sections of the coupons were then prepared using a CBN (carbon boron nitride) blade and mounted for examination. Grinding with Grit 600 SiC grinding paper followed by polishing with mono-crystal diamond solutions of 9 µm, 3 µm, and 1 µm in incremental steps was performed on the mounted cross-sections. These cross-sections were further analyzed using confocal laser microscopy, SEM, and EDS techniques.

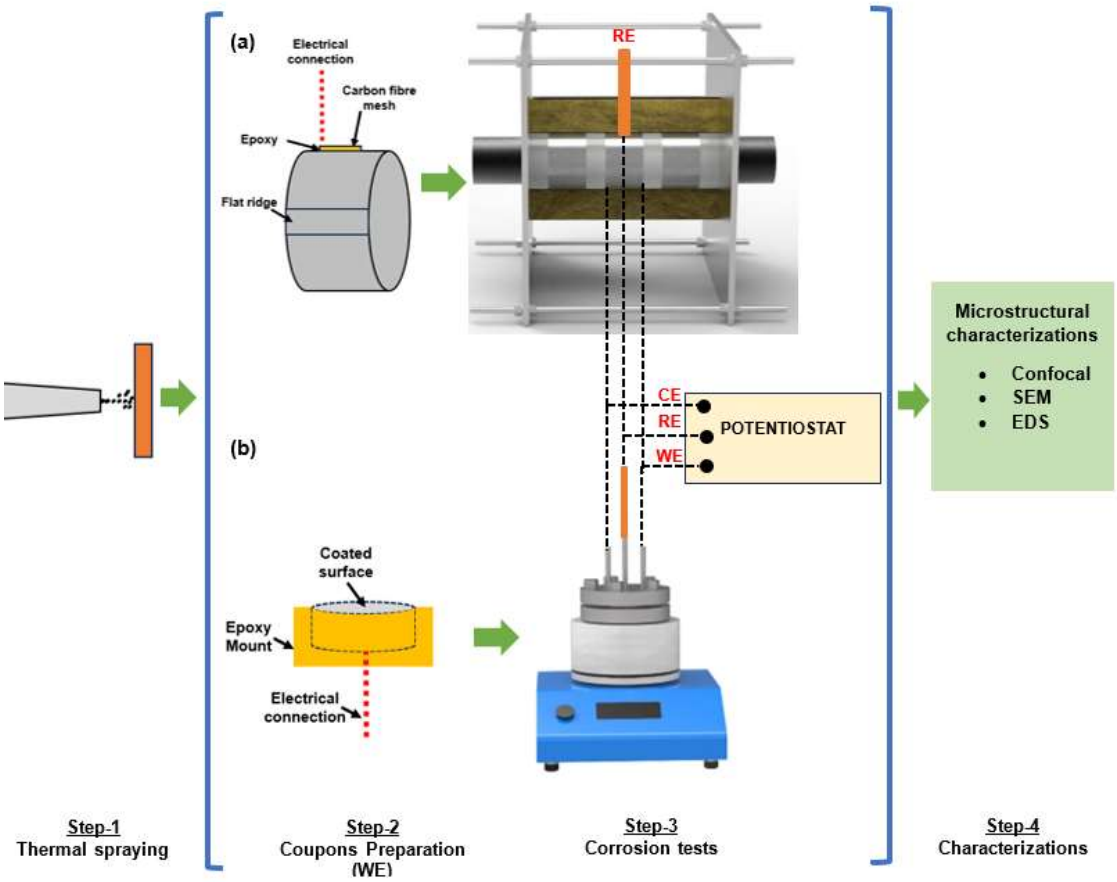

Figure 6-2 Experimental setup for (a) CUI simulation test (b) autoclave immersion tests

Table 6-3 Testing conditions for the CUI simulation and autoclave immersion tests

TEST TYPE	TEST CONDITION	DURATION (hrs)	ELECTROLYTE	TEMPERATURE (ºC) FOR IMMERSION HEATER	TEMPERATURE (ºC) @ COUPON SURFACE
CUI simulation (ASTM G189-07)	Isothermal wet (IW) *	72	100 ppm NaCl	170ºC	100ºC
	Cyclic wet (CW) **	96		170ºC ~ 100ºC	100ºC ~ 70ºC
Autoclave Immersion	Isothermal wet (IW) *	72	Insulation leachate extract per ASTM C871	-NA-	100ºC
	Cyclic wet (CW) **	96		-NA-	100ºC ~ 70ºC
* For IW, temperature was held constant for three days ** For CW, temperatures on odd days (i.e., 1 & 3) was kept at high end of temperature cycle, and on even days (i..e, 2 & 4) temperature was at low end of temperature cycle					

6.5 RESULTS

Figure 6-3 (a-d) illustrates the pre-and post-test conditions of the ring-shaped coupons and cylindrical pucks exposed to IW conditions. The ring-shaped coupon subjected to IW conditions exhibited scattered white and reddish-brown spots, as shown in Figure 6-3 (b). In contrast, the autoclave immersion coupon in Figure 6-3 (d) displayed a dark grey appearance. Further microscopic analysis using confocal laser scanning revealed that the reddish-brown spots on the ring-shaped coupons (under both IW and CW conditions) were distributed over the surface in both isolated and interconnected patterns, as seen in Figure 6-4 (a-b) and Figure 6-5 (a-b). As shown in Figure 6-4 (c-d) and Figure 6-5 (c-d), the cylindrical pucks subjected to autoclave immersion tests did not exhibit noticeable surface damage or reddish-brown rust stains, unlike the CUI simulation coupons. A concurrent analysis of Figure 6-4 (c-e) and Figure 6-5 (c-e) shows that the autoclave immersion coupons maintained a similar appearance to pristine coupons, with no significant pits or reddish-brown rust stains, in contrast to the ring-shaped coupons from the CUI simulation test.

Table 6-4 presents the surface roughness (S_z) and electrochemical results for all tested coupons. The ring-shaped coupons exposed to CUI simulation tests under both IW and CW conditions exhibited significantly higher surface roughness compared to both the pristine

coupons and the cylindrical pucks after autoclave immersion tests. The ring-shaped coupons from the CUI simulation tests displayed blunt surface features and interconnected voids, while the cylindrical pucks subjected to autoclave immersion showed minimal surface voids and a texture similar to the pristine coupons. The surface roughness of the autoclave immersion pucks under IW and CW conditions was 156.26 µm and 154.97 µm, respectively, slightly lower than the pristine coupon, which had a roughness of 171.29 µm (with a deviation of ±10%).

Figure 6-6 (a-d) illustrates the daily LPR trends for the CUI simulation and autoclave immersion tests under IW and CW conditions, respectively. Polarization resistance (R_p), calculated corrosion densities (i_{corr}) per equation 6-1, and corresponding corrosion rates per equation 6-2 are detailed in Table 6-6. For the ring-shaped CUI simulation coupon under IW conditions, the corrosion rate escalated from 0.247 mm/year on Day 1 to 2.765 mm/year on Day 3, accompanied by a decrease in Rp from 1.143 KΩ to 0.103 KΩ. In the CW condition, there was a steady daily increase in the corrosion rate, rising from 0.279 mm/year to 1.288 mm/year from Day 1 through Day 4, with a corresponding decline in Rp from 1.01 KΩ to 0.22 KΩ. For the autoclave immersion tests, the corrosion rate for the cylindrical puck under IW conditions gradually decreased from 0.37 mm/year on Day 1 to 0.295 mm/year on Day 3. Conversely, for the CW condition in the autoclave immersion test, the corrosion rate spiked from 0.324 mm/year on Day 1 to 1.08 mm/year on Day 2, then decreased to 0.662 mm/year on Day 3, followed by a sudden rise to 1.268 mm/year on Day 4.

Figure 6-7 (a-e) presents the SEM micrographs of the post-test TSA surfaces alongside the pristine TSA. The pristine TSA surface exhibits pores primarily within the 50 µm to 100 µm range, as seen in Figure 6-7 (e). In contrast, the ring-shaped CUI simulation coupons display significant voids, measuring approximately 300 µm to 400 µm, as illustrated in Figures 6-7 (a-b) for IW and CW conditions, respectively. However, the autoclave immersion pucks shown in Figures 6-7 (c-d) lack these voids, differing from the CUI simulation coupons. Additionally, the autoclave coupons subjected to IW and CW conditions exhibit no major porosity, resulting in a smoother surface compared to the

pristine TSA coupon shown in Figure 6-7 (e). This observation aligns with the surface roughness trends in Table 6-4, where autoclave immersion coupons under IW and CW conditions demonstrate a ~10% reduction in surface roughness compared to the pristine TSA (171.29 μm). Repeated experiments indicate that the post-test specimen roughness is dependent on the initial roughness of the pristine samples. Consequently, Table 6-4 reports the relative increase or decrease in surface roughness instead of absolute roughness to ensure consistency.

Table 6-4 Tribological and electrochemical results for the candidate coupons

TEST TYPE	**TEST CONDITION**	**RELATIVE CHANGE IN SURFACE ROUGHNESS, (vs PRISTINE)**	**DAY & (SURFACE TEMP.)**	**CORROSION CURRENT DENSITY (mA/cm^2)** $\pm$ 2%	**POLARIZATION RESISTANCE, R_p (kΩ)** $\pm$ 2%	**CORROSION RATE (mm/yr.)** $\pm$ 2%
CUI simulation (ASTM G189-07)	Isothermal wet (IW)	2-2.5 folds*	Day 1 (100ºC)	22.8	1.143	0.247
			Day 2 (100ºC)	72	0.362	0.781
			Day 3 (100ºC)	255	0.103	2.765
	Cyclic wet (CW)	2-2.5 folds*	Day 1 (100ºC)	25.7	1.01	0.279
			Day 2 (70ºC)	64.7	0.40	0.701
			Day 3 (100ºC)	110.2	0.23	1.195
			Day 4 (70ºC)	118.8	0.22	1.288
Autoclave Immersion	Isothermal wet (IW)	−10%**	Day 1 (100ºC)	34	0.384	0.369
			Day 2 (100ºC)	30.4	0.43	0.330
			Day 3 (100ºC)	27.2	0.48	0.295
	Cyclic wet (CW)	−10%**	Day 1 (100ºC)	29.9	0.437	0.324
			Day 2 (70ºC)	99.3	0.131	1.08
			Day 3 (100ºC)	61.1	0.214	0.662
			Day 4 (70ºC)	117	0.112	1.268

* Increase in surface roughness
** Decrease in surface roughness

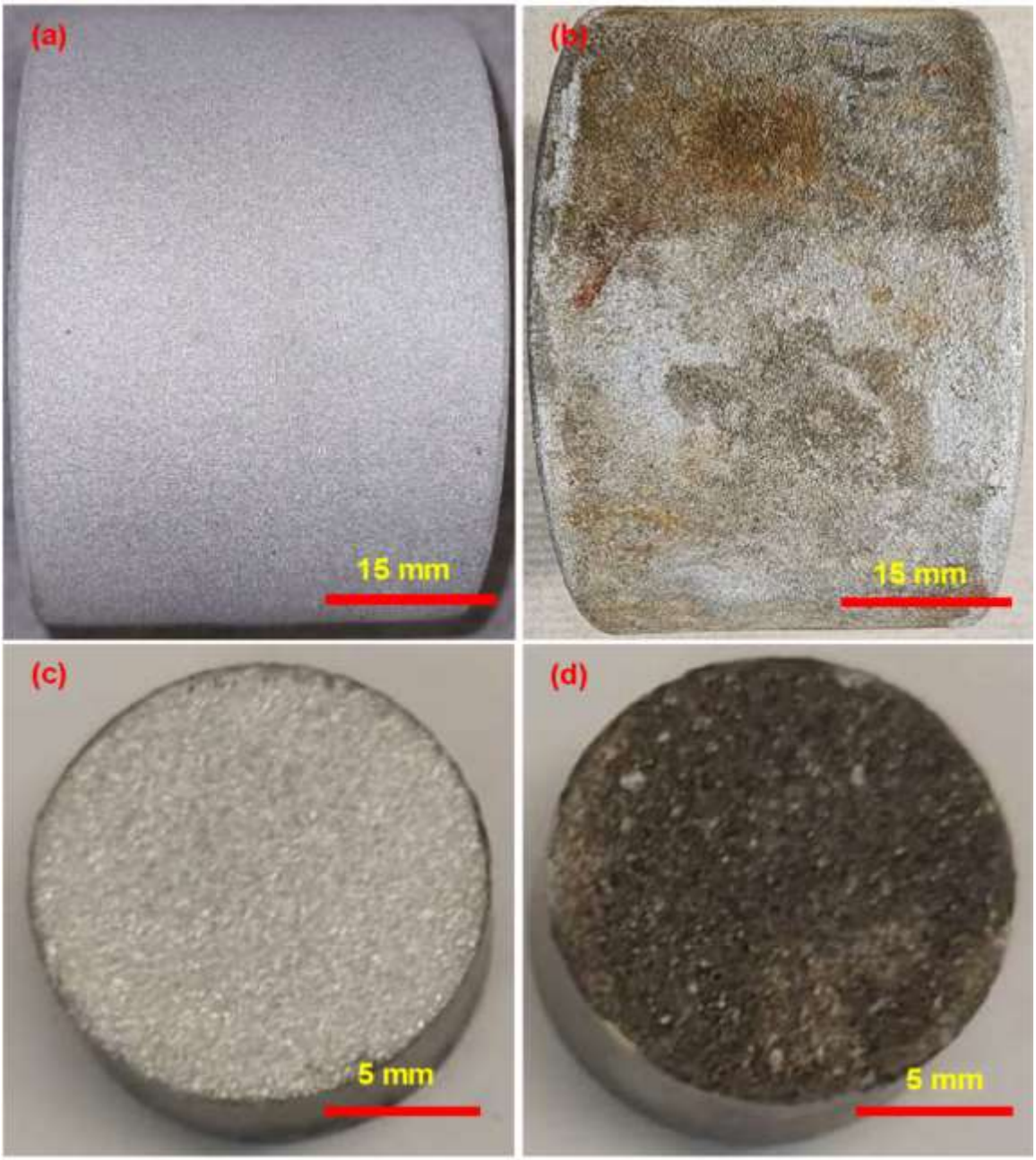

Figure 6-3 Photographs for TSA coupons as: (a) pristine ring-shaped coupon for CUI simulation test (b) post-CUI simulation test under IW (c) pristine cylindrical puck for autoclave immersion test (d) post-autoclave immersion test under IW

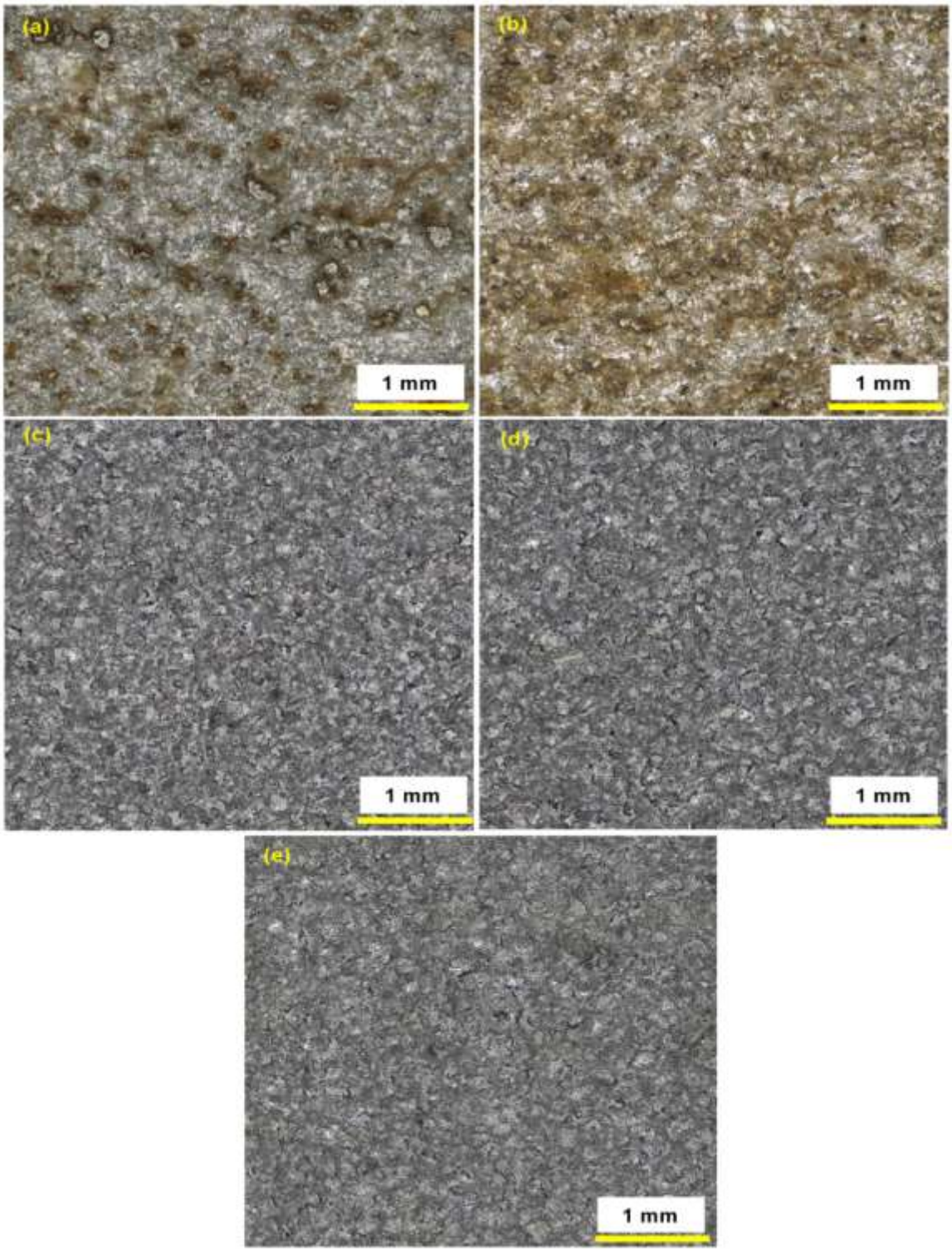

Figure 6-4 2D micrographs (mag. 100x) at the surface for (a) post-CUI simulation test under IW (b) post-CUI simulation test under CW (c) post-autoclave immersion test under IW (d) post-autoclave immersion test under CW (e) pristine TSA

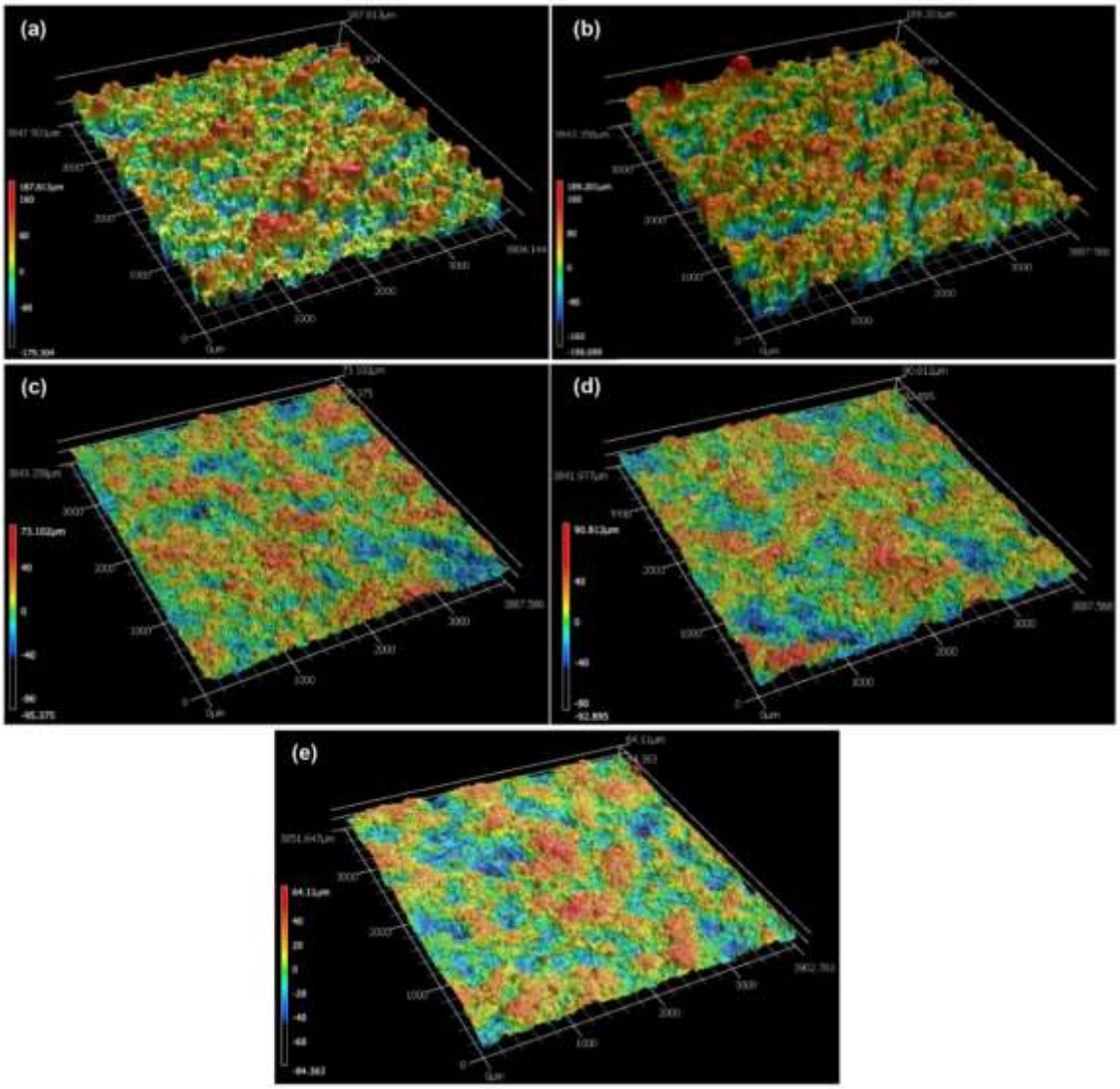

Figure 6-5 3D topo graphs (aspect ratio 1:1:2) at the surface for (a) post-CUI simulation test under IW (b) post-CUI simulation test under CW (c)) post-autoclave immersion test under IW (d)) post-autoclave immersion test under CW (e) pristine TSA

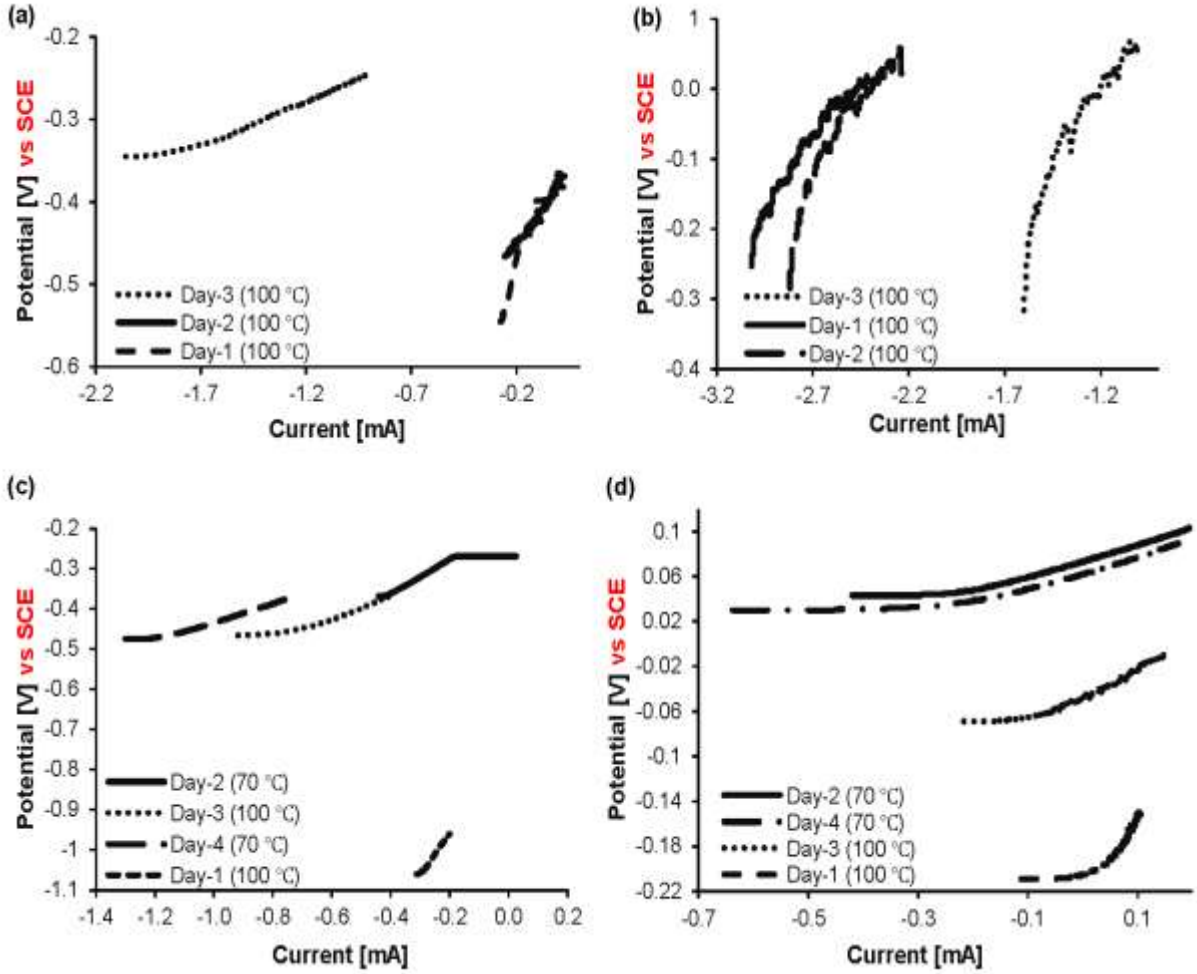

Figure 6-6 Day-wise LPR variations of TSA coupons from: (a) CUI simulation tests under IW (b) autoclave immersion test under IW (c) CUI simulation test under CW (d) autoclave immersion test under CW

Figure 6-8 (a-e) presents the cross-sectional micrographs of the post-test coupons from the CUI simulation tests, autoclave immersion tests, and as-sprayed pristine coupon. The CUI simulation coupons exhibit crevices that correspond to surface voids, as shown in Figures 6-8 (a-b). In contrast, the autoclave immersion coupons in Figures 6-8 (c-d) do not display any crevices. For both test types, there is no evidence of delamination between the substrate and the TSA, and no cracks or blisters are observed.

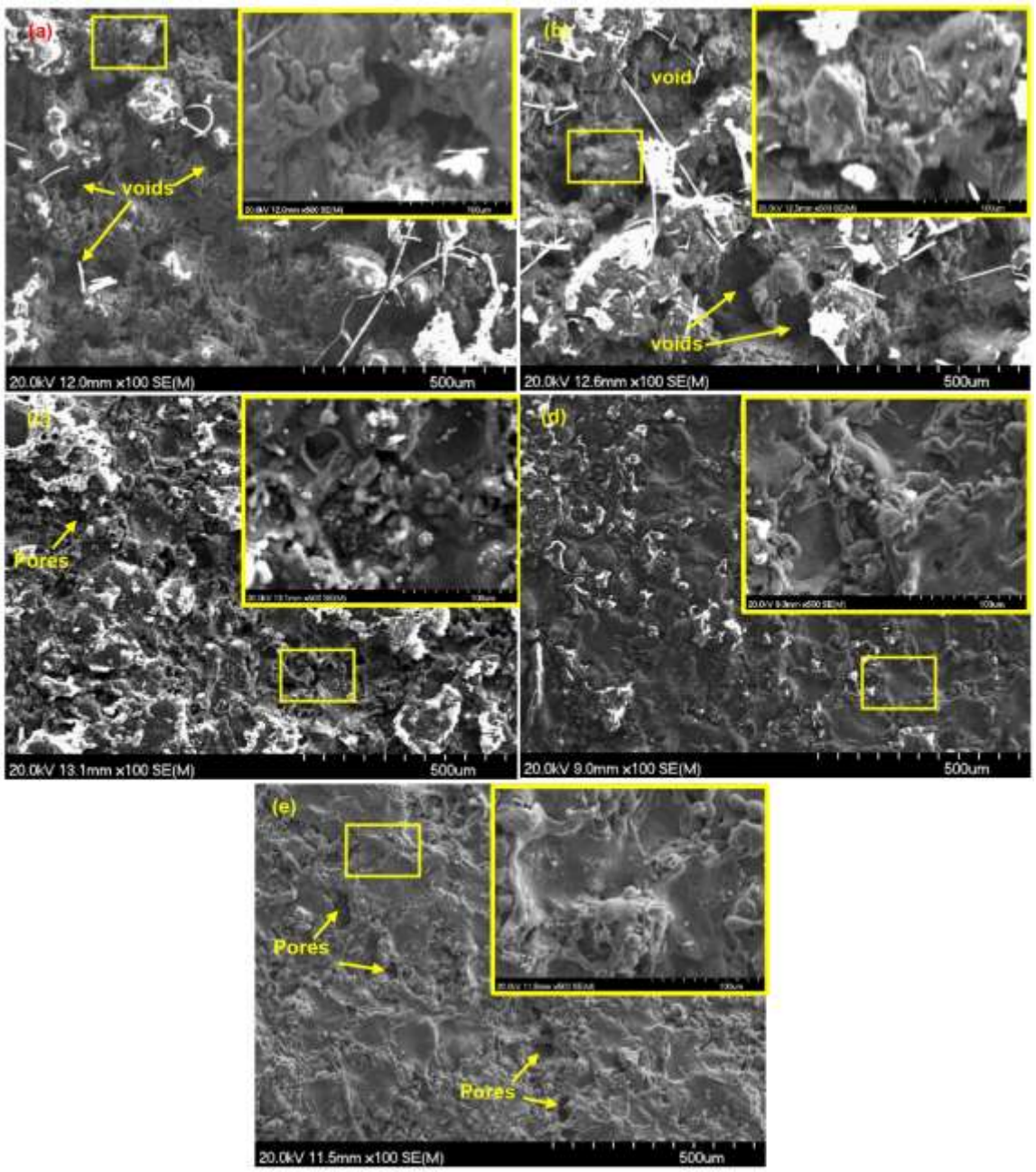

Figure 6-7 SEM micrographs at the surface for (a) post-CUI simulation test under IW (b) post-CUI simulation test under CW (c)) post-autoclave immersion test under IW (d)) post-autoclave immersion test under CW (e) pristine TSA

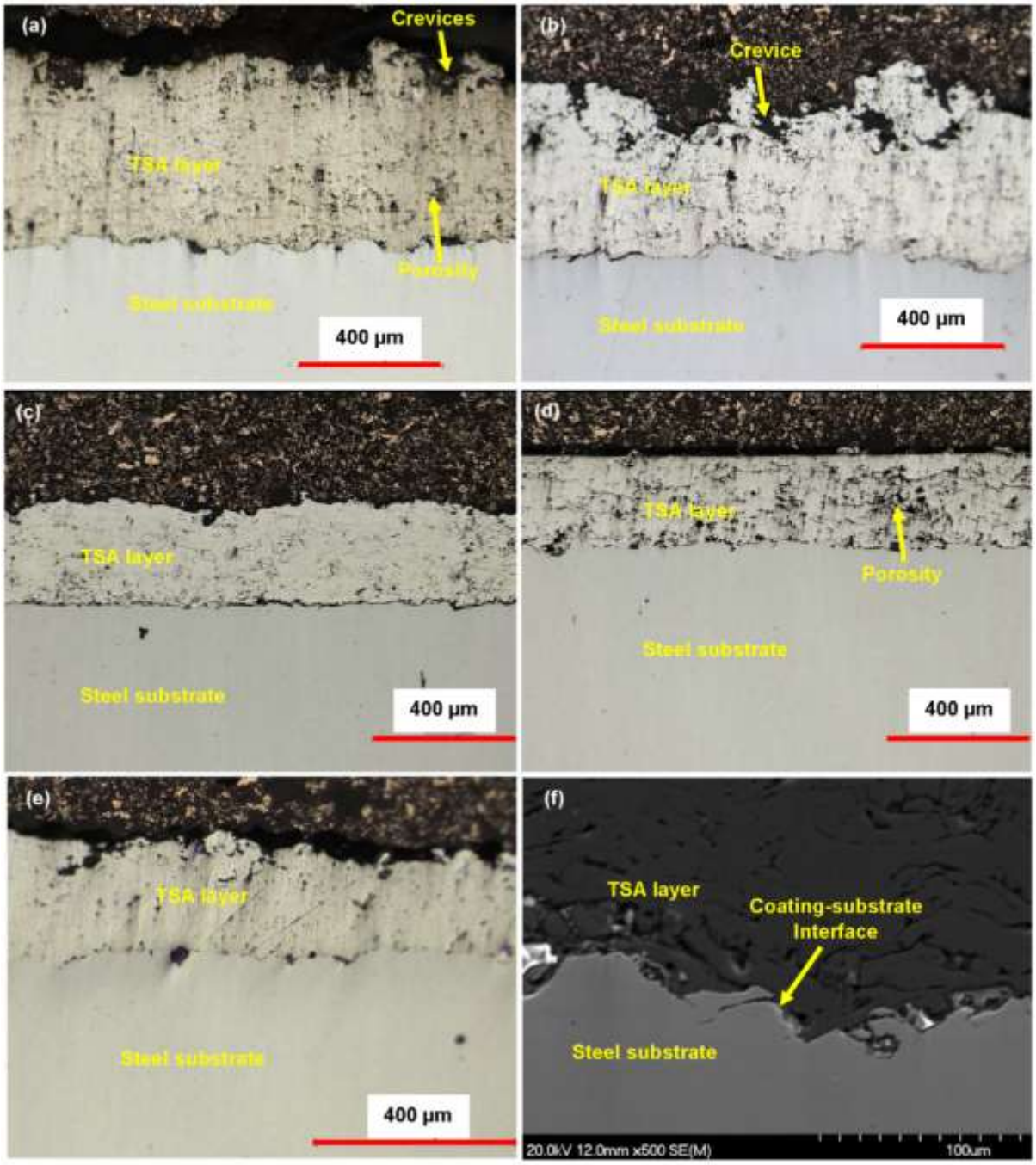

Figure 6-8 Micrographs (mag. 100 x) along cross-sections for: (a) post-CUI simulation test under IW (b) post-CUI simulation test under CW (c) post-autoclave immersion test under IW (d) post-autoclave immersion test under CW (e) pristine TSA coupon and (f) SEM micrograph for post-CUI simulation test under CW

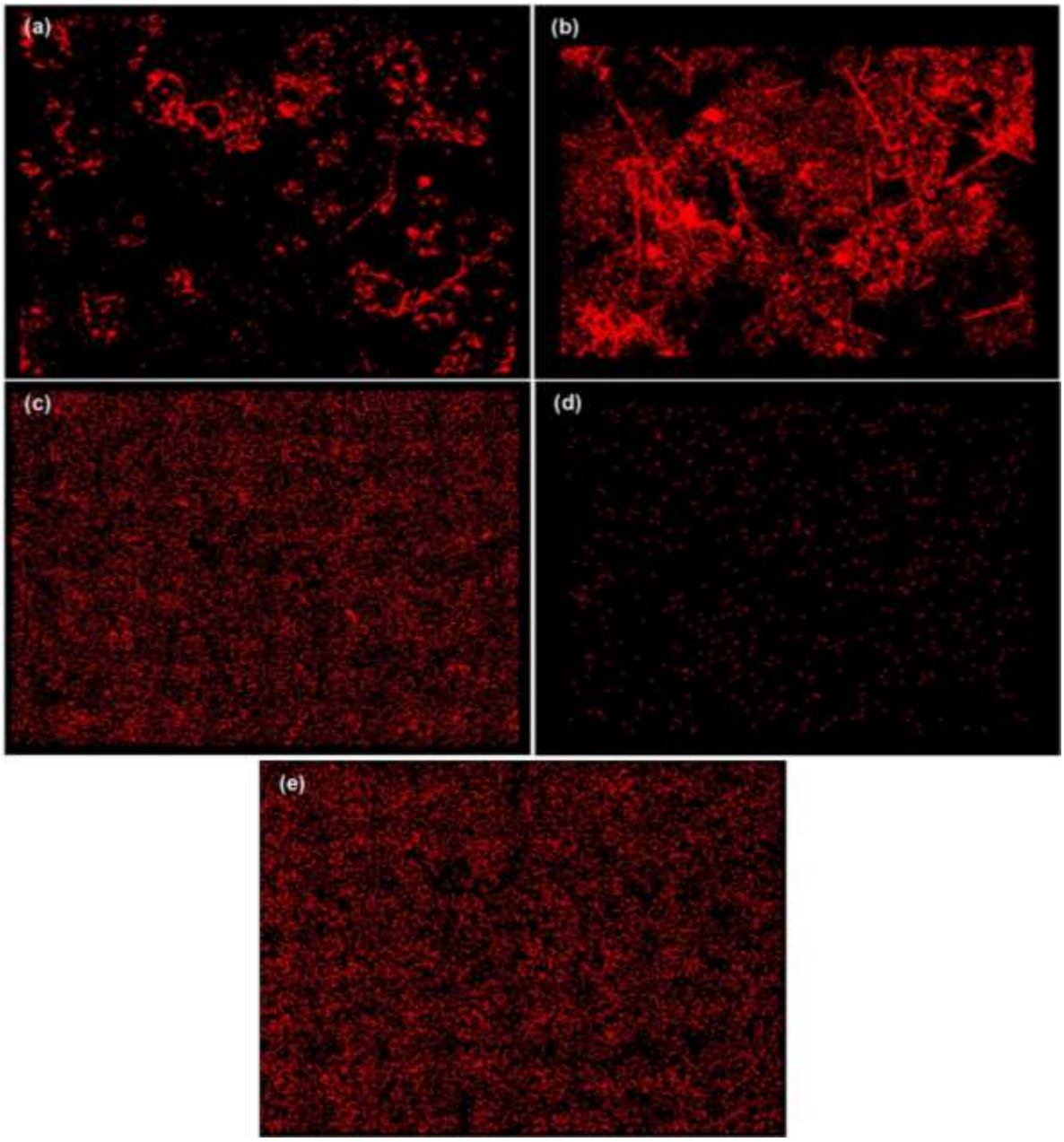

Figure 6-9 EDS map for Iron at the surface for (a) post-CUI simulation test under IW (b) post-CUI simulation test under CW (c) post-autoclave immersion test under IW (d) post-autoclave immersion test under CW (e) pristine TSA coupon

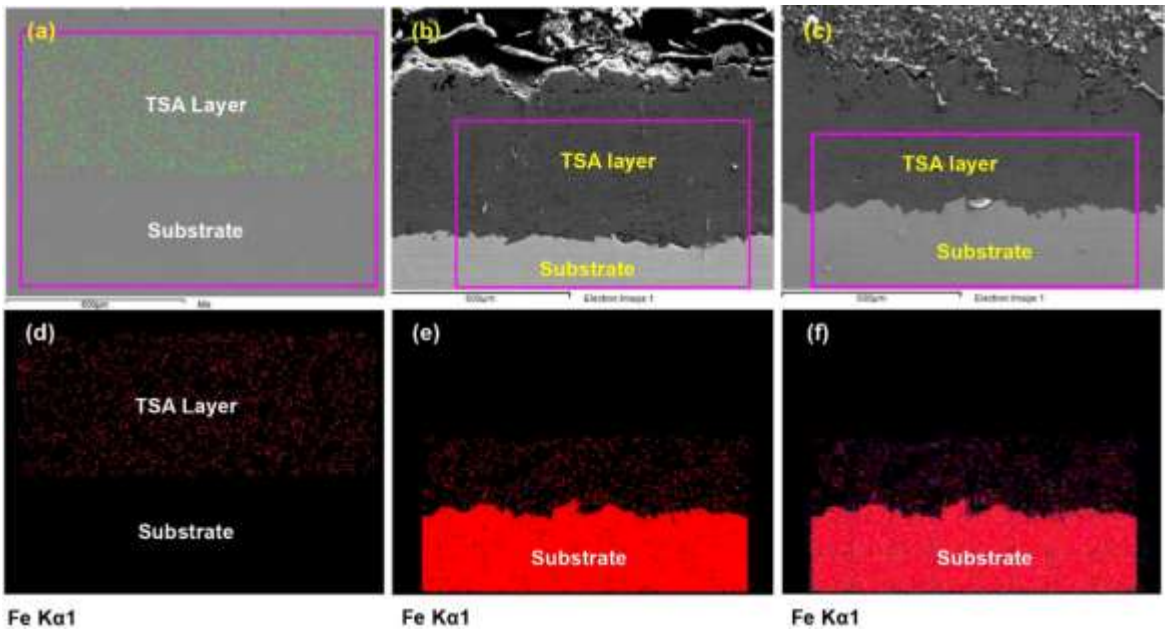

Figure 6-10 SEM micrographs & EDS along cross-sections (a) & (d) pristine TSA coating (b) & (e) post-CUI simulation test under IW (c) & (f) post-CUI simulation test under CW

6.6 DISCUSSION

Coupons subjected to the CUI simulation cell under IW conditions displayed a heterogeneous morphology with a varied surface profile and multi-colored rust stains (white, reddish-brown, etc.), as illustrated in Figure 6-3 (b). The reddish-brown rust stains likely indicate the presence of specific iron corrosion byproducts. In contrast, samples tested in the autoclave exhibited dark grey spots on their surfaces, as shown in Figure 6-3 (d), suggesting the formation of aluminum sulfide (Al_2S_3), which occurs in the presence of sulfur and carbonate ions. ICP analysis of the leachate extracts confirmed the presence of sulfur and alkaline metals (K, Ca, Na, Mg), typically found in stone wool insulations as carbonates and bicarbonates [27], [64].

Further surface characterization of the CUI simulation coupons and cylindrical pucks tested under both IW and CW conditions, as shown in Figures 6-4 (a-b) and 6-5 (a-b), revealed that the reddish rust stains were associated with deeper features, suggesting potential holidays on the TSA surface [57]. The CUI simulation coupons exhibited highly rough features and interconnected voids under both IW and CW conditions. According to Table 6-4, the surface roughness of the CUI simulation coupons was approximately twice that of

the pristine TSA and the cylindrical pucks subjected to autoclave immersion tests. The reduced surface roughness observed in the autoclave immersion tests under IW and CW conditions, as shown in Figures 6-5 (c-d), can be attributed to the buildup of passive layers, deposits in pores, and/or dissolution of asperities [65]. SEM micrographs of the CUI simulation coupons, shown in Figures 6-7 (c-d), revealed larger voids compared to those found in the autoclave immersion pucks (Figure 6-7 (b)) and the pristine TSA coupon (Figure 6-7 (a)). This can be attributed to the rupture and coalescence of pores due to the flashing conditions at the insulation-TSA interface in the CUI simulation cells, a phenomenon not present in the autoclave environment. The wear behavior of TSA from flashing is consistent with previous findings [20], [66].

The electrochemical analysis presented in Table 6-4 unveils a distinct pattern observed in the cylindrical pucks subjected to autoclave immersion tests. Those exposed to isothermal wet (IW) conditions exhibited a consistent daily decline in corrosion current density (i_{corr}), indicative of a gradual stabilization in corrosion activity. Conversely, the pucks under cyclic wet (CW) conditions displayed a notable surge in i_{corr} on Day 2, followed by a decrease on Day 3, and yet another substantial increase on Day 4. Interestingly, Day 1 i_{corr} values were virtually identical across both IW and CW conditions. This behavior aligns with expectations, considering the alkaline nature of the leachate extract (pH > 7) and the elevated test temperature of 100°C, factors conducive to heightened aluminum corrosion activity.

The modest decline in i_{corr} observed for IW on Days 2 and 3 can be linked to the accumulation of corrosion byproducts and alkaline metal deposits like aragonite, calcite, gibbsite, and bayerite [56]. This trend echoes findings from previous research indicating that the corrosion rate of TSA diminishes over time due to these deposits obstructing pore ingress, thereby reducing the number of active corrosion sites [23], [24]. The sharp i_{corr} surge on Day 2 for CW-conditioned pucks likely stems from a temperature drop to 70°C, triggering aluminum passivation and enabling active corrosion of iron contaminants within the TSA matrix. Given aluminum's cathodic nature to iron, an unfavorable cathode-to-anode ratio ensued, resulting in a notably elevated i_{corr} [34]. As the temperature returned to

100°C on Day 3, aluminum regained activity, manifesting in a reduced i_{corr} compared to Day 2 but still higher than Day 1. This uptick on Day 3 can be attributed to freshly exposed aluminum sites post active iron dissolution on Day 2. Day 4 saw another i_{corr} spike as the temperature fell to 70°C, re-passivating aluminum and initiating active corrosion of iron contaminants once again.

The persistent increase in i_{corr} observed under both IW and CW conditions for the CUI simulation coupons is the result of a complex interplay between corrosion and wear catalyzed by the fluctuating moisture environment. Under IW conditions, the notable spike in i_{corr} is particularly evident due to the exposure of coupons to a 100°C temperature, prompting active dissolution of aluminum at a nearly neutral pH level. Additionally, the wear and tear on TSA layers caused by the intermittent moisture exposure constantly exposes underlying aluminum layers within the TSA matrix. pH variations (<7) within crevices, arising from wear-induced mechanisms, contribute to aluminum re-passivation and subsequent active dissolution of iron, collectively contributing to the observed increase in i_{corr}. In CW conditions, the cycling surface temperature to 70°C on Day 2 triggers a phase of aluminum re-passivation, leading to active iron dissolution from both the TSA matrix and the substrate. However, the i_{corr} increase on Day 2 in the CUI simulation exhibits a lesser magnitude compared to autoclave immersion, primarily due to substrate exposure altering the Surface Area Cathode/Surface Area Anode ratio, thus tempering the corrosion rate amplification. On Day 3, the i_{corr} escalation can be attributed to aluminum reactivation alongside wear from intermittent moisture exposure as the surface temperature reverts to 100°C. Finally, a slight i_{corr} uptick on Day 4 can be attributed to aluminum re-passivation at temperatures below 70°C, resulting in anodic dissolution of iron contaminants and the substrate, albeit to a lesser extent than observed on previous days.

In the CUI simulation cell, the soaking of the coupon occurs as the moisture-saturated insulation remains in contact with the coupon. This situation creates flashing conditions for moisture, as it evaporates to seek areas of lower relative humidity. At the interface between the insulation and TSA, these flashing conditions lead to the formation and collapse of bubbles. Due to its lower hardness, the TSA surface experiences cavitating

wear, resulting from the coalescence of pores and the creation of voids. These voids act as crevices, allowing the electrolyte to seep in. The concentration of chlorides within these crevices, compared to the outer TSA layer, creates a lower pH environment. This lower pH, below neutral, triggers the re-passivation of aluminum even as it undergoes cavitating wear. Over time, these crevices deepen to the steel substrate's surface while the aluminum remains passivated due to the lower pH environment. When exposed to moisture, the steel substrate undergoes active dissolution, facilitated by the cathodic aluminum within the crevices. This process is evident from the reddish rust visible in Figure 6-3 (b) and the surface micrographs depicted in Figure 6-4 (a-b).

Knudsen et al. observed that as the temperature rises to 95°C, the upper pH limit for aluminum passivation decreases to 7 [57]. This near-neutral pH of the leachate solution at the operating temperature of 100°C compromises aluminum passivation, leading to active dissolution. Additionally, higher temperatures result in a reduced concentration of dissolved oxygen in the solution. Under de-aerated conditions, pure aluminum experiences a higher corrosion rate as the oxide films become more porous, offering minimal resistance to hydrogen diffusion [22]. Figure 6-8 (c) illustrates that the surface of the IW coupon appears more dissolved compared to the CW coupon in Figure 6-8 (d). This disparity stems from the IW coupon being consistently exposed to higher temperatures (>95°C) than the CW coupon, which undergoes cycling between 100°C and 70°C.

To gain deeper insights into the physical and chemical properties of the corroded surfaces, EDS mapping was performed on the surface and cross-sections of both pristine and post-test coupons, with a specific focus on iron concentration and distribution within the TSA matrix. Commercially available aluminum powders often contain trace amounts of iron as contaminants. During the EDS analysis of pristine and post-test TSA coatings, the EDS map of Fe Kα1 (as shown in Figure 6-1 (b) for aluminum powder) served as a reference to differentiate between the effects of pre-existing iron contamination in aluminum powders. Figure 6-9 (a-b) displays the EDS maps for both IW and CW coupons from the CUI simulation test, indicating prominent iron clusters compared to Figure 6-1 (b) for aluminum powder and Figure 6-9 (e) for pristine TSA coating. Cross-sectional EDS maps for CUI

simulation coupons in Figures 6-10 (e) and 6-10 (f) show no clusters alongside the TSA coating thickness, suggesting that the observed iron clusters in Figure 6-9 (a-b) stem from the substrate rather than pre-existing iron contaminants within the TSA matrix. Conversely, the EDS map for pucks from autoclave immersion tests under IW condition in Figure 6-9 (b) reveals iron concentrations consistent with pristine TSA in Figure 6-9 (e), indicating minimal iron dissolution in the autoclave immersion test under IW condition. This finding corroborates with the electrochemical data showing consistent passivation over three days, where Rp increased from 0.384 kΩ on Day 1 to 0.48 kΩ on Day 3, resulting in active corrosion of aluminum rather than iron.

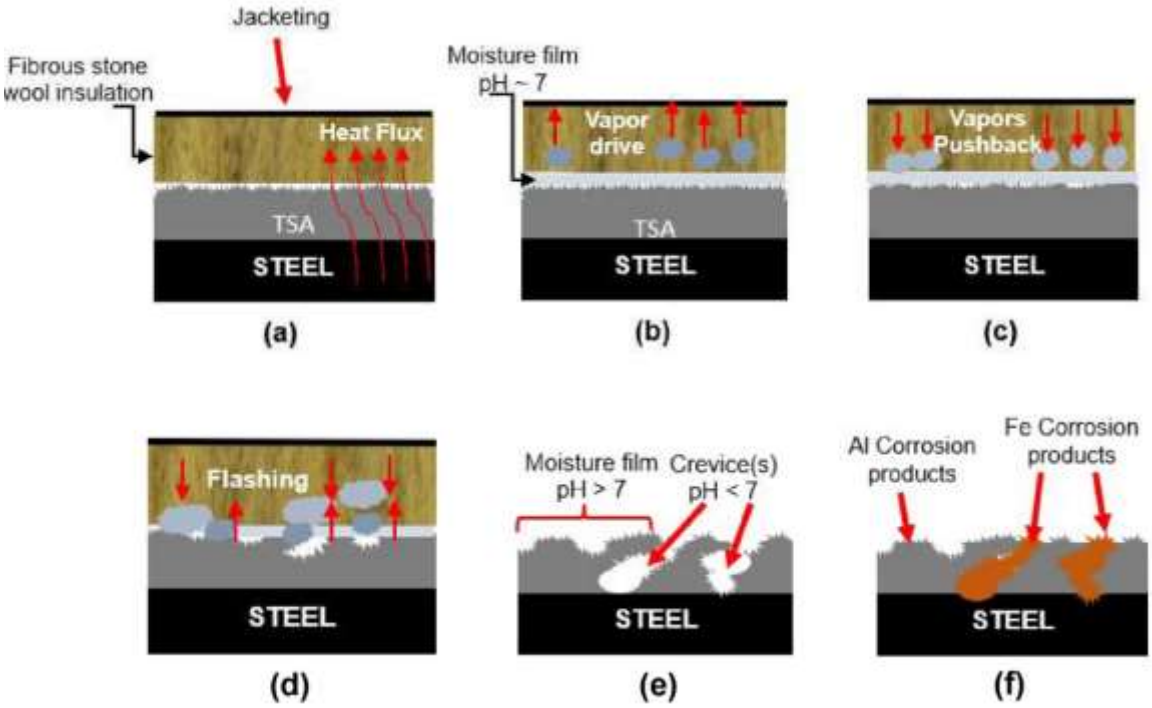

Figure 6-11 Schematic of TSA damage in an autoclave with leachate extracts immersion

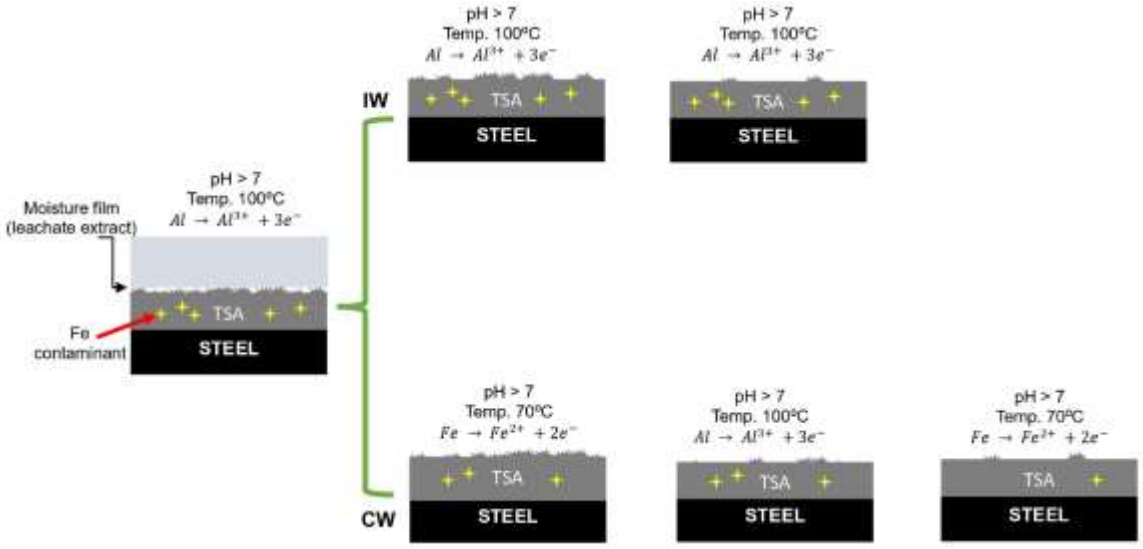

Figure 6-12 Schematic of TSA damage in a CUI simulation test

Conversely, the EDS map of the puck from the CW autoclave immersion reveals minimal iron presence on its surface, explaining the spikes in corrosion rates on Day 2 and Day 4 due to the active dissolution of iron contaminants (owing to aluminum passivation), as depicted in Figure 6-9 (d). Schematic representations of corrosion damage for the CUI simulation and autoclave cells are presented in Figures 6-11 and 6-12, respectively.

6.7 CONCLUSIONS

Using thermal sprayed aluminum (TSA) coating on mild steel substrates, employing commercially available aluminum 1350 powder was conducted within an industrial framework, marking a pivotal stride in corrosion resistance engineering. The experimental paradigm encompassed dual scenarios: first, entwined with fibrous stone wool insulation within a meticulously designed corrosion under insulation (CUI) simulation test cell, meticulously crafted to replicate direct insulation-TSA interaction per ASTM G189-07 standards, and exposed to isothermal wet (IW) and cyclic wet (CW) conditions; second, submerged in an autoclave under similar IW and CW conditions utilizing leachate extract from fibrous stone wool insulation. This rigorous testing regimen was complemented by sophisticated analytical techniques, including linear polarization resistance (LPR) methodology and comprehensive microstructural evaluations via cutting-edge tools like

confocal laser microscopy, 3D topography analysis, scanning electron microscopy (SEM), and energy dispersive spectroscopy (EDS).
The findings from this groundbreaking study have unveiled profound insights that promise to revolutionize corrosion mitigation strategies:

1. TSA coatings deployed under IW conditions amidst fibrous stone wool insulation exhibited an intriguing surge in corrosion current density (i_{corr}), underscoring the dynamic interplay between environmental factors and coating resilience. Conversely, immersion in the autoclave environment showcased a subtle decline in i_{corr} and corrosion rate over the experimental timeline, hinting at the robustness of TSA coatings under controlled conditions.

2. Delving into the realm of CW conditions, TSA coatings nestled within insulation demonstrated a subtle downtrend in i_{corr} and corrosion rates compared to their IW counterparts, a phenomenon intricately linked to nuanced temperature fluctuations below the flashpoint threshold. Meanwhile, the autoclave environment unraveled intriguing i_{corr} fluctuations, reflecting the intricate dance between temperature dynamics and material behavior, particularly aluminum's response.

3. The striking visual of TSA coatings within the CUI simulation cell, engaged in a direct tussle with insulation, revealed an intricate tapestry of large void formations, a testament to the adversarial battle against moisture-induced wear and tear. This visual spectacle, accompanied by heightened surface roughness and corrosion rates, painted a vivid picture of the challenges posed by real-world environmental stressors.

4. Noteworthy was the resilience of TSA coatings, showcasing no signs of disbanding, delamination, or structural compromise under both harsh autoclave immersion and demanding CUI simulation conditions, a testament to their durability and engineering prowess.

5. The strategic proposition of alternative insulation paradigms incorporating breathable systems emerged as a beacon of hope, offering a pathway to mitigate moisture-related challenges and elevate corrosion resistance strategies to unprecedented heights.

This scientific odyssey has not only unraveled the intricate nuances of TSA coatings' behavior under varying environmental stresses but also paved the way for transformative advancements in corrosion mitigation methodologies, setting a new benchmark for engineering ingenuity and resilience in the face of adversities.

CHAPTER 7. CONCLUSION

Corrosion, particularly Corrosion Under Insulation (CUI), represents a critical challenge in the engineering and maintenance of industrial facilities. Its insidious nature, coupled with the difficulty of detection until significant damage has occurred, makes it a paramount area of research. CUI's economic, safety, and operational implications necessitate comprehensive studies to develop effective mitigation and management strategies. The research within this thesis contributes to this critical field by offering insights into the mechanisms, detection, and prevention of CUI, thereby underpinning the broader efforts to enhance asset integrity and operational reliability in industries prone to this phenomenon.

This thesis provided an in-depth forensic investigation of CUI by analyzing rust scale samples from various industrial settings. The complexity of CUI, as influenced by environmental conditions and operational practices, was underscored. Key findings highlighted the role of effluents, such as SO_2 and marine vapors, in exacerbating CUI rates and the formation of heterogeneous scales due to oxygen concentration cells. The study concluded that direct insulation-metal contact significantly heightens pitting risks, emphasizing the need for robust design and maintenance protocols. Forensic analysis through scab studies emerged as a promising yet nascent tool in CUI management, indicating the need for further research to refine these methodologies and enhance predictive capabilities.

Further exploration delved into the implications of insulation aging on CUI, comparing laboratory and field samples of mineral wool and calcium silicate. The research demonstrated that insulation aging is a significant factor in CUI risk assessment, leading to altered physical properties and increased corrosion susceptibility. Advanced analytical techniques, including inductively coupled plasma spectroscopy and various corrosion tests, were employed to evaluate the degradation processes. Findings revealed that field-aged insulations exhibited more severe degradation than lab-aged samples, highlighting the importance of realistic environmental simulations in CUI studies. This reinforced the

necessity of continuous monitoring and developing more resilient insulation materials to mitigate CUI.

A practical case study on the premature failure of coatings on boiler tubes was presented, providing an example of how improper coating application and environmental factors can lead to rapid degradation. The investigation revealed that the failure was primarily due to inadequate surface preparation and environmental exposure, which compromised the coating's integrity. This underscored the importance of adhering to stringent coating application protocols and the need for regular inspections to identify early signs of coating deterioration. The insights gained from this case study offer valuable lessons for improving coating practices and enhancing the longevity of protective systems in high-temperature environments.

The behavior of thermal sprayed aluminum (TSA) coatings under varying environmental conditions, including isothermal wet (IW) and cyclic wet (CW) scenarios, both within the insulation and in autoclave environments, was thoroughly explored. The findings indicated that TSA coatings exhibit remarkable resilience, showing no signs of disbanding or delamination, even under harsh conditions. However, the challenges posed by moisture-induced wear and tear, particularly in CW conditions, were also highlighted. Notably, the research proposed adopting breathable insulation systems as a strategic approach to enhance moisture management and reduce CUI risks. These insights contribute significantly to advancing corrosion mitigation strategies and underscore the potential of TSA coatings in extending the service life of industrial components.

The comprehensive investigations presented in this thesis collectively offer a multifaceted understanding of CUI and its mitigation. The forensic analysis of rust scales provided foundational knowledge on corrosion compounds and their formation drivers. The aging study of insulations emphasized the impact of environmental exposure on insulation properties and subsequent CUI risks. The case study on coating failures illustrated practical challenges and underscored the importance of rigorous coating protocols. Finally, the evaluation of TSA coatings demonstrated their robustness and highlighted innovative

approaches for moisture management. Together, these studies build a cohesive narrative that addresses CUI's theoretical and practical aspects, offering valuable insights for industry stakeholders.

7.1 FUTURE WORK

The author recommends expanding forensic investigation via scale analysis to broaden industrial applications and reduce uncertainties in CUI damage assessment. Additionally, the author plans to conduct laboratory simulation tests to evaluate the performance of various insulation materials on coated substrates, incorporating electrochemical testing for a more comprehensive analysis. Furthermore, the author intends to investigate damage modes and mechanisms of phenolic epoxy and inorganic zinc coatings at elevated temperatures through detailed laboratory simulations.

BIBLIOGRAPHY

[1] Zaki Ahmad, Principles of Corrosion Engineering and Corrosion Control. 2006. [Online]. Available: www.icheme.org.

[2] Corrosion Control, “Corrosion Control,” https://www.corrosioncost.com/.

[3] Canada’s cost of corrosion, “Canada’s cost of corrosion,” https://canada.constructconnect.com/dcn/news/economic/2023/03/canadas-cost-of-corrosion-a-51-9-billion-problem.

[4] S. Bin Mujib, S. Mukherjee, Z. Ren, and G. Singh, “Assessing corrosion resistance of two-dimensional nanomaterial-based coatings on stainless steel substrates,” R Soc Open Sci, vol. 7, no. 4, Apr. 2020, doi: 10.1098/rsos.200214.

[5] B. J. Fitzgerald, P. L. Iii, R. M. Kay, and S. Winnik, “03029 - STRATEGIES TO PREVENT CORROSION UNDER INSULATION IN PETROCHEMICAL INDUSTRY PIPING,” 2003.

[6] A. R. K. Rana, M. Yang, J. Umer, T. Veret, and G. Brigham, “Influence of Robust Drain Openings and Insulation Standoffs on Corrosion Under Insulation Behavior of Carbon Steel,” Corrosion, vol. 77, no. 6, pp. 681–692, Jun. 2021, doi: 10.5006/3749.

[7] N. Wilds, “Corrosion under insulation,” in Trends in Oil and Gas Corrosion Research and Technologies: Production and Transmission, Elsevier Inc., 2017, pp. 409–429. doi: 10.1016/B978-0-08-101105-8.00017-6.

[8] A. R. Hayrullin, A. I. Haibullina, and A. M. Gusyachkin, “Thermal Conductivity of Insulation Material: Effect of Moisture Content and Wet-Drying Cycle,” 2023. [Online]. Available: www.scientific.net.

[9] S. Caines, F. Khan, J. Shirokoff, and W. Qiu, “Experimental design to study corrosion under insulation in harsh marine environments,” J Loss Prev Process Ind, vol. 33, pp. 39–51, Jan. 2015, doi: 10.1016/j.jlp.2014.10.014.

[10] Y. Xu, Y. Q. Zhang, X. Y. Liu, C. Ma, and L. J. Liu, “Research on thermal insulation performance of composite energy storage pipeline with phase change materials,” J Energy Storage, vol. 55, Nov. 2022, doi: 10.1016/j.est.2022.105711.

[11] M. Morcillo, D. De La Fuente, I. Díaz, and H. Cano, “Atmospheric corrosion of mild steel,” Sep. 2011. doi: 10.3989/revmetalm.1125.

[12] R. A. Antunes, I. Costa, D. Lúcia, and A. De Faria, “Characterization of Corrosion Products Formed on Steels in the First Months of Atmospheric Exposure 403 Characterization of Corrosion Products Formed on Steels in the First Months of Atmospheric Exposure,” 2003.

[13] P. S. Brown, O. D. L. A. Atkinson, and J. P. S. Badyal, “Ultrafast Oleophobic–Hydrophilic Switching Surfaces for Antifogging, Self-Cleaning, and Oil–Water Separation,” ACS Appl Mater Interfaces, vol. 6, no. 10, pp. 7504–7511, May 2014, doi: 10.1021/am500882y.

[14] Ahmad Raza Khan Rana, Graham Brigham, and Andrew Buchanan, “CUI Management Through Moisture Barrier System and Field Assessment,” 2021.

[15] H. Saito, M. Ito, and K. Mabuchi, “Empirical Model for Predicting Corrosion Under Insulation Considering the Effects of Temperature, Salinity, and Water Content,” Corrosion, vol. 79, no. 11, pp. 1267–1276, Nov. 2023, doi: 10.5006/4359.

[16] S. Winnik, “Design for the prevention of CUI,” in Corrosion-Under-Insulation (CUI) Guidelines, Elsevier, 2016, pp. 67–73. doi: 10.1016/b978-0-08-100714-3.00008-1.

[17] M. Cui, Y. Shen, H. Tian, Y. Yang, H. Feng, and J. Li, “Influence of water adhesion of superhydrophobic surfaces on their anti-corrosive behavior,” Surf Coat Technol, vol. 347, pp. 38–45, Aug. 2018, doi: 10.1016/j.surfcoat.2018.04.064.

[18] Q. Cao, I. Oluwoye, T. Pojtanabuntoeng, H. Farhat, and M. Iannuzzi, “Evaluation of epoxy-based coating degradation under thermal insulation at elevated temperatures on different steel substrates,” Prog Org Coat, vol. 180, Jul. 2023, doi: 10.1016/j.porgcoat.2023.107544.

[19] SSPC-SP 10/NACE no. 2, “SSPC: The Society for Protective Coatings,” 2007.

[20] A. López-Ortega, R. Bayón, and J. L. Arana, “Evaluation of protective coatings for offshore applications. Corrosion and tribocorrosion behavior in synthetic seawater,” Surf Coat Technol, vol. 349, pp. 1083–1097, Sep. 2018, doi: 10.1016/j.surfcoat.2018.06.089.

[21] N. Ce and S. Paul, “Thermally Sprayed Aluminum Coatings for the Protection of Subsea Risers and Pipelines Carrying Hot Fluids,” Coatings, vol. 6, no. 4, p. 58, Nov. 2016, doi: 10.3390/coatings6040058.

[22] S. Paul, “Behavior of damaged thermally sprayed aluminum (TSA) in aerated and deaerated seawater,” 2019.

[23] R. Grinon-Echaniz, P. Refait, M. Jeannin, R. Sabot, S. Paul, and R. Thornton, “Study of cathodic reactions in defects of thermal spray aluminium coatings on steel in artificial seawater,” Corros Sci, vol. 187, Jul. 2021, doi: 10.1016/j.corsci.2021.109514.

[24] H. S. Lee, J. K. Singh, and J. H. Park, “Pore blocking characteristics of corrosion products formed on Aluminum coating produced by arc thermal metal spray process in 3.5 wt.% NaCl solution,” Constr Build Mater, vol. 113, pp. 905–916, Jun. 2016, doi: 10.1016/j.conbuildmat.2016.03.135.

[25] S. Paul and D. Harvey, “Determination of the Corrosion Rate of Thermally Spayed Aluminum (TSA) in Simulated Marine Service,” 2020.

[26] G. A. Cragnolino, “Corrosion fundamentals and characterization techniques,” in Techniques for Corrosion Monitoring, Elsevier, 2020, pp. 7–42. doi: 10.1016/B978-0-08-103003-5.00002-3.

[27] K. D. Ralston, “Laboratory Testing in Leachate Environments to Understand Stress Corrosion Cracking on an Insulated Above-Ground Pipeline,” 2019.

[28] Y. S. Choi, M. K. Chung, and J. G. Kim, “Effects of cyclic stress and insulation on the corrosion fatigue properties of thermally insulated pipeline,” Materials Science and Engineering: A, vol. 384, no. 1–2, pp. 47–56, Oct. 2004, doi: 10.1016/j.msea.2004.05.068.

[29] F. Gui and C. S. Brossia, “Corrosion monitoring undercoatings and insulation,” in Techniques for Corrosion Monitoring, Elsevier, 2020, pp. 439–455. doi: 10.1016/B978-0-08-103003-5.00018-7.

[30] S. Winnik, “The risk-based inspection methodology for CUI,” in Corrosion-Under-Insulation (CUI) Guidelines, Elsevier, 2016, pp. 17–42. doi: 10.1016/b978-0-08-100714-3.00004-4.

[31] A. Hussein Khalaf et al., “Emerging AI technologies for corrosion monitoring in oil and gas industry: A comprehensive review,” Jan. 01, 2024, Elsevier Ltd. doi: 10.1016/j.engfailanal.2023.107735.

[32] Ahmad Raza Khan Rana, Shahzad Karim, Salwa Alachkar, Touqeer Sohail, Syed Umair Niaz Bukhari, and Graham Brigham, “Forensic Investigation Of Corrosion Under Insulation From Rust Scale Sample,” 2024.

[33] API RP 571, “Damage Mechanisms Affecting Fixed Equipment in the Refining Industry,” 2011. Accessed: Jun. 18, 2024. [Online]. Available: https://www.api.org/

[34] A. R. K. Rana and Z. Farhat, “Neighborhood Watch-Right Step Towards Asset Integrity,” 2020. [Online]. Available: https://www.researchgate.net/publication/342788457

[35] A. R. K. Rana et al., “Influence of Insulation Stand-Off Membranes and Moisture Drainage on the Corrosion Under Insulation Behavior of Out-of-Service Carbon Steel Piping,” Corrosion, vol. 78, no. 10, pp. 1003–1013, Oct. 2022, doi: 10.5006/4104.

[36] C. W. Turner and L. Chi, “FORMATION OF CORROSION PRODUCTS OF CARBON STEEL UNDER CONDENSER OPERATING CONDITIONS,” 2012.

[37] J. A. Sawicki and M. E. Brett, “CANDU BIIAINTENANCE CONFERENCE 1995 CORROSION-PRODUCT INVENTORY: THE BRUCE-B SECONDARY SYSTEM,” 1995.

[38] R. I. Ray, J. S. Lee, B. J. Little, and T. L. Gerke, “The anatomy of tubercles: A corrosion study in a fresh water estuary,” Materials and Corrosion, vol. 61, no. 12, pp. 993–999, Dec. 2010, doi: 10.1002/maco.201005739.

[39] M. Morcillo, D. De la Fuente, I. Díaz, and H. Cano, “Atmospheric corrosion of mild steel,” Revista de Metalurgia, vol. 47, no. 5, pp. 426–444, Oct. 2011, doi: 10.3989/revmetalm.1125.

[40] Tao Chen, Feng Liang, Frank Chang, and Steven Hochanadel, “Downhole Sour Corrosion and Scale Deposition in Oil Wells,” in AMPP Annual Conference + Expo, 2022.

[41] T. Pojtanabuntoeng, L. L. Machuca, M. Salasi, B. Kinsella, and M. Cooper, “Influence of drain holes in jacketing on corrosion under thermal insulation,” Corrosion, vol. 71, no. 12, pp. 1511–1520, Dec. 2015, doi: 10.5006/1861.

[42] A. R. K. Rana et al., “Influence of Insulation Stand-Off Membranes and Moisture Drainage on the Corrosion Under Insulation Behavior of Out-of-Service Carbon Steel Piping,” Corrosion, vol. 78, no. 10, pp. 1023–1033, Oct. 2022, doi: 10.5006/4104.

[43] https://web.archive.org/web/20240222134954/, “https://web.archive.org/web/20240222134954/https://static.aer.ca/prd/documents/bulletins/Bulletin-2021-36.pdf.”

[44] Ahmad Raza Khan Rana, Shahzad Karim, Salwa AlAchkar, Graham Brigham, and Syed Umair Niaz Bukhari, “Insulations Ageing & CUI Implications-A Comparison of Lab & Field Samples,” 2024.

[45] G. Brigham, A. Raza Khan Rana, O. Chaar, and S. Umair Niaz Bukhari, “Corrosion Scale And Moisture Assessments-An Improvement To On-Stream Inspections For CUI Management,” 2023.

[46] ASTM G 189-07, “ASTM G189-07(2021)e1 - Laboratory Simulation of Corrosion Under Insulation,” 2021.

[47] ASTM C 1617-19, “Standard Practice for Quantitative Accelerated Laboratory Evaluation of Extraction Solutions Containing Ions Leached from Thermal Insulation on Aqueous Corrosion of Metals 1,” 2019, doi: 10.1520/C1617-19.

[48] Ahmad Raza Khan Rana, Shahzad Karim, George Jarjoura, and Syed Umair Niaz Bukhari, “Case Study Of The Premature Coating Failure On The Boiler Tubes,” 2024.

[49] https://www.venus-boiler.com/, “https://www.venus-boiler.com/technical_paper_pdf/Visit%20to%20Penthouse.pdf.”

[50] https://web.archive.org/, “https://web.archive.org/web/20231030205222/https:/www.speccoats.co.za/DataSheets/Inorganic_Zinc_Primer.pdf.”

[51] https://web.archive.org, https://web.archive.org/web/20230908174823/https:/www.linkedin.com/pulse/sacrificial-coatingsprimers-immersion-buried-services-guan/.

[52] https://web.archive.org, "https://web.archive.org/web/20231019213455/https:/docs2.cer-rec.gc.ca/ll-eng/llisapi.dll/fetch/2000/90464/90552/418396/446070/489870/554336/A1J5C3_-_Hardisty_Tanks-_Specification_for_Tank_Hydrotest.pdf?nodeid=554340&vernum=-2."

[53] NACE SP0198-2017, SP0198-2017, "Control of Corrosion Under Thermal Insulation and Fireproofing Materials—A Systems Approach," Rev. 2010-6-25. Houston, Tex.: NACE International, 2017.

[54] A. R. K. Rana, S. Karim, S. AlAchkaar, J. Umer, G. Brigham, and G. Jarjoura, "An Investigation of Corrosion Behaviors of Thermally Sprayed Aluminum (TSA) at Elevated Temperatures Under Thermal Insulations and Autoclave Immersion Conditions," CORROSION, Jul. 2024, doi: 10.5006/4508.

[55] API RP 583, "API Recommended Practice 583 Corrosion Under Insulation and Fireproofing," 2014. [Online]. Available: www.api.org

[56] E. Hornus et al., "Growth Kinetics of Calcareous Deposits on Thermally Sprayed Aluminum Coatings in Natural Seawater," Corrosion, vol. 78, no. 12, pp. 1263–1274, Dec. 2022, doi: 10.5006/4118.

[57] O. Ø. Knudsen, J. Van Bokhorst, G. Clapp, and G. Duncan, "Technical note: Corrosion of cathodically polarized thermally sprayed aluminum in subsea mud at high temperature," Corrosion, vol. 72, no. 4, pp. 560–568, Apr. 2016, doi: 10.5006/1485.

[58] R. Arrabal et al., "Corrosion Behavior of Mg-Al Alloys with Aluminum Thermal Spray Coatings in Humid and Saline Environments," 2009. [Online]. Available: http://meridian.allenpress.com/corrosion/article-pdf/65/12/817/1537902/1_3319108.pdf

[59] R. D. Kane, M. Chauviere, and K. Chustz, "EVALUATION OF STEEL AND TSA COATING IN A CORROSION UNDER INSULATION (CUI) ENVIRONMENT," 2008.

[60] ASTM C 871, "ASTM C 871 - Leachates," 2018.

[61] ASTM G 59-23, "Standard Test Method for Conducting Potentiodynamic Polarization Resistance Measurements 1," 2023, doi: 10.1520/G0059-23.

[62] A. R. K. Rana, M. A. Islam, and Z. Farhat, “Effect of Graphene Nanoplatelets (GNPs) Addition on Erosion–Corrosion Resistance of Electroless Ni–P Coatings,” J Bio Tribocorros, vol. 6, no. 1, Mar. 2020, doi: 10.1007/s40735-019-0304-y.

[63] ISO 25178-6 2010, “ISO-25178-2010, ‘Geometrical Product Specifications—Surface Texture’ (Geneva, Switzerland: ISO, 2010).,” 2010.

[64] https://web.archive.org/web/20231222071252, “https://web.archive.org/web/20231222071252,” https://web.archive.org/web/20231222071252/https://www.biosynth.com/p/FA172944/1302-81-4-aluminum-sulfide.

[65] H. S. Lee et al., “Corrosion mechanism and kinetics of Al-Zn coating deposited by arc thermal spraying process in saline solution at prolong exposure periods,” Sci Rep, vol. 9, no. 1, Dec. 2019, doi: 10.1038/s41598-019-39943-3.

[66] O. Ø. Knudsen, J. Van Bokhorst, G. Clapp, and G. Duncan, “4196: Corrosion of Cathodically Polarized TSA in Subsea Mud at High Temperature,” 2014.